THE UNIVERSITY OF ALBERTA

RELEASE FORM

NAME OF AUTHOR ..Gary..Mann.....................

TITLE OF THESIS .Multichannel..Signal...........
.Enhancement...Techniques..For...
.Reflection..Seismic..Records...

DEGREE FOR WHICH THESIS WAS PRESENTED ..M.Sc...............

YEAR THIS DEGREE GRANTED ..1979.........................

Permission is hereby granted to THE UNIVERSITY OF
ALBERTA LIBRARY to reproduce single copies of this
thesis and to lend or sell such copies for private,
scholarly or scientific research purposes only.

The author reserves other publication rights, and
neither the thesis nor extensive extracts from it may
be printed or otherwise reproduced without the author's
written permission.

THE UNIVERSITY OF ALBERTA

MULTICHANNEL SIGNAL ENHANCEMENT TECHNIQUES FOR REFLECTION

SEISMIC RECORDS

by

(C) GARY DALE MANN

A THESIS

SUBMITTED TO THE FACULTY OF GRADUATE STUDIES AND RESEARCH

IN PARTIAL FULFILMENT OF THE REQUIREMENTS FOR THE DEGREE

OF MASTER OF SCIENCE

IN

GEOPHYSICS

DEPARTMENT OF PHYSICS

EDMONTON, ALBERTA

SPRING, 1979

THE UNIVERSITY OF ALBERTA

FACULTY OF GRADUATE STUDIES AND RESEARCH

The undersigned certify that they have read, and recommend to the Faculty of Graduate Studies and Research, for acceptance, a thesis entitled MULTICHANNEL SIGNAL ENHANCEMENT TECHNIQUES FOR REFLECTION SEISMIC RECORDS submitted by GARY DALE MANN in partial fulfilment of the requirements for the degree of MASTER OF SCIENCE in GEOPHYSICS.

ABSTRACT

Deep reflections from horizons within the Earth
have been recorded, at near vertical incidence, on
seismograms along three lines in southwestern Manitoba.
The data were digitally recorded on magnetic tape recorders
with a dynamic range of 84 decibels. Power spectral esti-
mates indicate that the reflected energy is contained in
the frequency band of 10 to 30 hertz. Through the
application of frequency filtering and common depth point
stacking, the primary reflections were enhanced relative
to the noise.

The methods of N-th root stacking, velocity filter-
ing and maximum likelihood filtering are discussed. These
techniques are applied to the reflection data and the
results are compared. Velocity filtering and N-th root
stacking were both found to be effective in enhancing
coherent signal, with very little success being obtained
from a three channel maximum likelihood filter. This was
the first time that the N-th root stack had been used for
enhancing reflection records. Main reflected energy was
located at depths of about 19 (6.6 seconds), 24 (8.1
seconds) and 37 (12.5 seconds) kilometers. Also, the N-th
root stack was found to be an excellent filter for deter-
mining the phase velocity of the reflected events.

ACKNOWLEDGEMENTS

TABLE OF CONTENTS

LIST OF FIGURES

CHAPTER 1
INTRODUCTION

1.1.   Understanding the Crust

The crust is comprised of the uppermost layers of
the Earth. This outer rind constitutes about one percent
of the Earth's volume, and only 0.5 percent of the Earth's
mass (Jacobs *et al.*, 1974). It has a mean thickness of
about 10 kilometers under the oceans and 40 kilometers
under the continents, and consists mainly of oxygen, sili-
con, aluminum and iron. Separated from the crust by the
Mohorovicic discontinuity, lies the mantle, and beneath
this is the core (figure 1.1). However, to fully under-
stand these deeper regions, in particular the mantle, one
must completely understand the crust.

Explosion seismology, and in particular the seismic
reflection technique, has proven to be the most valuable
method for investigating deep crustal structure. Both
reflection and refraction methods have produced much infor-
mation about the lower crust and upper mantle, but the
reflection technique has many inherent advantages. First,
the wavelengths of the reflected waves are many times
shorter than those of refracted waves yielding a larger
resolving power of the method, and thus increasing the pre-
cision in detailing fine structure (Kanasewich and Cumming,
1965). Spectral analysis of reflected waves provides
information about the reflective process. Also, the
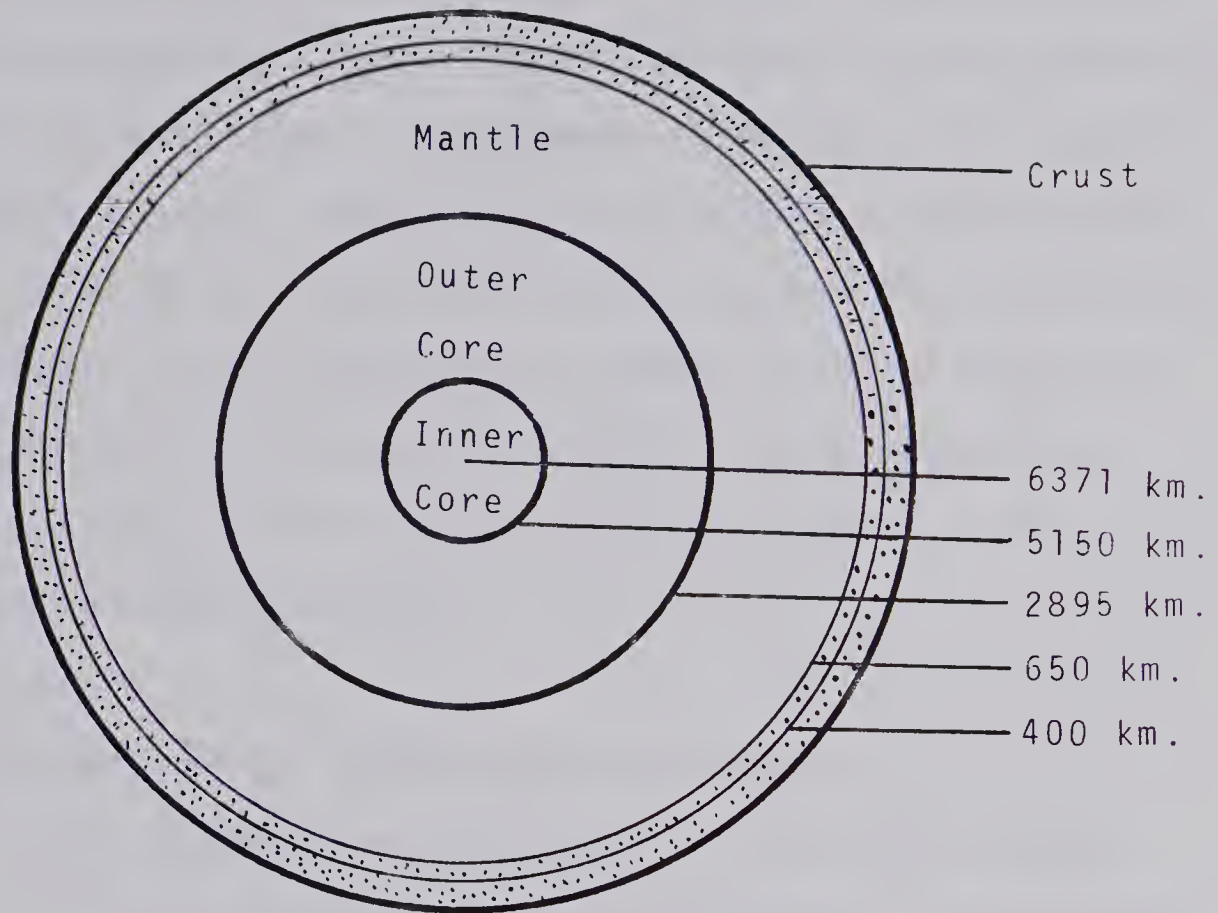
Figure 1.1: Depths to the major discontinuities of the Earth

The dotted region indicates complex structure in the upper mantle. A radius of 6371 kilometers is the result of assuming the Earth to be a perfect sphere with its true mass and volume.

method allows the determination of the average velocity down to any discontinuity, and the detection of all low velocity zones.

Through the use of digital recorders and high speed digital computers, seismic reflection data may be processed through various signal enhancement techniques very quickly and inexpensively. Thus, seismic sections exhibiting the very fine detail of deep structures within the Earth may be produced. These sections may then be correlated with other geophysical information obtained from refraction, magnetic and gravity surveys, to produce large scale pictures of the Earth's crust.

1.2. History of the Reflection Technique

The development of the seismic reflection method began in 1917 at the University of Oklahoma, in the hopes of developing a new technique to locate oil reserves (Schriever, 1952). Mr. J.C. Karcher and Dr. W.P. Haseman met at the university, and discussed the advantages and disadvantages of using reflected seismic waves to locate oil bearing structures. This idea was left alone until 1919, when they again met, leading to the design and construction of equipment for the recording of seismic reflections. The world's first exploration record was made in 1919 by Dr. Karcher in a rock quarry near Washington D.C., using dynamite as the source. This was followed by the first field tests on June 4, 1921. Drs. J.C.

Karcher, W.P. Haseman, I. Perinne, and Mr. W.C. Kite com-
prised this first field crew. To this day, the reflection
technique is still the most useful petroleum prospecting
technique (Dobrin, 1976).

Deep crustal reflections were first recorded by
Junger (1951), on a seismic section shot in Big Horn County,
Montana. He had observed that a charge of 11.4 kilograms
would create a long lasting, low frequency disturbance.
To determine the duration of this pulse, the recording
camera was allowed to run for ten seconds. A distinct
reflection was observed at 8.5 seconds on the record. This
experiment was repeated in adjacent areas, with reflections
being observed at 7.0 to 7.5 seconds. Junger effectively
argued that these reflections must be reflections from near
horizontal layers beneath the basement, and not multiple
reflections from shallower horizons. Other reports concern-
ing the early use of the reflection technique for studying
the lower crust may be found in Steinhart and Meyer (1961).
James and Steinhart (1966) followed this up with a review
of seismic reflection studies of the lower crust from all
parts of the world, for the period of 1960 to 1965. Some
of these will be mentioned in the following pages.

Since the work of Mintrop (1949), there have been
many reports of deep crustal reflections in Europe. In
these early reports, the criterion for an event to be con-
sidered a reflection, was that it had to have a high
apparent velocity. Many such records obtained from France

and Hungary during the 1950's exhibited such features.
However, many of these European records contain only poor
quality reflections. This is the case with Bath and
Tryggvason (1962), who report on the first seismic investi-
gations of deep crustal structure in Fennoscandia. Their
project was to investigate near vertical incidence reflec-
tions from crustal discontinuities. The sources of energy
were quarry blasts in iron ore mines, and the information
was recorded with refraction equipment. They obtained
depths to the Conrad and Mohorovicic discontinuities of 19
and 34 kilometers, but their reflections were erratic and
very weak. In Greece, Papazachos *et al.* (1966), reported
on the crustal structure near Athens. Through the analysis
of reflections obtained from near earthquakes, he produced
a three layered model for the Earth's crust. Again, though,
his results were not very well substantiated.

The application of the reflection technique for deep
crustal studies became popular in Germany when Dohr and
Schulz recorded their first profiles in 1954. In the eval-
uation of the data, Dohr applied statistical methods to
the deep reflections (Dohr and Fuchs, 1967). He found that
on many occasions late reflections were observable, but
that it was impossible to correlate them over more than 400
meters. Using several hundred seismograms, histograms of
the number of deep reflections, in time intervals of 0.1
to 0.2 seconds, for particular regions of about 100 to 300
square kilometers were plotted against arrival time. Some

of these histograms exhibited one or more peaks which
Dohr interpreted as reflected events from intracrustal
discontinuities and the Mohorovicic discontinuity.
Liebscher (James and Steinhart, 1966) later applied these
statistical techniques to a number of areas in southern
Germany. The histograms constructed for these areas also
exhibited many peaks. Liebscher applied a chi-square test
to the peaks, and found them significant at the 99 percent
level. The statistical results of these tests suggest
that he has indeed recorded primary reflections from
within the Earth.

Dohr and Fuchs (1967) also discuss the statistical
nature of deep seismic reflections as performed on the
several thousands of seismograms collected up to
1965. By performing chi-square tests on many of the histo-
grams, the computed value of chi-square for the peaks was
found to be significant at the 95 percent level. This
indicates that the variations in the distributions are
larger than what would result from random variations. In
most cases, there were three main peaks observed. The width
of the peaks (0.5 to 1.3 seconds) was suggested to be the
result of the boundary between any two of the layers being
a transition zone, which Dohr and Fuchs estimated to be
1.5 to 4.0 kilometers in thickness. They also noted that,
in recording deep reflections, better results were
obtained when the recording arrays consisted of groups of
geophones with higher frequencies than the corresponding

refraction equipment.

To verify the conclusions drawn from the statistical method, a wide angle reflection survey was conducted in southern Germany in 1964, utilizing the common depth point technique. Meisnner (1966) reported on the initial results of this survey. Four different reflecting horizons, the basement, the Conrad discontinuity, a sub-Conrad discontinuity, and the Mohorovicic (Moho) discontinuity were noted, with the Moho being the strongest reflector. The travel time curves were not exactly hyperbolic, and he explained this as the result of the lack of sharp boundaries between the horizons, with a gradient zone $2.0 \pm .7$ kms. thick.

In 1968, seismic reflection measurements were taken along a 17 kilometer long profile in order to investigate the structure of the Ries Crater in southern Germany. The seismic signals were recorded digitally for up to 14 seconds, with the digitizing interval being 4 milliseconds. A total spread length of 1380 meters was used, and each subsurface point had 300 percent coverage. After stacking, frequency and optimum filtering, the main reflection zones were noted at 3 to 4 seconds, 6 to 7 seconds, and 9 to 10 seconds (Angenheister and Pohl, 1971). This last reflection corresponds to the Mohorovicic discontinuity.

Two six kilometer profiles were conducted in the Rhinegraben area by Dohr as part of the Upper Mantle Project in 1971 (Dohr and Meissner, 1975). Then, in 1973, a deep crustal project was performed across a large fault

zone separating the Rhenish Massif and the Saar-Nahe trough in southern Germany. A 21 kilometer reflection profile across the fault zone was recorded. Geophones were organized into a 36-unit arrangement, and a 300 percent subsurface coverage was obtained. Charges were up to 100 kilograms. The spread length was 2.4 kilometers, and 24 traces were recorded per shot. Many high frequency reflections from the sediments were recorded, along with reflections from the Conrad, a sub-Conrad, and the Mohorovicic discontinuities. The fault zone was observed down to the crust-mantle transition zone, separating two large blocks of variable dipping crustal layers (Bartelsen *et al.*, 1976).

Deep crustal studies using reflected waves in the Soviet Union were first proposed by G.A. Gamburtsev in 1939 (Zverev, 1967). From 1948 to 1950, he directed the first experiments for the recording of reflected waves from horizons within the lower crust. In 1956, the deep seismic sounding method was adopted for large scale seismic projects. By 1961, more than 5000 kilometers on land and 11,000 kilometers on sea of seismic reflection profiles, had been recorded.

From the period of 1962 to 1965, many Soviet geophysicists studied the crust beneath the Black and Caspian Seas (James and Steinhart, 1966). They noted that both seas did not have the granitic layer (P-wave velocity of 6.0 kilometers per second) beneath them, whereas the

surrounding regions did. The crust beneath the Black Sea appeared to be basaltic and at most 20 kilometers in thickness. Beneath the Caspian Sea, the crust was found to be more acidic.

Sollogub (1973) presents the results of deep seismic sounding in central and southeastern Europe. The study is based on approximately 13,000 kilometers of reflection seismic profiles. Crustal thicknesses were found to vary from 20 to 65 kilometers. He suggests that the crust is a heterogeneous body whose numerous local discontinuities comprise the thick transition zones between the main layers, in particular, between the crust and the mantle.

For North America, only isolated instances of deep crustal reflections have been recorded for the period up to 1961. Narans *et al.* (1961) performed seismic surveys in Utah in an effort to obtain normal incidence reflections from within the lower crust. In order to distinguish between random noise and possible reflections, the seismograms were analyzed statistically as in Germany. They obtained peaks in their histograms corresponding to discontinuities at 8.5 and 26.3 kilometers. However, their results were based on only ten records.

Dix (1965) applied standard reflection prospecting methods to the study of deep crustal structure in the Mojave Desert. To eliminate the problems of multiple reflections from sedimentary layers, he recorded in an area of thin sedimentary cover. From the 22 records, he

found strong events that had arrival times consistent with that of the Mohorovicic discontinuity.

The first deep reflection study at the University of Alberta was a near vertical incidence reflection investigation in southern Alberta (Kanasewich and Cumming, 1965). A tapered array consisting of 12 evenly spaced geophones over 134 meters, with an additional 4 geophones at the central location, was used. The distance between geophone units was 293 meters. This type of array, along with multiple holes, was found to be an effective filter for attenuating long period surface waves. From a T^2 versus X^2 analysis, the average velocity to a strong reflector at 11.4 seconds was found to be 6.37 kilometers per second. The depth calculated to this reflector, now known as the Riel discontinuity, was 34 kilometers.

Seismic reflections were investigated along 4 profiles comprising some 90 kilometers in southern Alberta (Clowes *et al.*, 1968). The data was recorded on FM analog magnetic tape, and the results were later digitized. Through power spectra calculations, the energy of the reflected wavelets was found to be in the 5 to 15 hertz band. Along one profile, the Riel discontinuity was located at 11.6 seconds, and correlated over 25 kilometers. A T^2 versus X^2 analysis yielded an average velocity of 6.2 kilometers per second to a depth of 34 kilometers.

Seismograms obtained from the studies in southern Alberta were later investigated to determine the attenuation

properties of the crust, and the characteristics of the reflecting layers (Clowes and Kanasewich, 1970). The study made use of synthetic seismograms with depth and frequency dependent attenuations. The data was inverted by comparing the autopower spectra of particular time intervals on the field records with the spectra computed from the synthetic seismograms. A transition zone model comprised of alternating high and low velocity sills satisfied the recorded observations.

During the summer of 1969, two linear arrays were operated through a joint project conducted by Princeton and the University of Alberta (Perkins and Phinney, 1971). These arrays were located near Riverton, Wyoming. The shot and geophone patterns were as described by Kanasewich and Cumming (1965). Charge weights were between 9 and 13 kilograms, and were detonated at 30 meter depths. Data was collected on FM magnetic tape recorders as well as on a galvanometer camera. Following recording, the data was digitized so that signal enhancement techniques could be applied. From the results, good reflections were noted at 11 and 35 kilometers.

A near vertical incidence reflection survey was conducted in north-central British Columbia (Mair and Lyons, 1976). The five shot points were separated by 1.5 kilometers, and the 42 recording sites were spaced at 250 meters. They also used the 16 geophone tapered array of Kanasewich and Cumming (1965), and recorded a subsurface

coverage of 500 percent. Two 7 channel FM tape recorders were used to record the data, which was later digitized with a sampling interval of 10 milliseconds. Coherent energy was seen to exist at 8 and 11 seconds. The event at 11 seconds is continuous over much of the profile, and is believed to be from the Mohorovicic discontinuity. All attempts to enhance the signal from the Moho by the common depth point (C.D.P.) stack met with failure, and they suggest that this is the result of the crust-mantle transition zone being a many layered complex of high and low velocity beds, with a total thickness of only a few kilometers.

In 1973, an additional 40 kilometers of reflection records were obtained in southern Alberta to complement those already gathered by the University of Alberta (Cumming and Chandra, 1975). The investigations have used power spectra analysis and predictive deconvolution of the primary discontinuities within the crust to increase our knowledge of their nature.

Several reflection profiles were shot just north of Edmonton, and the results from the study indicate dips within the lower crust of 15 to 20 degrees southeast (Ganley and Cumming, 1974). Reflections were observed at 20, 32 (Riel discontinuity) and 35.5 (Mohorovicic discontinuity) kilometers.

A near vertical incidence reflection profile was carried out over three lines in Hardeman County, Texas (Oliver et al., 1976). The profile, containing 368 kilo-

meters of subsurface coverage, was recorded by the Vibro-
seis technique utilizing large vibrators and low frequency
waves. Deep reflections were not continuous over more
than a few kilometers. Within the crust, zones of low
reflector density were thought to be the result of plutons,
and curvature of the reflections to indicate deep folded
structures. The Mohorovicic discontinuity was located at
14 to 15.4 seconds.

Smithson and Brown (1977) propose a model for the
lower crust based on geological, geochemical and geophysi-
cal information. Their geophysical data comes from both
refraction and reflection studies. Discussion of the field
procedures and the initial results of the refraction study
are reported by Smithson and Shire (1975). Smithson
and Brown suggest that the lower crust is a heterogeneous
body, with lateral heterogeneity being shown by the seismic
wave anomalies across the arrays. The number of reflectors
in the lower crust, and the presence of composite reflec-
tions, are best interpreted as layering found in metamor-
phic rocks. They suggest that the lower crust consists of
granite and syenite gneiss, as well as amphibolite, which
are interlayered and intruded by gabbro. The characteris-
tic discontinuity of deep reflections are thus the result
of disruptions of the layers, tight folding, changes in
dip and layer thickness, and intrusions.

1.3. The Reflection Method

The seismic reflection technique was developed for detailing the structure of the Earth by measuring the times necessary for a seismic pulse to travel from a source to a reflector, and back to the surface again. In seismic operations, a signal is induced into the Earth either by the detonation of a charge in a shot hole, or by some mechanical means such as Vibroseis or Dinoseis (Dobrin, 1976) (figure 1.2). Upon encountering various discontinuities in the Earth, some of the propagating energy is reflected back to the Earth's surface. The quantity of energy that is reflected depends primarily on the velocity and density distribution found in the Earth. This reflected energy is collected along arrays of geo-phone groups, each group consisting of several geophones. From the geophones, the reflected signals are time multi-plexed, amplified, converted to digital form, and written onto magnetic tape (Mercado, 1973).

Through the use of digital computers, the reflected signals are brought into proper time alignment, so as to simulate normal incidence seismic reflection profiling. This data is then passed through various filters to enhance the signal relative to the noise. The subject of this thesis is first to discuss those techniques used to bring reflected events into proper time alignment, and then to investigate which methods best enhance the signal with respect to the noise.
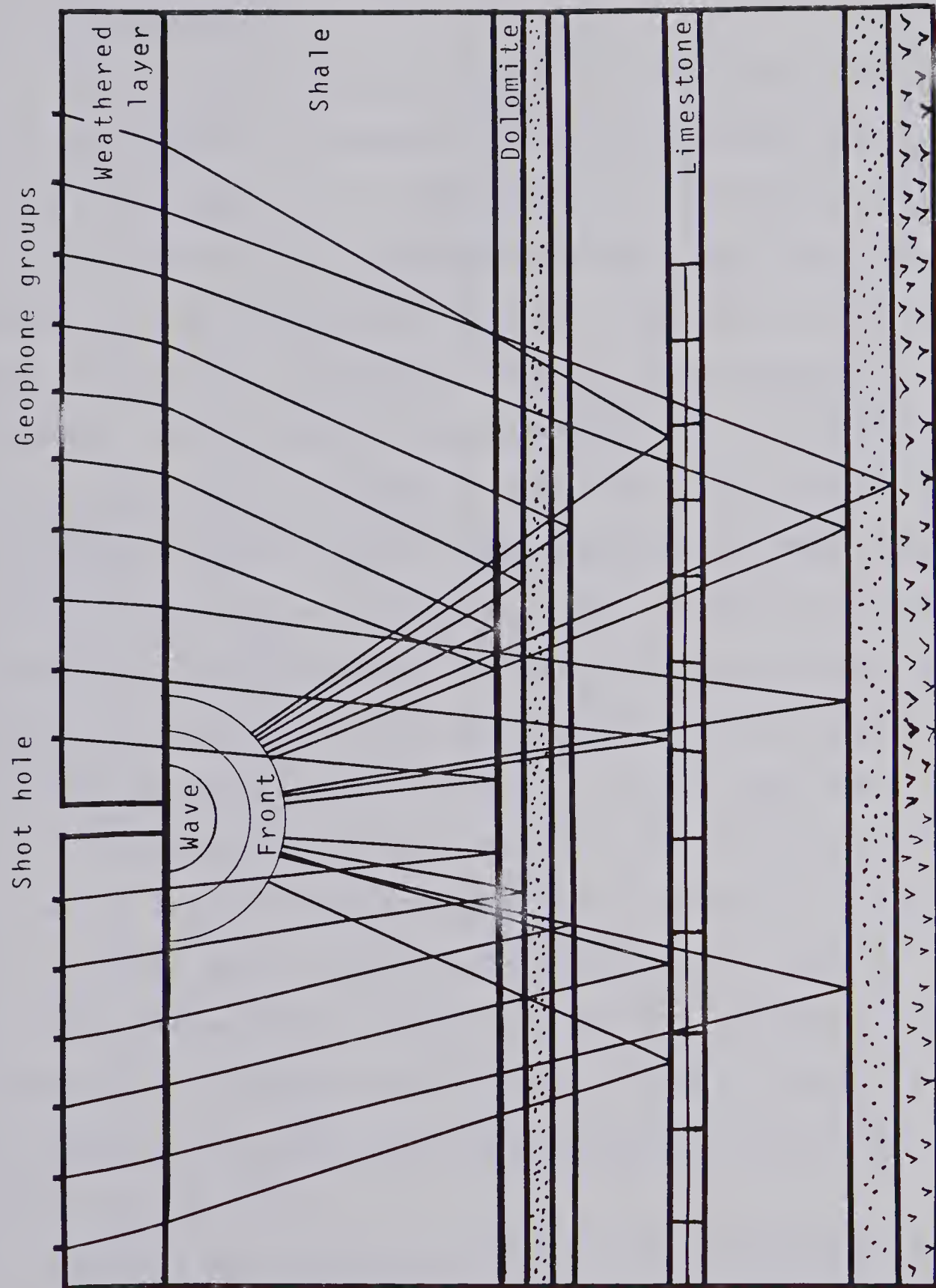
Figure 1.2: The reflection technique.

CHAPTER 2
THE CRUSTAL STUDY

2.1. Introduction

The transition zone between the Churchill (figure
2.1) and Superior structural provinces separates rocks
which differ not only in age, but in lithology and struc-
tural trends as well. In northeast Manitoba, structural
trends of the Superior Province are expressed in the east-
west orientations of metavolcanic and metasedimentary belts
(Goodwin, 1972). These supracrustal rocks are Archean in
age (K-Ar radiometric ages of about 2500 million years),
and lie in synformal bands which separate the much more
extensive granites and gneisses. The volcanic rich belts
(greenstone belts) consist of varied volcanic assemblages
with minor amounts of sediments, and have been extensively
intruded by granodioritic plutons. As one moves away from
the bounding granitic batholiths, the metamorphic grade
decreases from amphibolite facies to greenschist facies.
On the other hand, the metasedimentary belts contain
assorted metasediments along with schist, migmatite, and
paragneiss. The metamorphic grade is fairly uniform at
the amphibolite grade, but greenschist and granulite
facies may be found.

Within the Manitoba portion of the Superior province,
strong east-west magnetic and gravitational trends exist.
Positive Bouguer anomalies occur over the supracrustal
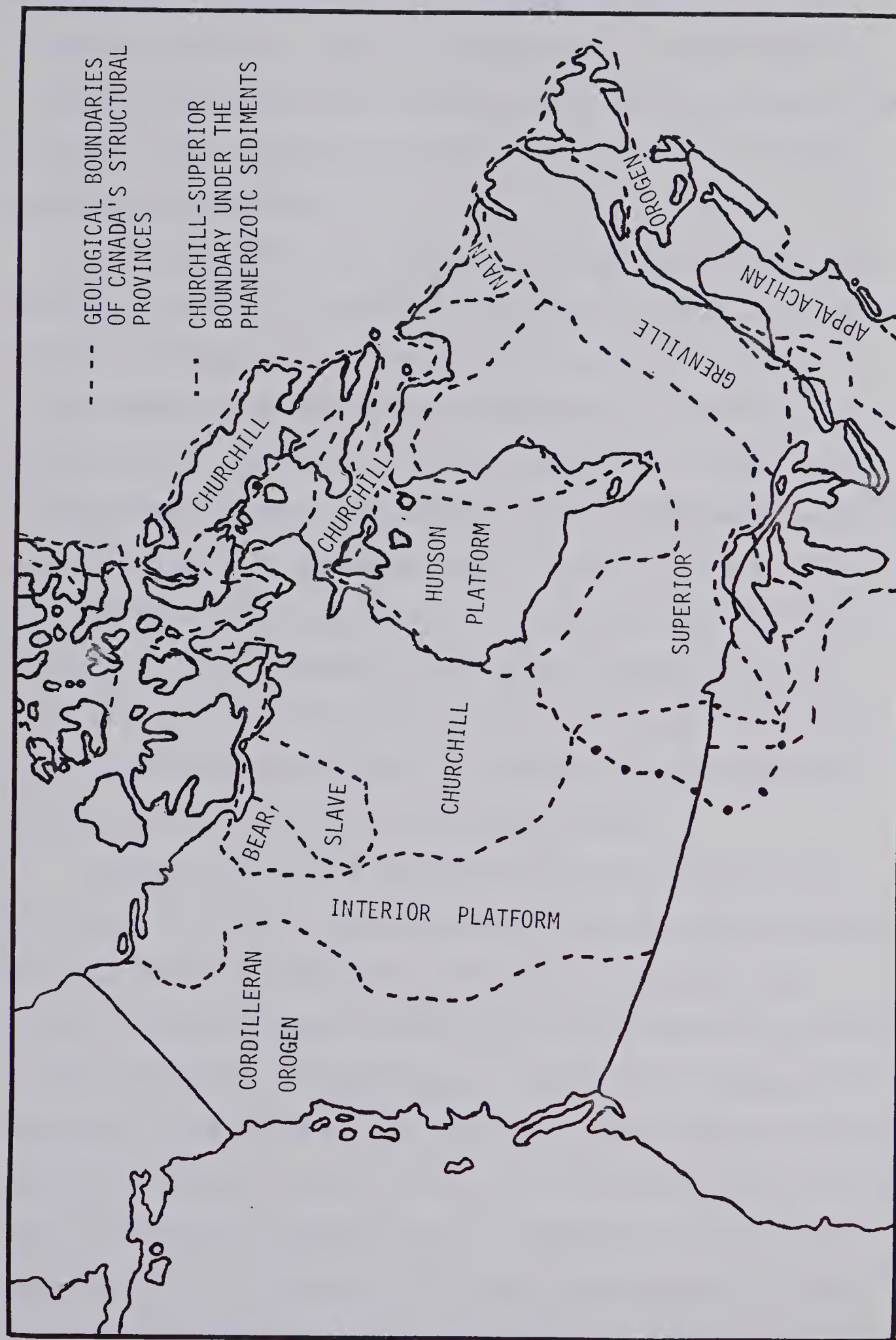
Figure 2.1: The structural provinces of Canada.

belts and granulite rocks, with negative anomalies over-
lying the granitic rocks. The stronger, linear magnetic
anomalies coincide with the greenstone belts and granulites,
with the low intensity areas corresponding to the para-
gneisses and granites.

The Churchill province in northern Saskatchewan is
underlain mainly by granitic and gneissic rocks. Curved
belts of metamorphosed and deformed lower Proterozoic
(K-Ar radiometric ages around 1800 million years) supra-
crustal rocks are found. These supracrustal rocks are
mainly metasediments, migmatites and slightly metamorphosed
volcanic rocks. The predominant structural trend in the
western half of the province is northeast, but it slowly
changes to the southeast as one moves towards the east.
Both the magnetic and gravity anomalies found within the
Saskatchewan portion of the Churchill province are highly
erratic, and do not show any strong trends.

Both geological and geophysical information have
been used to define, and investigate the boundary between
the Churchill and Superior structural provinces (Lee,
1977). Early attempts at defining the boundary are found
in Bell (1971a). Burwash *et al*. (1962) first proposed the
boundary to be a transition zone, which was later affirmed
by Bell (1971b). In his paper, Bell defined the transition
zone in northern Manitoba as the Pikwitonei subprovince.
However, Rb-Sr radiometric dating (Cranstone and Turek,
1976) in the boundary zone, along with evidence of

Pikwitonei rocks being traced into the Wabowden subprovince (Green *et al.*, 1977), suggest that this is insufficient. Thus, the Wabowden subprovince is now included in the boundary zone. In this boundary zone, rocks of the Pikwitonei subprovince are Archean in age (Cranstone and Turek, 1976), while in the Wabowden subprovince, ages are typically lower Proterozoic. Rocks of the Pikwitonei subprovince are predominantly granulite gneisses and charnockites (contain amounts of hypersthene) (Bell, 1971b). Migmatitic gneisses predominate in the Wabowden subprovince. The western edge of this subprovince comprises the Thompson Nickel Belt (Lee, 1977).

In the north, the boundary between the Wabowden and Pikwitonei subprovinces is a major fault zone (Assean Lake fault zone), as described by Bell (1971b). Cranstone and Turek (1976) suggest that the boundary zone is a meta-morphic transition zone under the Phanerozoic sediments.

Three lines of evidence indicate the extension of the Churchill-Superior boundary zone under the Phanerozoic sediments of the Interior Plains. Geochronological data from core samples show that both the Churchill and Superior provinces extend into southern Manitoba, Saskatchewan (Burwash *et al.*, 1962; Goldich *et al.*, 1966), and into North Dakota.

The Bouguer gravity map of eastern Saskatchewan and western Manitoba (figure 2.2) shows that the Nelson River
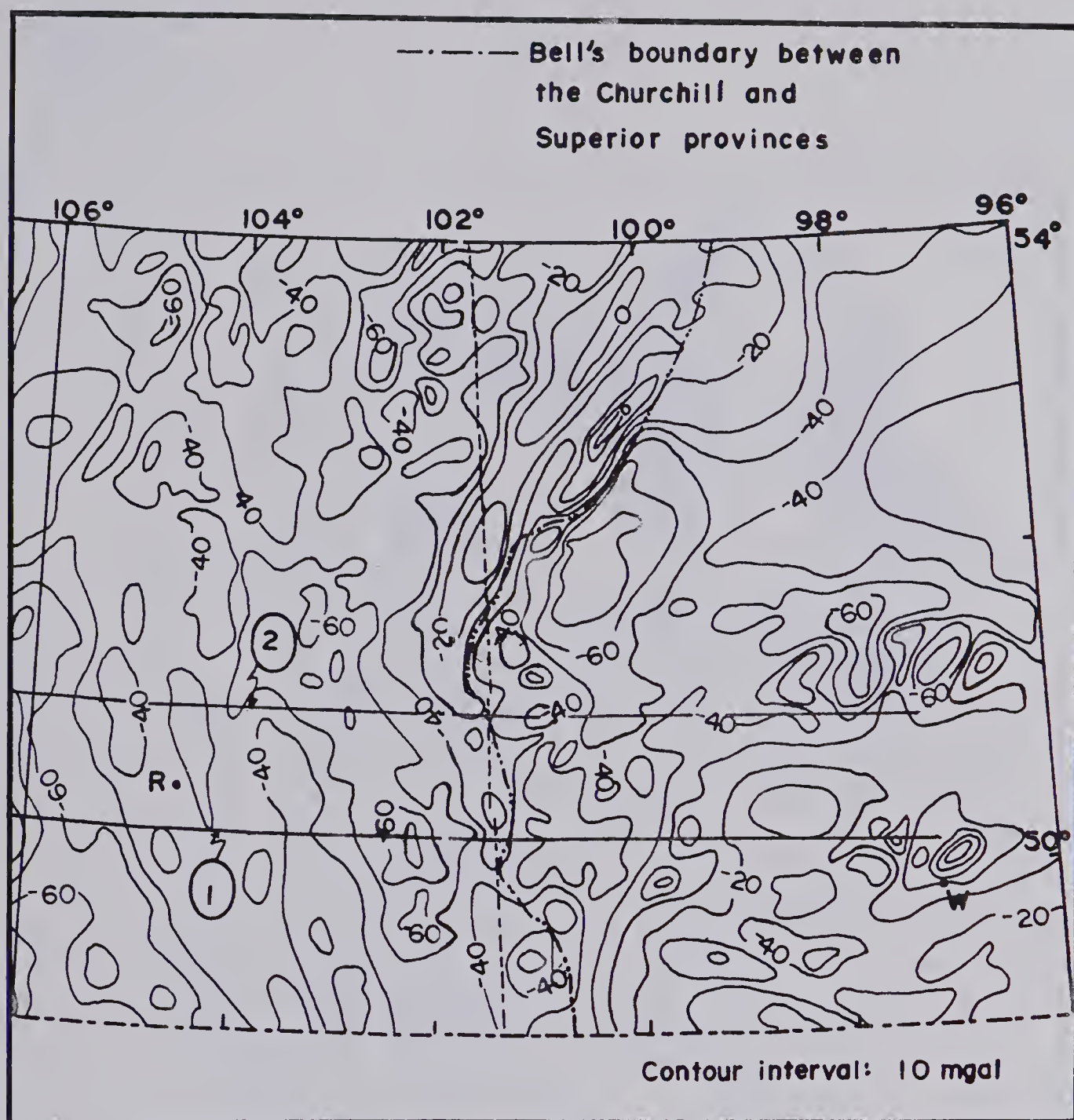
Figure 2.2: Gravity map of southern Saskatchewan and southern
Manitoba with R=Regina and W=Winnipeg (after Lee,1977).
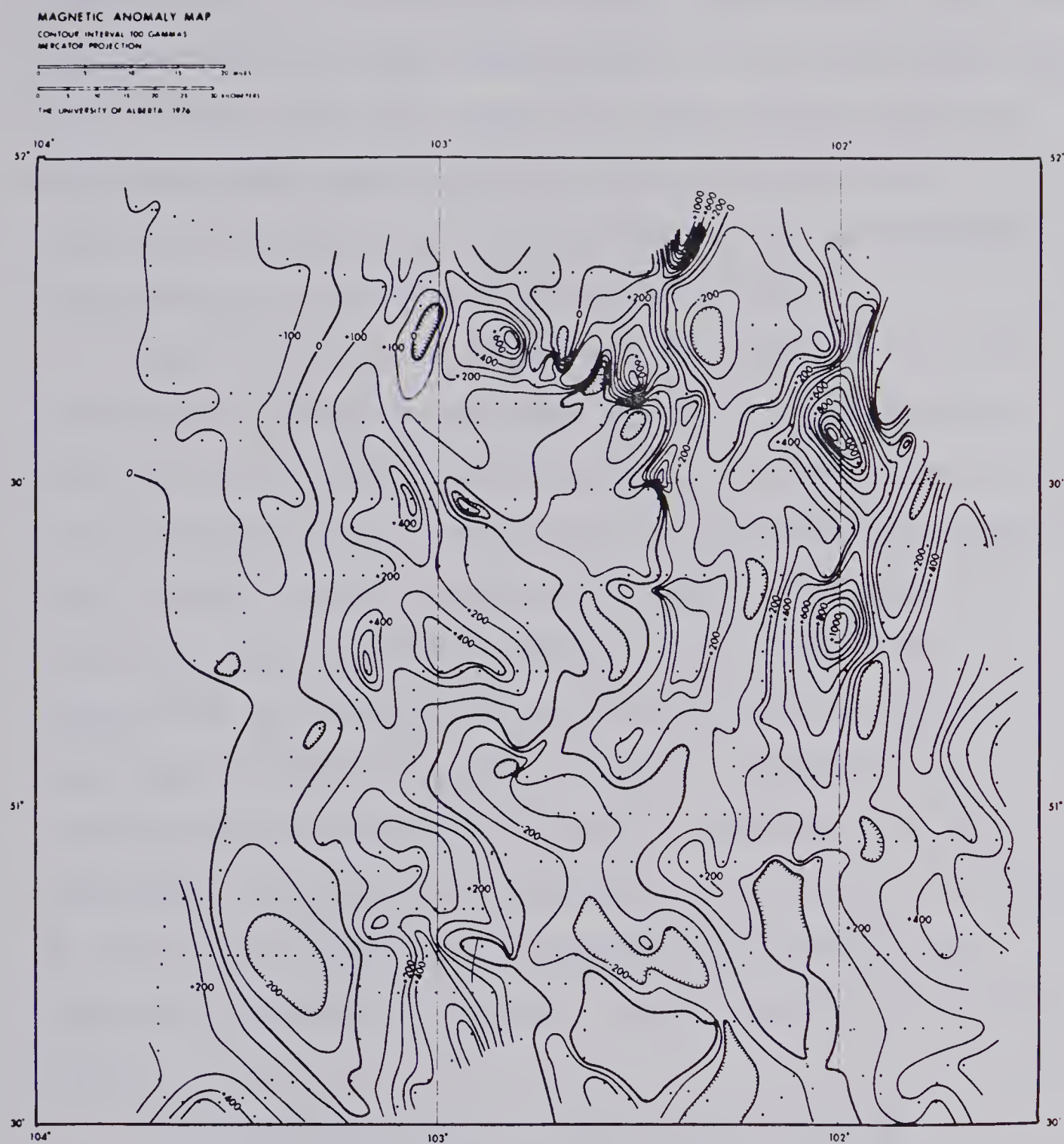
Figure 2.3: Magnetic map of southern Saskatchewan (after Lee,1977)

gravity high can be followed through the northern parts of Manitoba into southeast Saskatchewan. In northern Manitoba, Gibb (1968a, 1968b) has shown that this gravity high is associated with the high density granulites of the Pikwitonei subprovince. On the other hand, the Wabowden subprovince is associated with a gravity low.

The boundary zone in northern Manitoba is also well expressed in aeromagnetic maps (figure 2.3). Granulite gneisses of the Pikwitonei subprovince are expressed in a configuration of oval shaped high and low magnetic anomalies (Bell, 1971b; Kornik and Maclaren, 1966). In comparison with this, the migmatitic gneisses of the Wabowden subprovince are exemplified by high density, elongated anomalies, which trend to the northeast. Green *et al.* (1977) indicate that these elongated anomalies may be recognized in southeast Saskatchewan and southwest Manitoba. On this basis, Green has delineated the boundary zone under the Phanerozoic sediments to the Canada-United States border.

The overall picture of the Churchill-Superior transition zone as suggested by geophysical and geological data is that this zone may be an ancient Precambrian suture zone (Dewey and Burke, 1973). This boundary zone is associated with two important geological deposits (Green *et al.*, 1977). In northern Manitoba, nickel is mined from the Thompson Nickel Belt, one of the

world's largest nickel deposits. In the southern regions
of Saskatchewan and Manitoba, the Phanerozoic sediments over-
lying the transition zone have entrapped large quantities of
oil and gas. Though much of the cratonic movement between
the Churchill and Superior provinces would have ceased by
the Phanerozoic, these traps may be the result of slight
readjustments between the two plates, due to persisting
stresses, resulting in deformation of the overlying sediments.
Thus, locating these oil reserves, and perhaps other nickel
deposits, would be far easier if the geological evolution of
the rocks within the boundary zone were known. Therefore,
it was decided that a detailed geophysical study of the
Churchill-Superior boundary zone, including seismic, gravity
and magnetic studies, would be undertaken to increase our
knowledge of this boundary zone.

2.2. The Project

During 1975 and 1976, at the suggestion of Dr. E.R.
Kanasewich, a loose association of seismologists from the
universities of British Columbia, Alberta, Manitoba,
Toronto and Western Ontario and the Earth Physics Branch
of the Department of Energy, Mines and Resouces met
several times to form a Canadian Crustal Studies Group
(CCSG). In July 1977, the CCSG performed its first seismic
reflection survey in southern Saskatchewan and Manitoba
under the direction of Dr. A.G. Green. The project con-
sisted of a wide angle reflection/refraction profile,
along with a near vertical incident reflection survey.

The main purpose of this survey was to increase our know-
ledge of the transition zone between the Churchill and
Superior structural provinces.

A number of factors influenced the decision to have
the survey in southern Manitoba as opposed to its northern
regions, where the boundary zone is visible. First, there
was evidence for both deep and shallow reflecting layers
in the crust, with good control on depths and nature of
the shallow layers from oil company drill holes. The topo-
graphy was extremely flat, with a highly unconsolidated
surface layer which allowed for easy drilling of shot holes.
Also, there was a complete network of roads available which
yielded easy access for drilling, shooting and recording.

The combined survey consisted of a 245 kilometer
north-south and a 242 kilometer east-west refraction sur-
vey, and a 84.54 kilometer east-west near vertical incident
reflection survey (figure 2.4). The reflection survey was
conducted over three lines which were 44.17, 19.31 and
21.06 kilometers in length (figure 2.5), with an average
subsurface coverage of 400 percent (figure 2.6). Alto-
gether, there were 58 shots detonated at an average depth
of 18 meters in holes that were 15 centimeters in diameter.
The explosive used consisted of 60 percent geogel in 46 by
13 centimeter sticks. For the spread, there were a total
of 47 takeouts. With a takeout distance of 292.55 meters,
this yielded a spread length of 12.87 kilometers (figure
2.7). Each trace was recorded with a linear array of nine
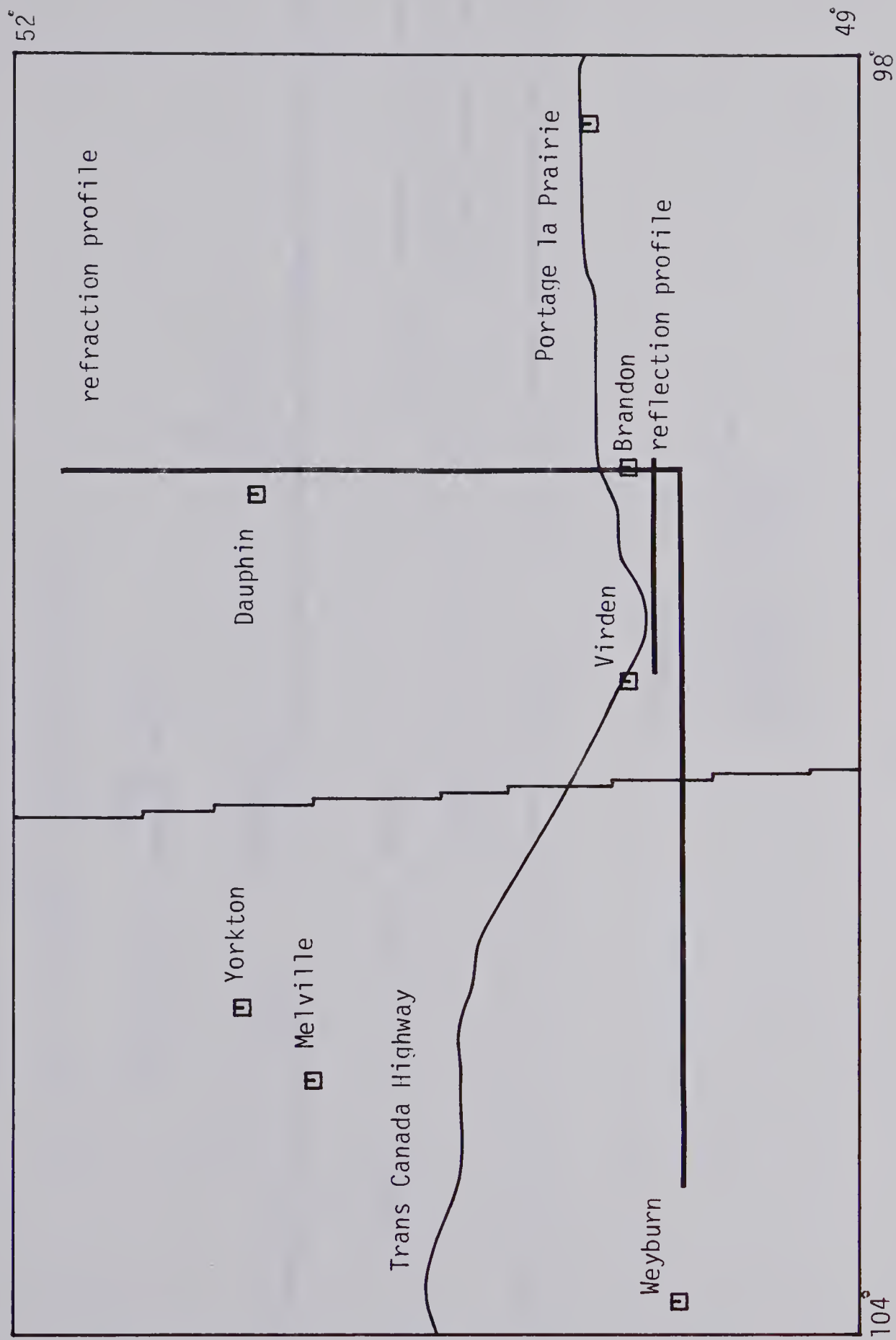
Figure 2.4: Map of the project.
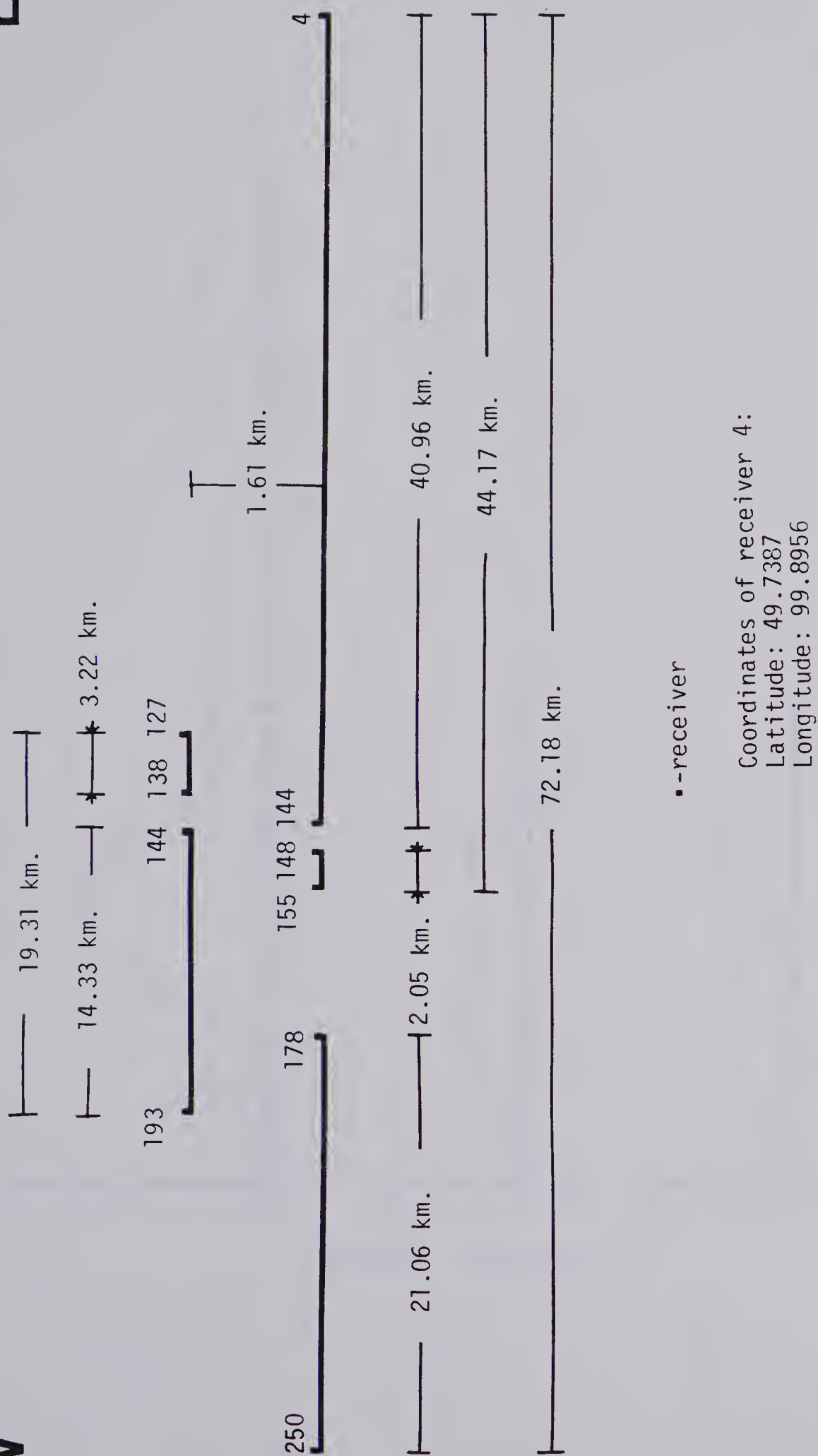
Figure 2.5: The reflection survey.
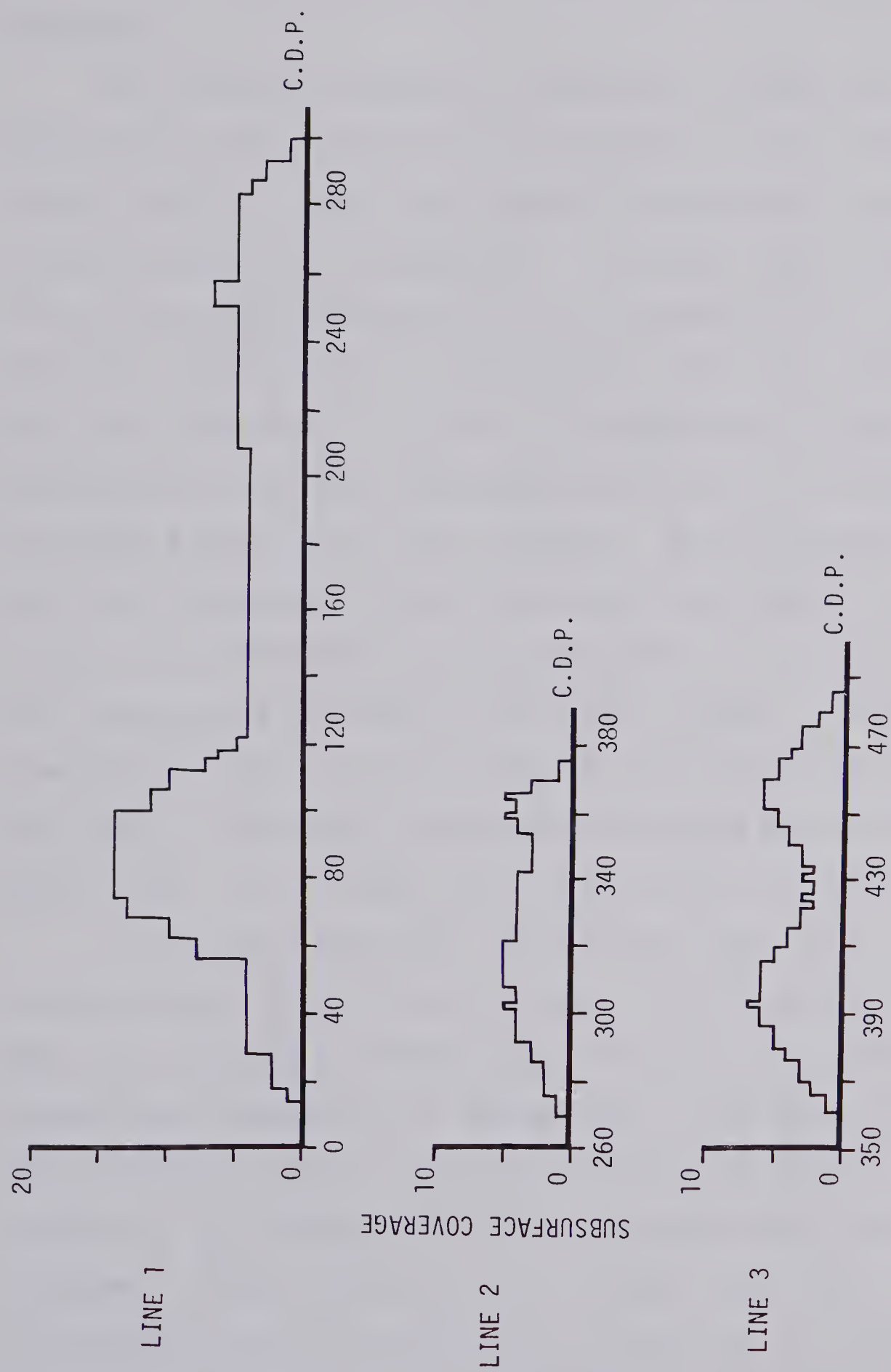
Figure 2.6: Histograms of subsurface coverage.

L-15A, 600 ohm-10 hertz geophones on a 73 meter A30 DDC
stringer. At the shot hole, an uphole geophone was also
recorded.

The shooting sequence is depicted in figure 2.8. In
most cases, the shot holes were located at every fifth or
sixth receiver. After four shots, the complete spread was
moved westward 6.44 kilometers. For every shot the detona-
tion circuit was connected to the recording cable of the
Manitoba system, and to a chronometer unit that detonated
the shot (Green *et al.*, 1977). The WWVB radio signal was
synchronized with the chronometer unit so as to provide
accurate timing of the shot instant. The chronometer unit
was also connected to the time break cables which recorded
a tone break when the shot was detonated. This tone break
was transmitted by radio to the other systems. The shot
instant was taken to be the time of the tone break, with
the delay in detonation from the 0.0 second mark on the
WWVB signal and the tone break being about 42 milliseconds.

In recording the data, three trucks were used,
corresponding to the three systems. The University of
Manitoba employed a DS1590 automatic gain varying digital
system, and recorded at a sample rate of one millisecond.
They recorded traces 11 through 34 along the spread. The
University of Saskatchewan had a programmed gain analog
recorder. Traces 34 to 45 were recorded with their system.
A fixed gain digital system which sampled at 5.6 milli-
seconds was employed by the University of Alberta. This
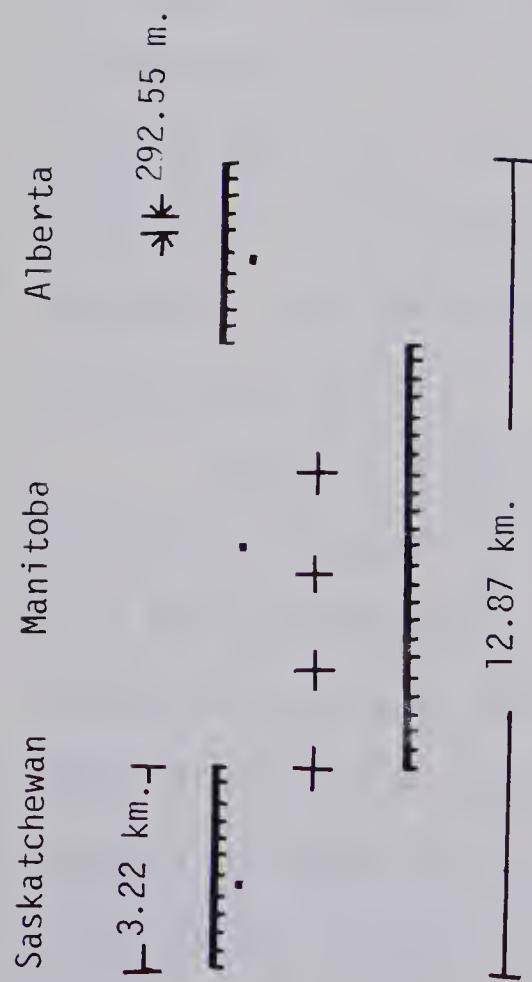
Figure 2.7: The spread picture (modified from Green *et al.*, 1977).
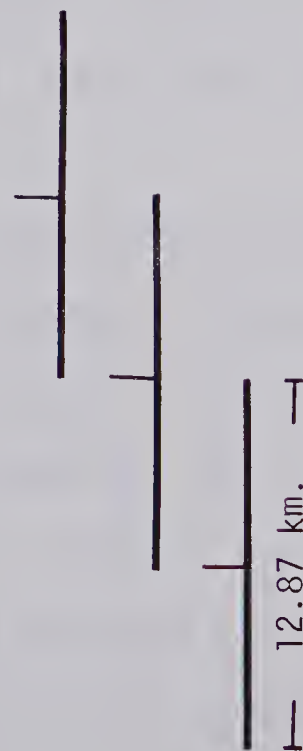
A shot is detonated every fifth geophone group location. After four shots, the entire spread is moved 6.44 km. to the west.

Figure 2.8: The shooting sequence (modified from Green *et al.*, 1977).

system was responsible for recording traces 1 to 11. Trace 1 was recorded at the most easterly receiver, and the two overlapping traces allowed a tie between the three systems.

Since much preliminary work had to be done on the data before it could be put into a form suitable for analysis, it is worthwhile, at this time, to discuss our system, and its mode of data collection.

2.3. The Digital Recording System

The University of Alberta's recording system is a digital recording system. With the system, 14 channels of information may be digitally recorded onto an 800-bytes per inch, nine-track synchronous tape recorder. The tape velocity is 6.25 inches per second, yielding a 5000 bytes per second transfer rate. During the survey, channel 7 was used to record the WWVB radio signal, channel 14 to record the tone break, and channels 1 through 5 and 8 through 13 were used to record the seismic signals. These channels, excluding the dead channel 6, were also recorded photographically.

Figure 2.9 details the complete recording system. The tape recorder is a model 7830-9 write-only transport, and the multiplexer, A to D converter and 5 kilohertz crystal clock are contained within a modified model 120 Data Acquisition System (Allsop *et al.*, 1972). One to twenty channels may be recorded with a maximum of 4096 samples per channel. Several records may be sequentially
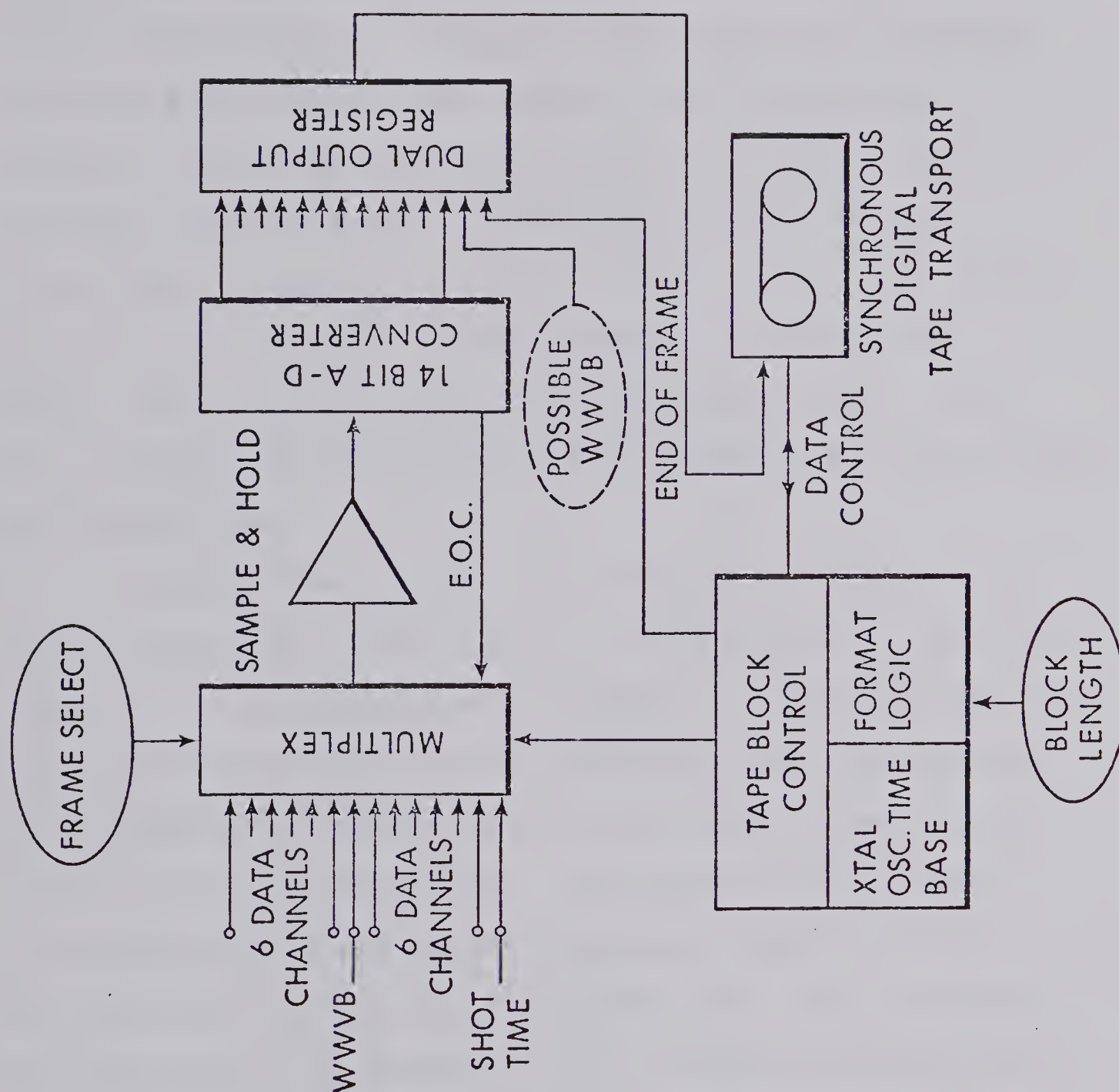
Figure 2.9: The digital recording system(after Allsop et al,1972).

written, with an interrecord gap of 0.096 seconds.

The signal is converted from analog to digital form by a 14 bit converter (13 bits plus sign) with a dynamic range of 84 decibels. Since two 8-bit bytes are required to store each sample, 2500 samples are recorded per second. During the survey we recorded 14 channels, and thus the sampling rate is 14/2500 (or 0.0056) seconds. This yields a Nyquist frequency of 89.3 hertz. The length of the record written was 4096 samples in integer *2 words, and thus we recorded 22.94 seconds of data. With the collection of 14 channels, that results in a block length of 114,688 bytes.

The amplifier circuit is presented in figure 2.10, and is discussed in some detail by Ganley (1973). Briefly, though, it may be described as follows. A fixed gain 40 db preamplifier is driven by an 18 db gain input transformer. This preamplifier feeds the main amplifier through a two-pole high-pass Bessel filter. The Bessel filter yields zero-phase shift, and may be bypassed. Output from the main amplifier (which has switchable gain, with increments of 10 db from 0 db through 60 db) is passed through a four-pole Bessel aliasing filter with a 50 hertz corner. The gain and phase response of the amplifier are discussed fairly completely by Dickins (1973).

Figure 2.11 exhibits one of the photographically recorded seismic sections. Again, channel 7 is the WWVB signal and channel 14 is the tone break. Due to the high

Figure 2.10: The amplifier circuit (after Allsop et al,1972)

gain setting necessary for recording deep reflections, the information in the early section is clipped. This same section, as output from the digital recording system, is seen in figure 2.12 (the WWVB radio signal, the dead channel 6, and the tone break are not shown). The separation of the individual channels in this display makes visual interpretation of the seismic section much simpler. Also, it is possible to compress the channels into a much smaller length as compared to the photographic record which, on the average, is about three meters in length.

Figure 2.11: Photographic record for shot 123.
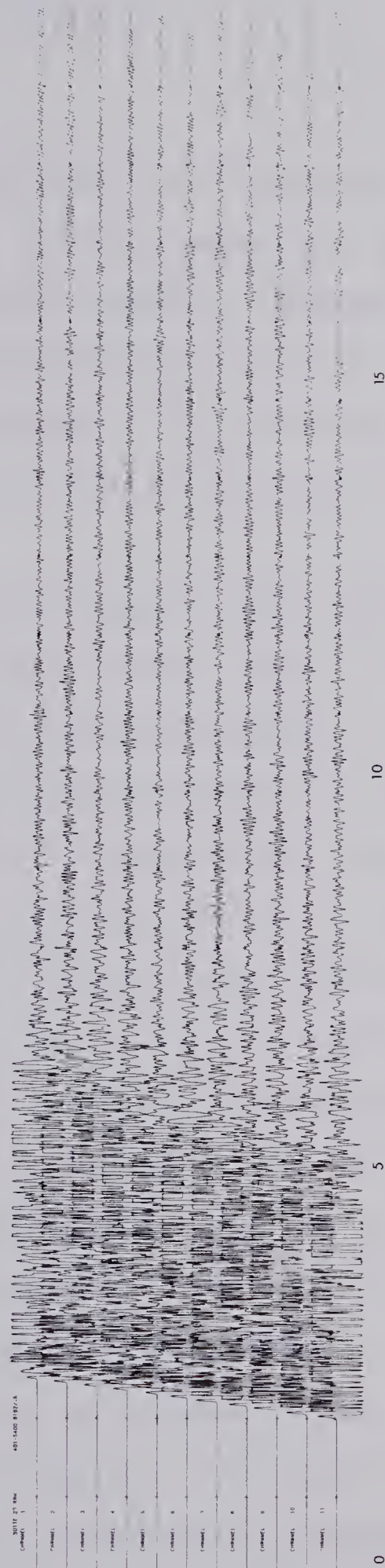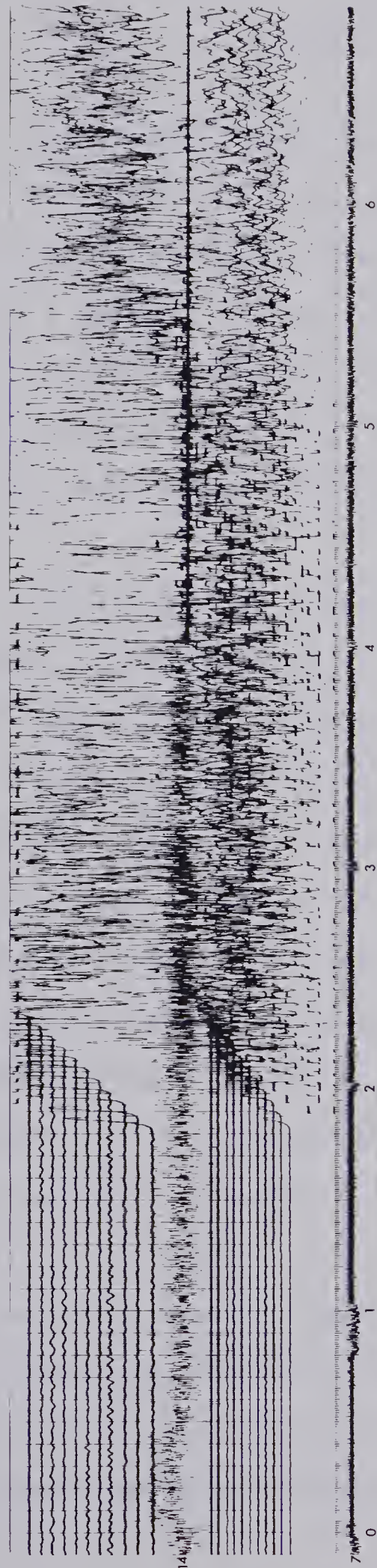
Figure 2.12: Digital output plot for shot 123(after redigitization).

CHAPTER 3
DIGITAL ANALYSIS

3.1. Preliminary Analysis

The reflection seismic profile was gathered on three different recording systems in the common depth point (C.D.P.) format. To be able to properly interpret the data, all of it must be contained on one tape, and in an order suitable for C.D.P. studies. Thus, our data had to be first made compatible with that of the other universities.

The first step in the treatment of the field recorded data was to demultiplex it, and write it onto a single tape. Each file of this first tape consisted of the fourteen channels, each containing 4096 samples, recorded for each shot. Next, the data was converted from integer *2 words to real *4 words, and then redigitized so that all of the universities' information had the same sampling interval. The sampling interval chosen was four milliseconds, yielding seismic traces with 250 samples per second. In the course of his research, D. Ganley has written a program that will resample a time series from one sampling interval to another. His algorithm makes use of the spline interpolation theory found in Pennington (1970). Basically, the program connects each pair of adjacent points with a section of a third degree polynomial, such that the first and second derivatives at each point are continuous.

Also, at each end, the second derivative is a linear extra-
polation of the value at (X(2),Y(2)) and (X(N-1),Y(N-1))
that is, the third derivative is continuous at these
points (N is the number of points in the original time
series; where X and Y are coordinates of points in the input
time series). The result of this redigitization may be
seen in figure 3.1. This illustration, in the upper half
(traces a and b), compares the input and output traces;
the output series now containing 5734 points. In the
clipped portions of the output trace (b), we notice that
small spikes have been generated on the edges of the
blocks. These peaks are very high frequency, and are
eliminated through frequency filtering (trace c of figure
3.1). Figure 3.2 shows the output power of the trace
before (a) and after (b) redigitization. The plots are
quite similar, except for a large peak at 118 hertz for
the redigitized trace. This is due to the small spikes
generated in the redigitization process. We should also
note, at this time, that the new Nyquist frequency is 125
hertz.

Following redigitization, it was necessary to locate
all sensors that were connected with reverse polarity in
the field. This required scanning the analog monitor
records of all the shots and picking out traces with first
motion opposite to the other traces on the record. Only
a few sensors were reversed. At this time, it was conven-
ient to make sure that all of the records had the same

Figure 3.1:   Comparison of a seismic trace before and
              after redigitization. Trace (a) is the
              original seismic channel. Trace (b) is the
              same channel after redigitization and the
              addition of 450 points of noise. It has
              also been divided through by four. This
              channel, after 8 to 40 hertz band-pass
              filtering, is seen as trace (c).

ORIGINAL 22:240-1311   SCALE   32768
CHANNEL   9

a

REDIGITIZED 22:451-   SCALE   819
CHANNEL   9

b

FILTERED 22:451-1950   SCALE   16384
CHANNEL   9

c

0.00   0.75   1.50   2.25   3.00   3.75   4.50   5.25   6.00

TIME IN SECONDS
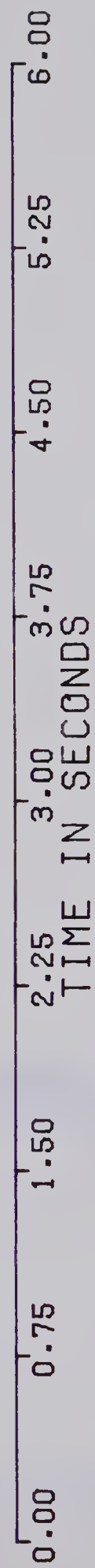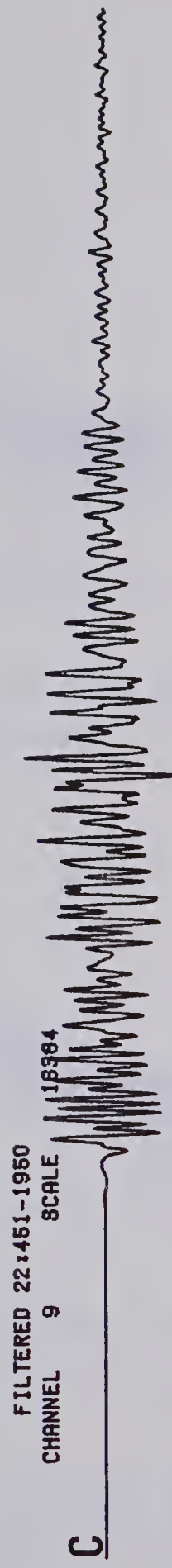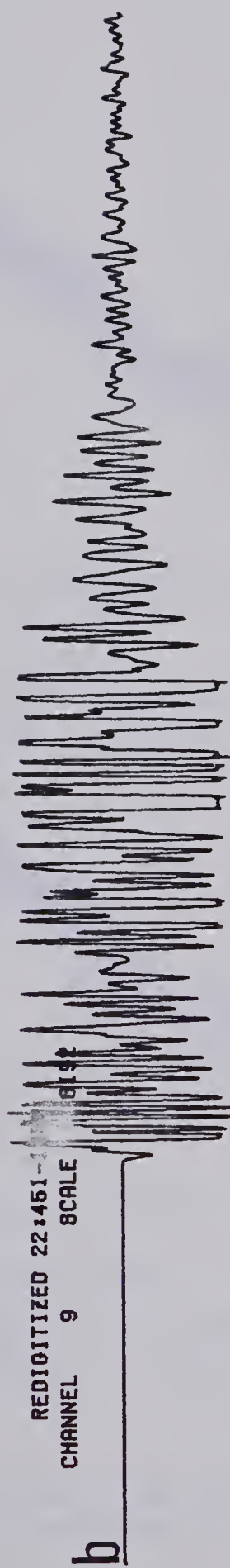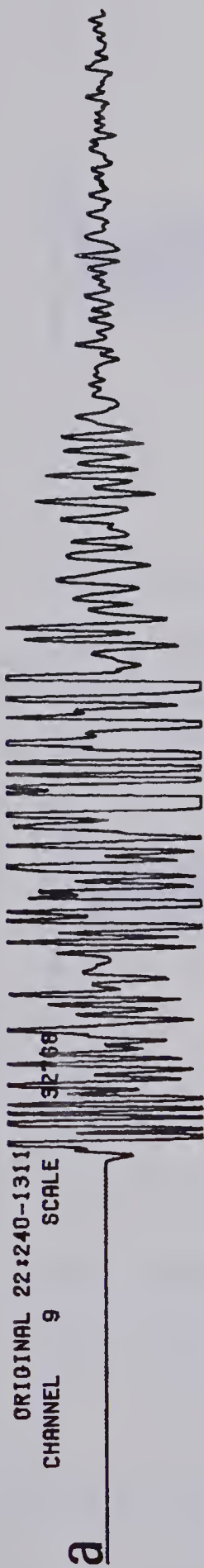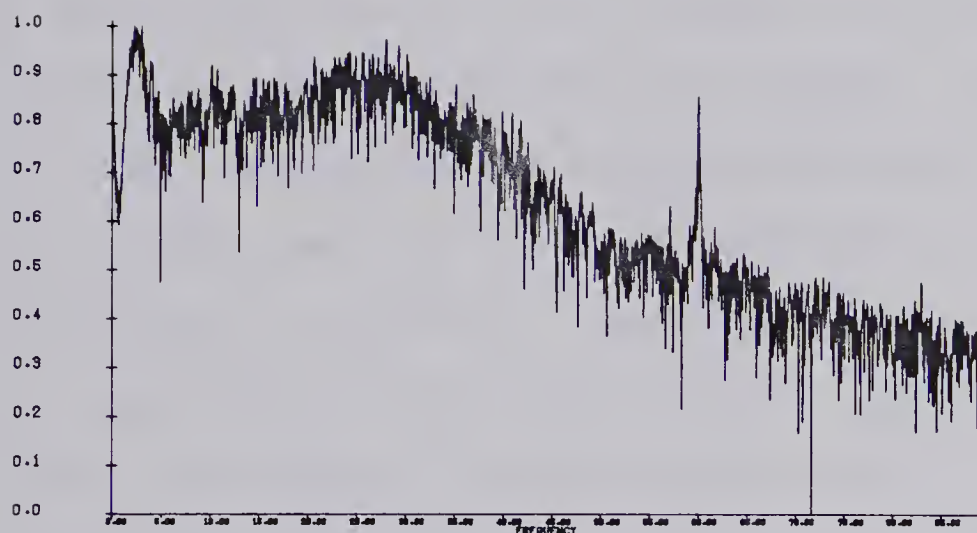
a POWER-OUTPUT:REC-22

AMPLITUDE MAX: 7.609E+00   MIN: -2.971E+00   MID VALUE: 2.319E+00

SCALE: 1.058E+00 UNITS/CM   NO. DATA POINTS: 2048
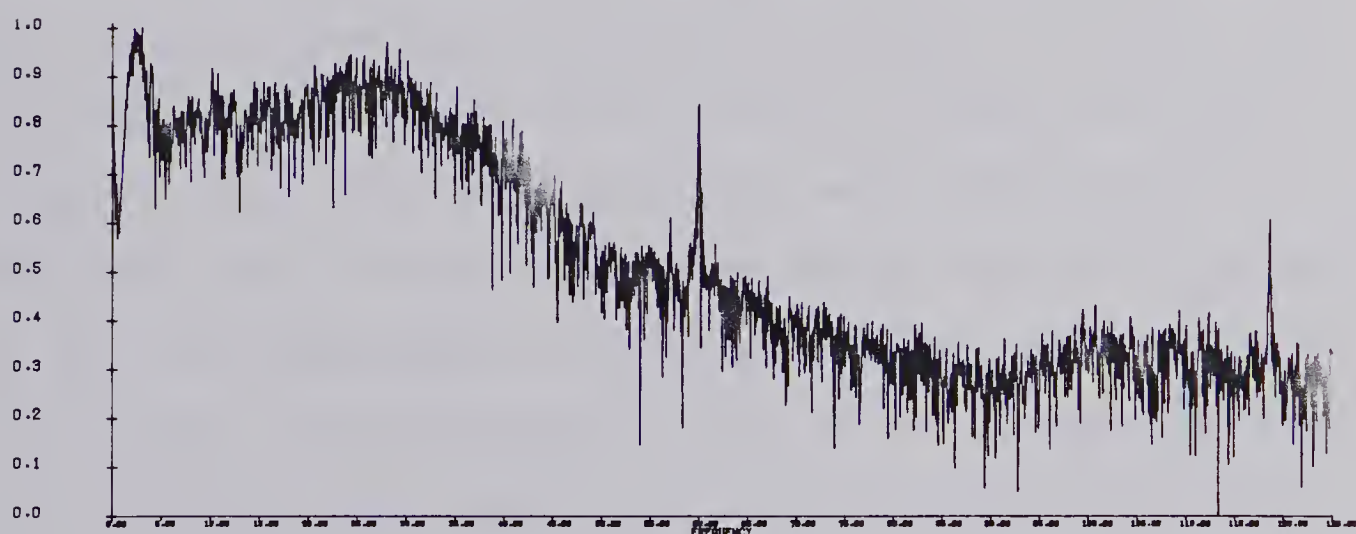
b POWER-OUTPUT:REC-22

AMPLITUDE MAX: 6.544E+00   MIN: -3.572E+00   MID VALUE: 1.486E+00

SCALE: 1.012E+00 UNITS/CM   NO. DATA POINTS: 2048

Figure 3.2: Comparison of the log of the power for the seismic channel of figure 3.1 before and after redigitization.

block length and that the shot instant was superimposed on all traces. It was decided that each trace would contain 450 points of noise before the shot instant and 5100 points of data, yielding a block containing 5550 samples. To accurately pick the shot instant for each trace, a relatively simple procedure was adopted. Each file of the tape, containing the fourteen channels for each shot, were plotted out and compared with the corresponding field photographic recording. Using the photographic record, the shot instant was picked exactly, knowing that the blaster introduced a 42 millisecond delay after the 0.0 time, which was shown on the WWVB radio signal immediately below. Then, knowing exactly when the shot instant occurred, times between various points along the traces and the shot tone were measured on the paper record. All of these time intervals were accurate to about one milli- second. These same time intervals were then measured on the plot, and in most cases, were within four milliseconds of the times measured on the paper record. However, in some cases, the tone break was not recorded digitally very well, and so it was necessary to use the times measured on the paper record to extrapolate the point corresponding to the shot instant on the plot. It was possible, in all cases, to pick the shot instant to an accuracy of one point.

The next step in the preparation of the tape was to filter the data. Since some of the cables were near

power lines (as evidenced by the peak in the power spectrum
at 60 hertz in figure 3.2), an upper cutoff frequency of
55 hertz was chosen. A lower cutoff frequency of 3 hertz
was also chosen. Digital filtering of the data will be
discussed in more detail in section 3.4, but basically
the data were passed through a zero-phase shift, eight-pole
recursive algorithm based on a Butterworth function with
attenuation outside the passband being 96 db per octave.
The data were also filtered with an 8 to 40 hertz filter.

Finally, we had to convert the data back into
integer *2 words. The final tape consisted of nine files;
three files containing the three lines of raw data, three
files with the 3 to 55 hertz filtered data, and three files
with the 8 to 40 hertz filtered data. The files contained
only the data channels for each shot, and each trace had
a label containing information on the shot and receiver
locations. Since each trace made up a block, the block
length was 11,000 + 100 (label) bytes. This tape was sent
to Manitoba where the data from all three of the universi-
ties was sorted according to subsurface coverage point,
and compiled onto one tape. This new tape contains three
files corresponding to the three lines, with the informa-
tion being stored in integer *2 words. The Manitoba and
Alberta traces have had a 3 to 55 hertz filter applied to
them, and the Saskatchewan traces have been subjected to
a 0 to 55 hertz filter. For the sake of safety, a copy
of this tape was made.

3.2.   Static Corrections

To process C.D.P. data properly, all of the traces
corresponding to a particular subsurface point must be
brought into proper time alignment. Timing corrections
are of two forms. Static corrections are based on spatial
variations of velocity and on the variations of elevation,
and dynamic corrections are time dependent due to varia-
tions in ray parameter, and will be discussed in section
3.5. Each static correction is the sum of an elevation
correction plus a near surface low velocity (weathered) cor-
rection (Telford *et al.*, 1976). Because of the anomalously
low velocity in this layer, any changes in layer thickness
will overly affect the travel times of the reflected waves,
and thus, it must be corrected for (Dobrin, 1976). The
elevation correction placed all shot points and receivers
at a common datum of 380 meters above sea level. By
measuring the time interval between the tone breaks and
the first breaks on the uphole geophones at all of the
shot points, the velocity of the seismic waves in the
weathered layer was determined to be 1.89 kilometers per
second. For those receiver locations that were not used
as shot points, the weathering corrections were interpol-
ated. These corrections were applied to the entire tape,
and in conjunction with this, the data was converted into
real *4 format.

My thesis is primarily concerned with investigating
the various techniques used to interpret seismic reflection

data, and so only small sections of the tape were worked
with at any one time. With the data being stored in
C.D.P. format, each subsurface point could comprise data
from one, two or all three of the universities. The
sections of data that I chose involved traces recorded by
both the universities of Alberta and Manitoba. Since each
university independently picked the shot instants for each
shot, they were probably picked differently. However, in
order to obtain proper time alignment between traces, the
shot instant must occur at the same time for each trace
corresponding to each subsurface point. This was easily
assured by comparing the two overlapping traces for each
shot (traces 11 and 12). A program was written which cross
correlates two seismic traces, and then plots them both
out. By visually comparing the two traces, and utilizing
the cross correlation coefficients, I was able to give
the traces recorded by the two universities the same shot
instant. An example of this procedure is shown in figures
3.3 and 3.4. The first figure exhibits the two overlapping
traces for shot 34A. The lower trace was recorded by the
Univerisity of Alberta, and was used as the standard trace
in the cross correlation program. Figure 3.4 is the cross
correlation curve showing that trace 11 is ahead of trace
12, that is, the Manitoba data is two lag points behind
the Alberta data for shot 34A. In all cases, I assumed
that I had picked the shot instances correctly, and thus,
Manitoba's traces were adjusted accordingly. Generally

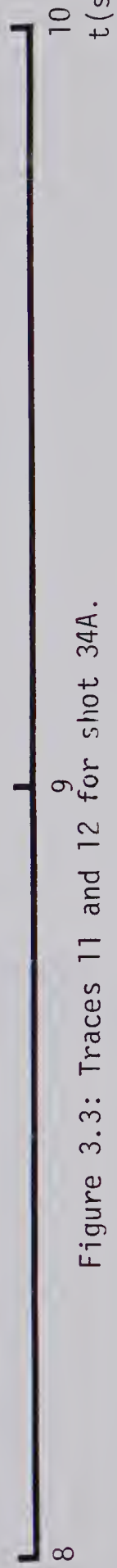BLOCK   220   SCALE   72

BLOCK   223   SCALE   51
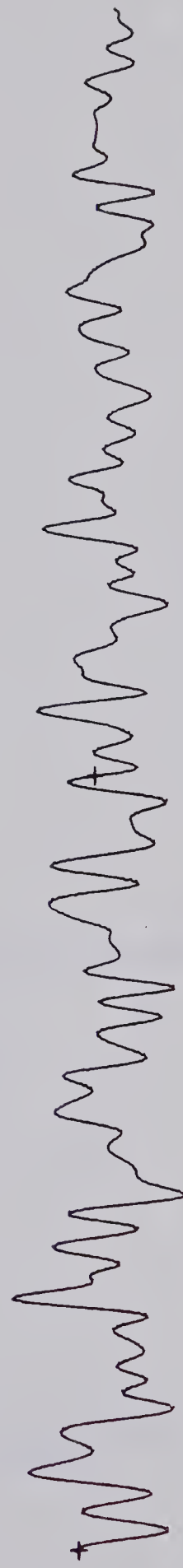
Figure 3.3: Traces 11 and 12 for shot 34A.

t(sec)
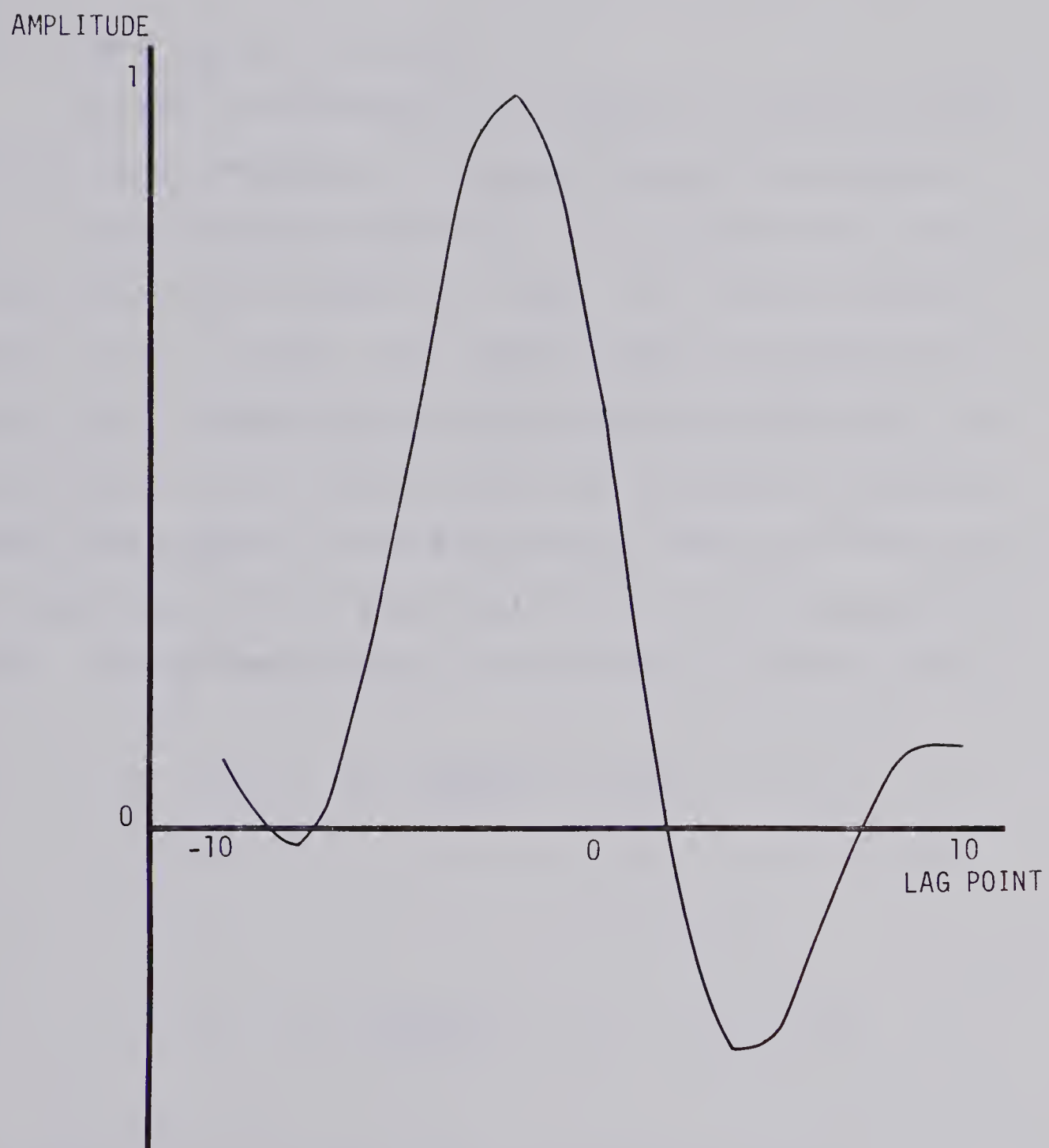
Figure 3.4: Cross correlation curve between traces 11 and 12 for shot 34A. Trace 11 is the reference channel.

though, the shot instances were picked within three points
of one another.

3.3.   Power Spectral Analysis

     In order to determine the frequency content of the
reflection seismograms, a computer program was written
which computed power spectrums. The program first selects
a particular time window of a trace to analyze, and then
stores it in a vector. To prevent power from being gener-
ated at all frequencies by the presence of sharp end dis-
continuities, the first and last ten percent of the data
points are tapered to the mean value, which is often zero.
The taper consists of a pair of cosine bells (Kanasewich,
1975). For N data points, the nth point is multiplied by

$$W_n = \frac{1}{2} \left(1 + \cos \frac{\pi(n+L)}{M}\right) \quad -(L+M) < n < -L$$

$$\text{3.3.1}$$

$$= 1 \qquad\qquad -L \leq n \leq L$$

$$= \left(1 + \cos \frac{\pi(n-L)}{M}\right) \qquad L < n < L + M$$

The period of the cosine bell is determined by M.

     Following this, the digitized seismic trace is trans-
formed into the frequency domain through the use of the
discrete Fourier transform, which may be represented as

$$F(W) = \sum_{n=0}^{N-1} f(n)e^{-2\pi i Wn/N} \qquad W = 0, \ldots, N-1$$

3.3.2

where

f(n) = nth digital point

The algorithm used to calculate the Fourier transform is based on the fast Fourier transform (FFT) algorithms of Cooley and Tukey (1965). To employ the algorithm, the N data points are factored into K products. Then the computation of K shorter Fourier transforms combined with a series of recursive multiplications of these transforms (Kanasewich, 1975), will yield the Fourier transform of the seismic trace. The number of operations in the calculation reduces from N^2 to N $Log_2 N$. In the algorithm used, N, the number of data points, is factored into products of two, and thus, the number of data points must be a power of two. This is facilitated by padding both ends of the tapered trace with zeros to the nearest power of two (N'). The addition of the zeros to the trace does not alter its relative power spectrum, but does smooth the spectral window. The algorithm used to obtain the fast Fourier transform of the data was found in Claerbout (1976). For a complete discussion of Fourier transforms, including the FFT, one is referred to Kanasewich (1975), Claerbout (1976), Dobrin (1976), and to Lindseth (1967).

A Daniell spectral estimate is now computed by the

program. An ideal window would be one whose frequency
response is rectangular (figure 3.5), and the Daniell win-
dow approaches this ideal quite well. This window is
computed directly on the periodogram (Kanasewich, 1975) by

$$P(W) = \frac{N'}{N} \frac{1}{2m+1} \sum_{j=-m}^{m} F(W-j)F^*(W-j) \qquad W=0,1,\ldots,\frac{N'}{2}$$

3.3.3

The factor $\frac{1}{2m+1}$ normalizes the area under the
window to unity, and N'/N keeps the amplitude of the
power spectrum constant for all values of N'. Since the
data are real,

$$f(n) = f^*(n)$$

3.3.4

and thus

$$F(W) = F^*(-W)$$

3.3.5

The Fourier transform function is cyclic, and so

$$F(-W) = F(N-W)$$

3.3.6

Using equations 3.3.3, 3.3.5 and 3.3.6, the Daniell
spectral estimate may be written as

$$P(W) = \frac{N'}{N} \frac{1}{2m+1} \sum_{j=-m}^{m} F(W-j)(N-W+j) \qquad W = 0,\ldots,\frac{N'}{2}$$

3.3.7
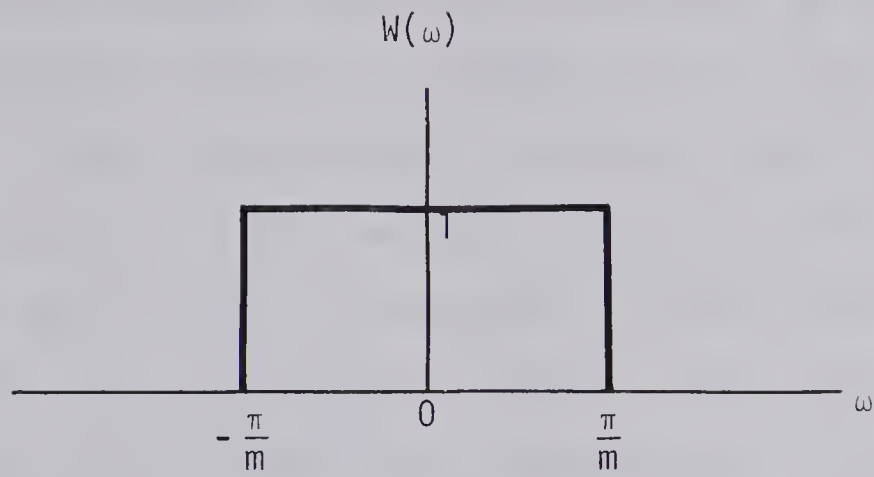
$$W(\omega)=1 \qquad -\frac{\pi}{m} \leq \omega \leq \frac{\pi}{m}$$

$$W(\omega)=0 \qquad \text{otherwise}$$

Figure 3.5: The ideal window (after Kanasewich,1975).

The power of various seismic channels was calculated over the time window from 6 to 18 seconds to determine their frequency content. In most cases, m was set equal to two. Figure 3.6 exhibits the power output of two traces. From the plots, we can see that the main power lies in the 10 to 30 hertz range. Assuming a crustal velocity of 6.5 kilometers per second, this suggests that the seismic energy from the crust and mantle is propagating with wavelengths of 200 to 450 meters. Thus, the resolution obtainable with this data will be of the order of 200 to 450 meters.

On the power plots of raw data, peaks are seen at about 3 and 60 hertz, and sometimes at even higher frequencies (figure 3.2). The very high frequency peaks (with exclusion of the 118 hertz peak) are likely due to wind noise, which often comes in with a frequency of about 85 hertz. The 60 hertz peak is the result of geophones being located near power lines, and the 3 hertz peak is likely due to ground roll. Ground roll (roller) is most likely the result of surface Rayleigh waves, and it is most strongly generated where the near surface material is highly unconsolidated and of very low velocity (Mateker, 1965). However, the proper arrangement of geophones and the use of multiple holes could have severely attenuated the ground roll (Kanasewich and Cumming, 1965), and greatly improved the quality of the records. For a complete discussion on the theory behind such patterned arrays, along with their amplitude responses,
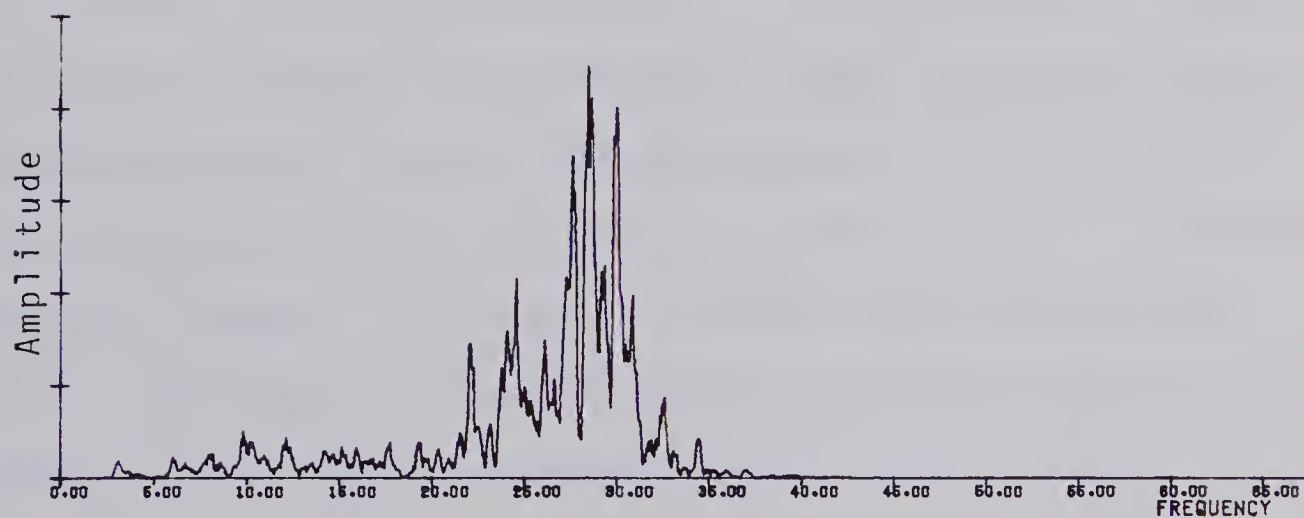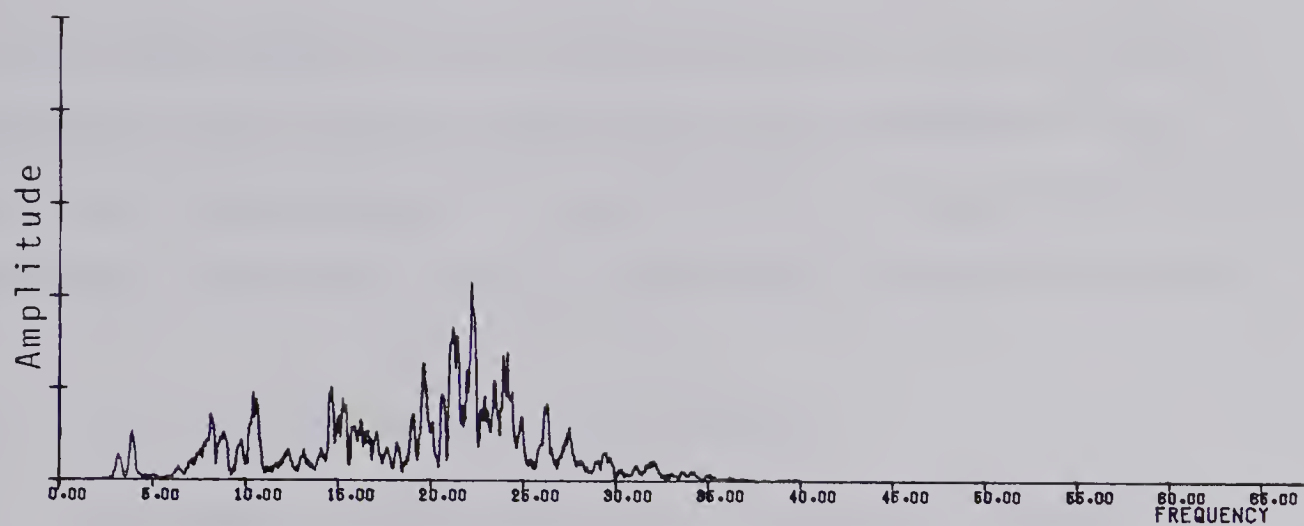
POWER-OUTPUT PLOTS.

SCALE: 5.000E+05 UNITS/CM

Figure 3.6: Daniell power spectral estimates for traces used in the study.

see Clowes (1966, 1969).

One final note regarding the plots in figure 3.6,
is that the power of the filtered traces (3 to 55 hertz)
seems to fall into two main bands, one between 10 and 15
hertz and one between 20 and 30 hertz. These bands likely
represent reflected energy from layers within the Earth.

3.4. The Zero-phase Band-pass Filter

The power spectra plots of figure 3.6 showed that
the reflected energy of the seismograms was contained
between the frequencies of 10 to 30 hertz. To eliminate
some of the unwanted noise in the traces, for example
surface waves, the data was subjected to a digital band-
pass filter. During the course of his research, D. Ganley
developed an eight-pole zero-phase shift recursive Butter-
worth band-pass filter. The Butterworth filter is design-
ed to separate signal and noise when they occur in distinct
frequency bands. This type of filter does not exhibit
Gibb's phenomena, a high frequency oscillation which super-
imposes itself upon the amplitude spectrum of the filter.
Since the filter is zero-phase shift, there is no lag
between different frequency components. Also, to prevent
aliasing problems, a bilinear Z transform was used in the
design of the filter.

Basically, the program works as follows (Kanasewich,
1975). First, the roots of the transfer function in the
complex Laplace transform variable (p) are calculated.

From these four poles, eight poles in complex conjugate
pairs, are computed by a transformation of a low to a band-
pass function (complex frequency, s). These are used to
calculate the filter gain, and the Z transform of the
Butterworth band-pass filter. The latter is given by

$$W(z) = \frac{(1-Z^2)^4}{B_1(Z)B_2(Z)B_3(Z)B_4(Z)} \qquad 3.4.1$$

where B_1, B_2, B_3 and B_4 are the filter coefficients
obtained from the S-poles. The filtered output, $Y(Z)$, is
obtained from

$$Y(Z) = W(Z) \cdot X(Z) \qquad 3.4.2$$

where '·' indicates a product. In the discrete time
domain, this convolution operator may be expressed as

$$Y_t = W*X = \sum_{i=0}^{m} W_i X_{t-i} \qquad 3.4.3$$

where N is the number of points in the input trace. A
recursive relation is used to obtain the final output
(figure 3.7). To obtain zero-phase shift, first the data
is convolved with the filter to produce an output trace.
This output trace is then time reversed and again convolved
with the filter. The output of this convolution is time
reversed to yield the desired filtered data. So that the
gain of the filter is unity, each point of the output
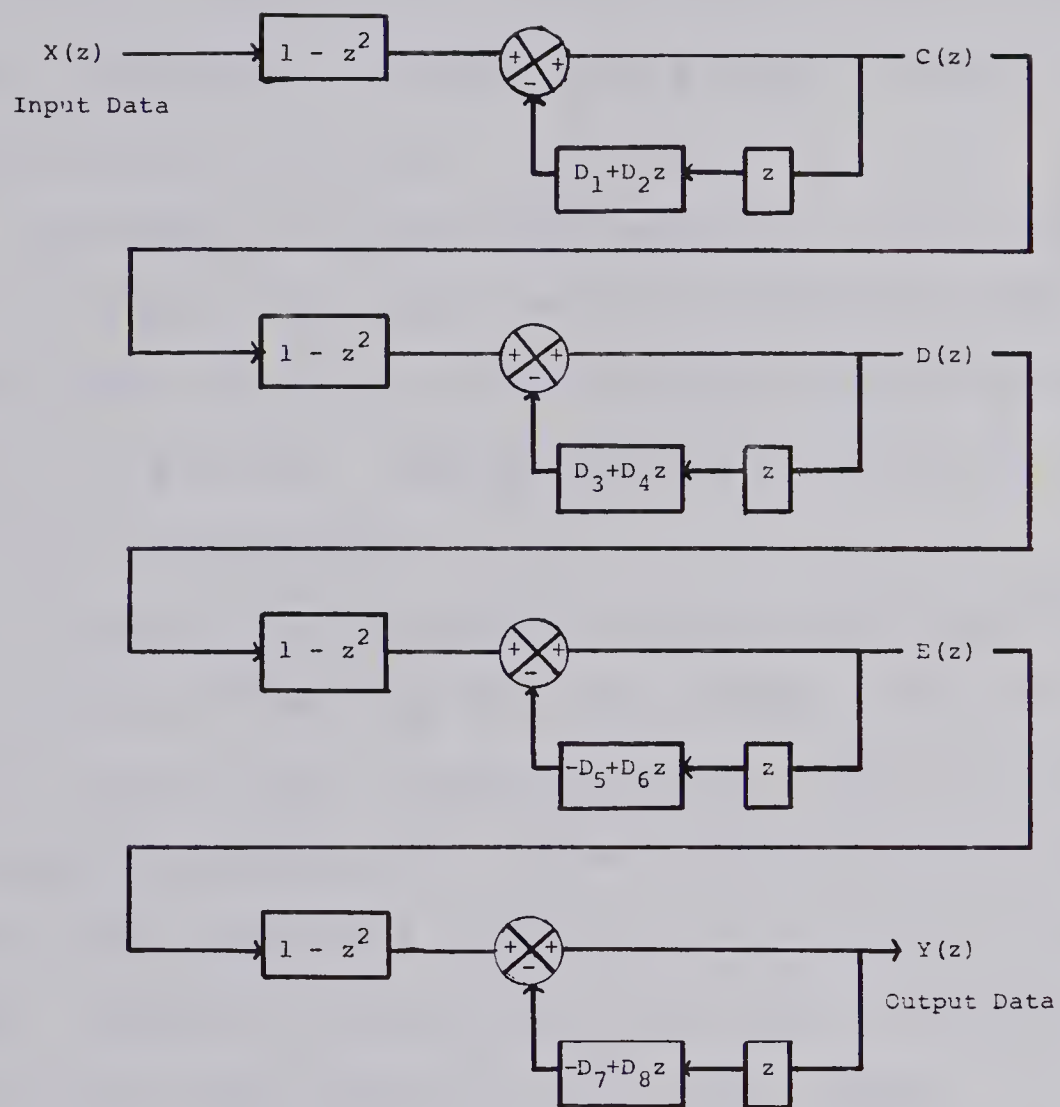
where D_i, $i=1,\ldots,8$ are coefficients of z
and z^2 of the Butterworth polynomials.

Figure 3.7: A recursive band-pass Butterworth filter with
eight poles and four zeros (after Kanasewich, 1975).

trace is divided by the gain of the filter.

In applying the filter to the data, it was decided that a relatively wide pass band would be used. Narrow band-pass filtering makes the output seismogram quite oscillatory, and destroys the character of the reflected pulse. Therefore, a filter having cutoff frequencies of 8 and 40 hertz was used.

An example of the effectiveness of the filter may be seen in figure 3.1. Here, we can see that the high frequency peaks generated in the clipped portion have been totally eliminated. However, this part of the trace is distorted and unusable.

Figure 3.8 also exhibits traces before and after the application of the 8 to 40 hertz filter. The first part of the figure shows a group of traces that are strongly disrupted by ground roll. Beneath this group of traces is the filtered output showing no sign of this long period noise. Overall, the quality of the record section can be seen to have been improved to a large degree.

Power spectral estimates were done on the filtered data (figure 3.9) to see where the power of the signal is confined. As previously mentioned, the power is confined to two bands, one centered at 13 hertz and one centered at 27 hertz. The lower frequency band is probably the result of signal from deeper layers, and the higher frequency band likely represents energy from shallower horizons.

Figure 3.8: Eleven traces of shot 34B before and after
8 to 40 hertz band-pass filtering. The
lower group of traces are the filtered
output. The origin is marked by the '0',
with the time between adjacent crosses being
1 second.
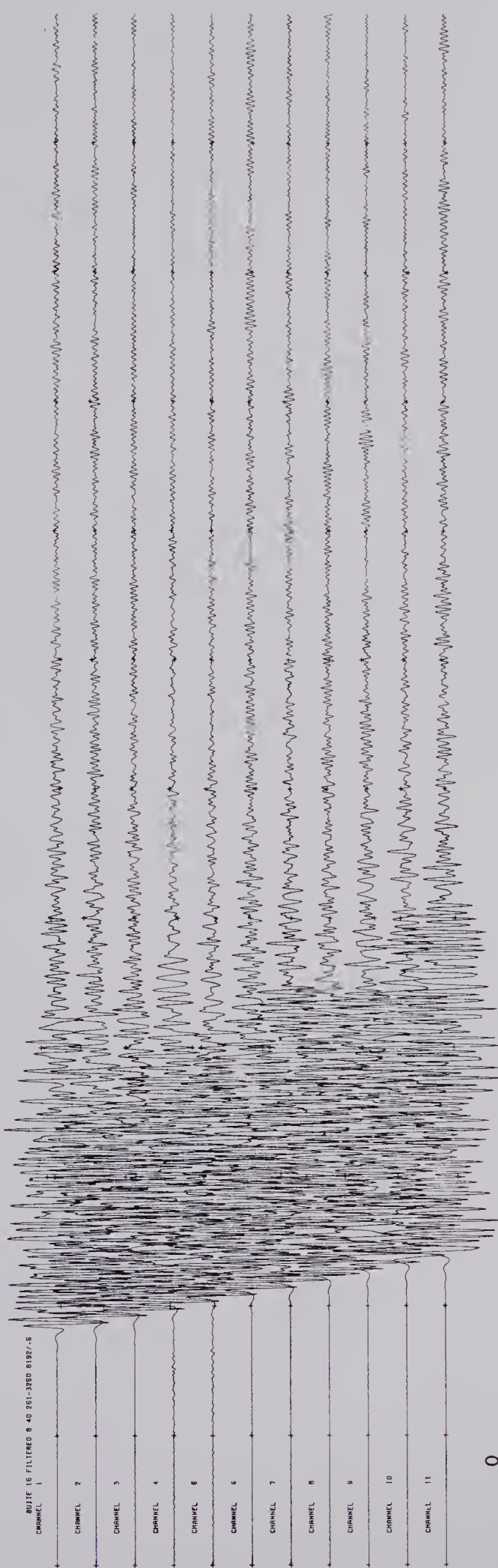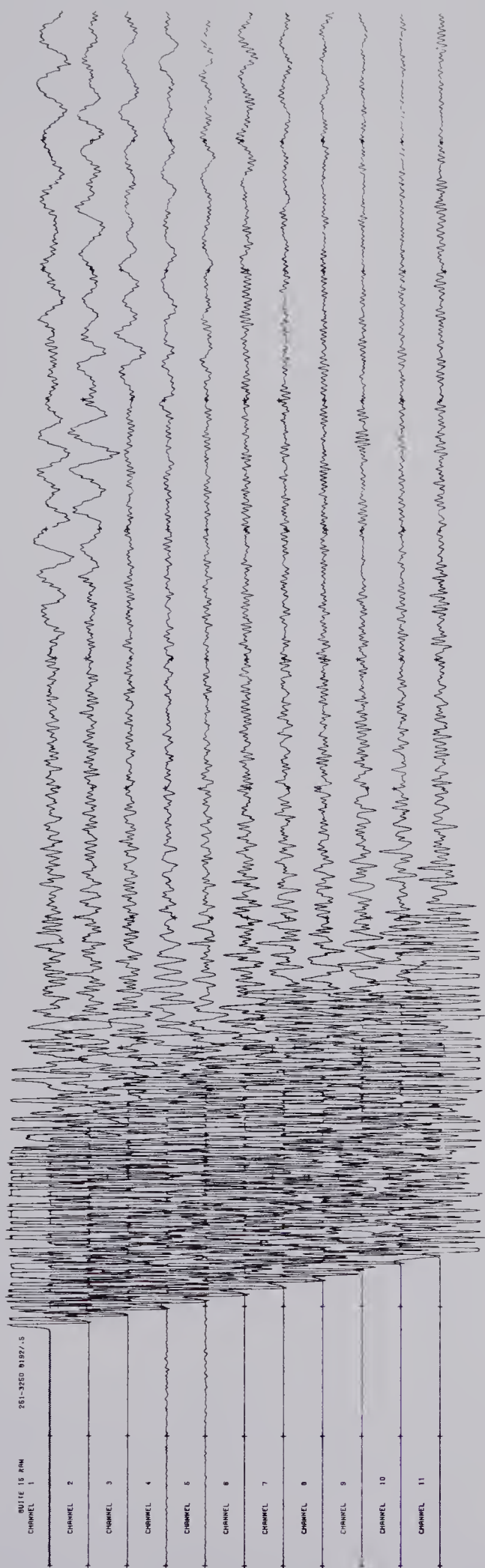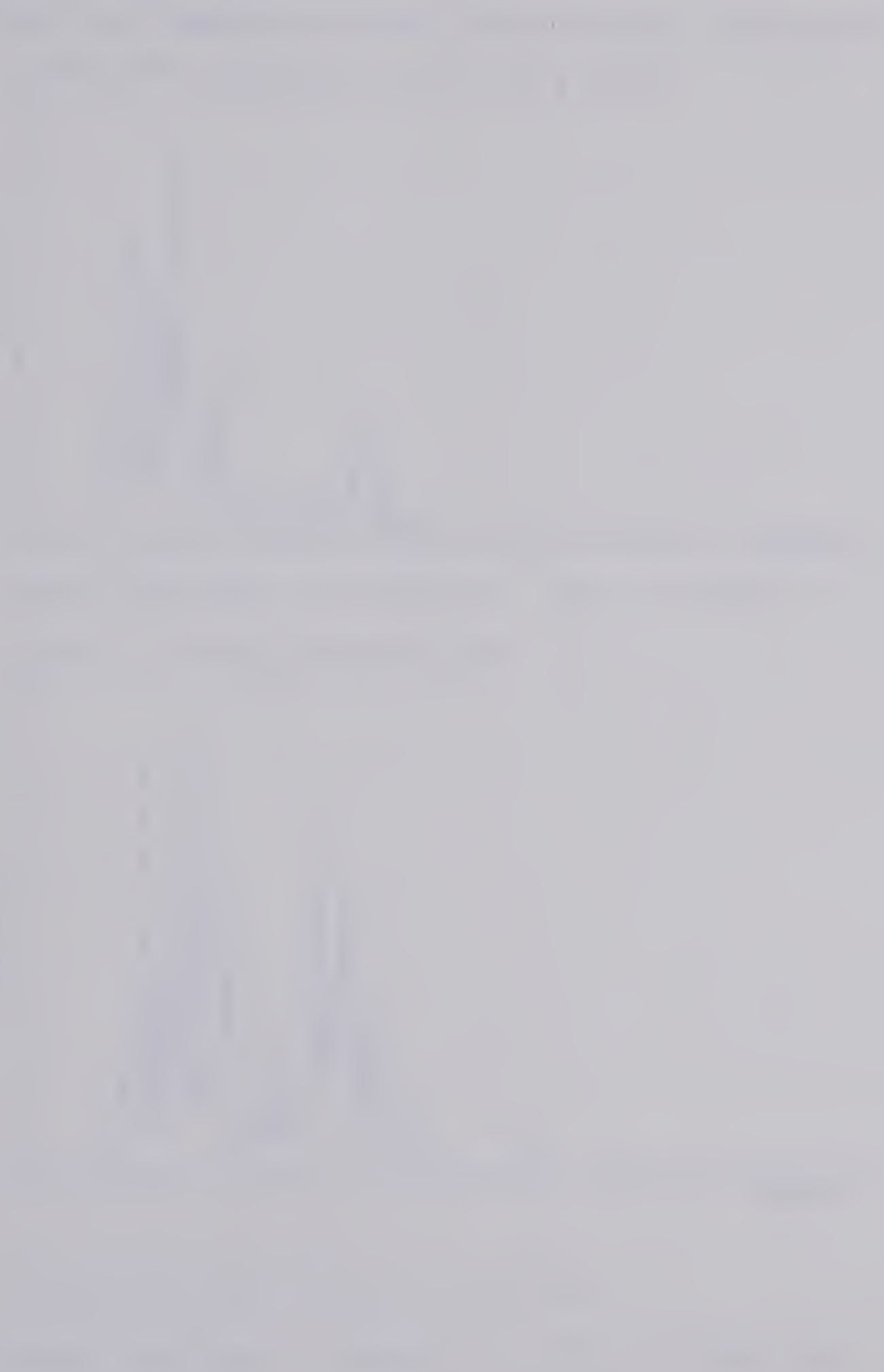
Figure 3.9: Daniell power spectral estimates for traces
after 8 to 40 hertz band-pass filtering.
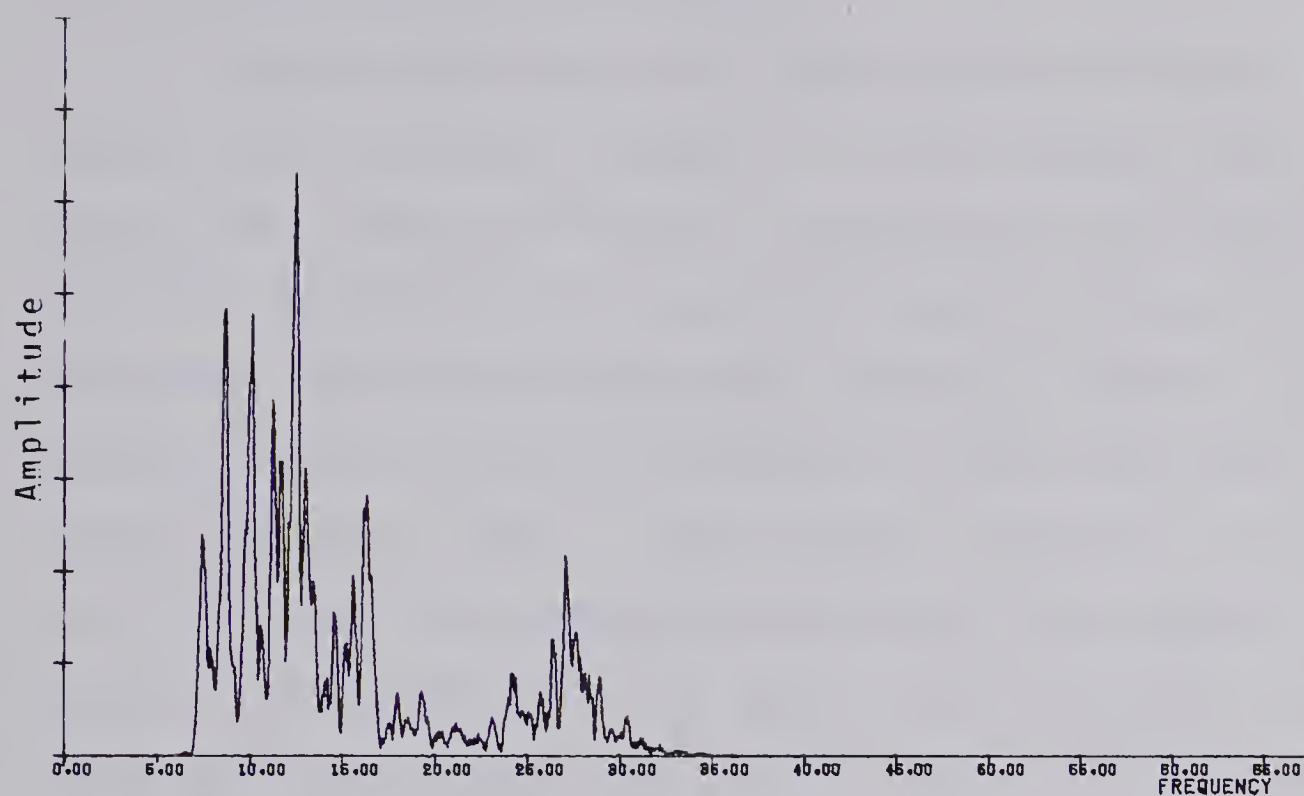
AMPLITUDE MAX: 3.153E+06   MIN: -3.689E-07

SCALE: 5.000E+05 UNITS/CM
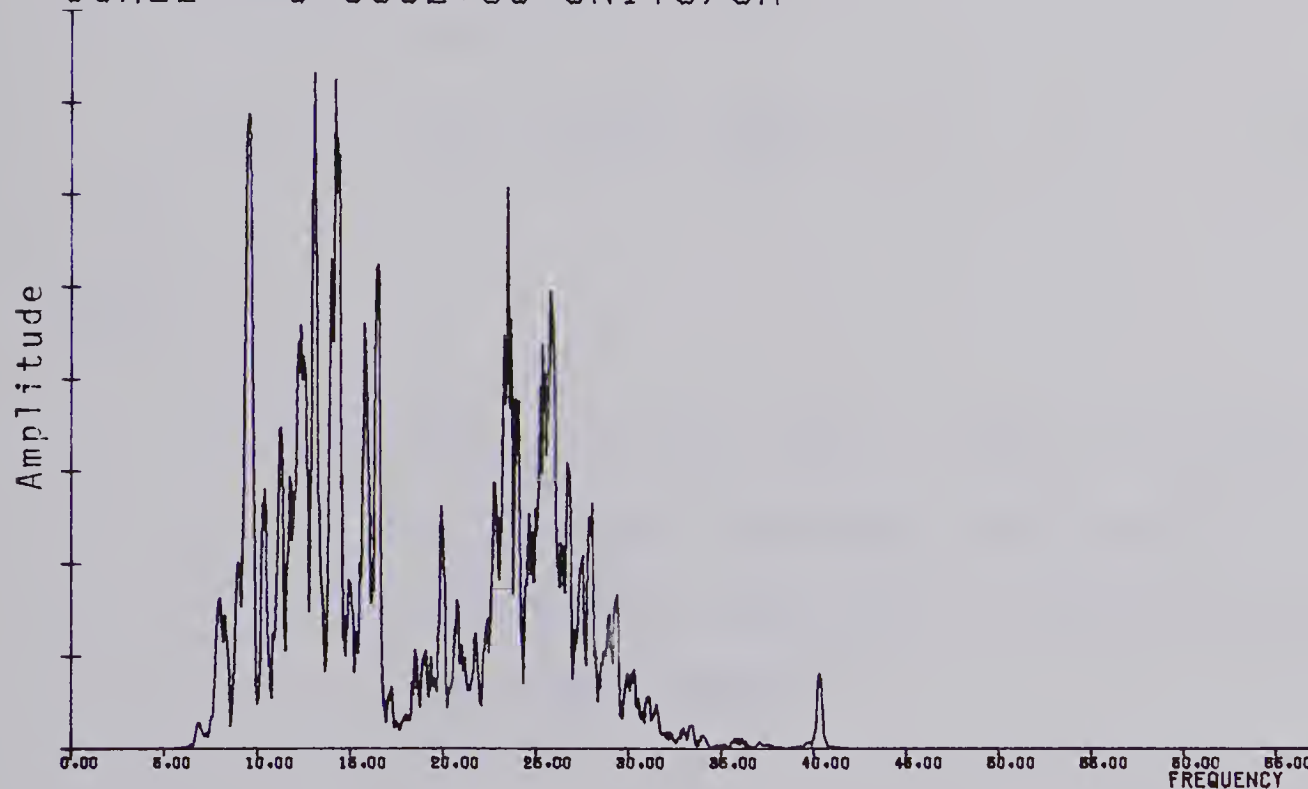
POWER-OUTPUT PLOTS.

AMPLITUDE MAX: 1.829E+03   MIN: -2.466E-10

SCALE: 2.500E+02 UNITS/CM

3.5. Normal Moveout Corrections

Dynamic corrections are displacements in time between the individual traces of a given record that vary with time. These corrections are applied to simulate a vertical ray path and so remove the normal moveout (or time lag) which depends upon the source to receiver dis- tance and the velocity distribution of the underlying ground (Mateker, 1965). From Fermat's principle we know that the wavefront is propagating along the shortest time paths. In regions where the layers are horizontal, or have very gentle dips, the arrival time of a reflection from the nth layer at a distance X is given by the infinite series (Taner and Koehler, 1969)

$$T(x,n)^2 = C_1 + C_2 X^2 + C_3 X^4 + \ldots \qquad 3.5.1$$

where

$T(x,n)$ = two-way travel time for the nth layer at a distance x from the shot location

C_i = coefficients dependent on interval velocity and layer thickness

A series of model studies by Al-Chalabi (1973) have demonstrated the accuracies that are possible by truncat- ing equation 3.5.1, and have shown that the accuracy is dependent upon the ratio of spread length to reflector

depth.   When this ratio was less than 1.0, the second

order approximation was correct to 0.5 percent.   For a

ratio equal to 2.0, the travel times were correct   to about

2.0 percent with a two term series.   In our case, the maxi-

mum shot to detector distance was about 10 kilometers,

yielding a ratio well below 1.0 for the reflectors of interest.

Thus, a two term truncation of the infinite series is suffi-

cient.

$$T(x,n)^2 = C_1 + C_2 x^2 \qquad\qquad 3.5.2$$

Taner and Koehler (1969) have calculated the coeffic-

ients C_1 and C_2, with the result

$$T(x,n)^2 = T(o,n)^2 + \frac{x^2}{\bar{V}(n)^2} \qquad\qquad 3.5.3$$

where

$\quad$ $T(o,n)$ = two-way normal incidence time for the

$\qquad\qquad$ nth layer

$$T(o,n) = 2\sum_{K=1}^{n} \frac{d(K)}{V(K)} \qquad\qquad 3.5.4$$

$\quad$ $d(K)$ $\quad$ = thickness of the Kth layer

$\quad$ $V(K)$ $\quad$ = interval velocity of the Kth layer

$\quad$ $\bar{V}(n)$ $\quad$ = time weighted, root mean square velocity

$\qquad\qquad$ as described by Dix (1955)

$$\bar{V}(n)^2 = \frac{\sum_{K=1}^{n} V(K)^2 t(K)}{T(o,n)} \qquad 3.5.5$$

$t(K)$ = two-way normal incidence time in the Kth

layer

$$t(K) = \frac{2d(K)}{V(K)} \qquad 3.5.6$$

Equation 3.5.3 defines a hyperbola (figure 3.10), and is accurate to within 0.5 percent of the actual travel times as given by the exact solution, which is more than adequate for deep reflections.

To remove the normal moveout in the data, a two part procedure was adopted. First, a model was assumed for the Earth's crust in the region of the survey. An average shallow structure was determined from a cross-section con- tained in Green *et al.*'s (1977) report, whereas a first approximation to a deep structure is from Gurbuz (1970). This model is presented in figure 3.11. Using this model, a computer program was written which computed the travel times for rays which assumed reflectors at intervals of 0.04 seconds of normal incidence time for 35 shot to detector distances. The travel time curves for reflectors at the lower three layers in the model are shown in figure 3.12, exhibiting the characteristic hyperbolic form. Next, a program was written which applied the normal moveout corrections, and it worked in the following manner. First, the program linearly interpolated the values for the travel
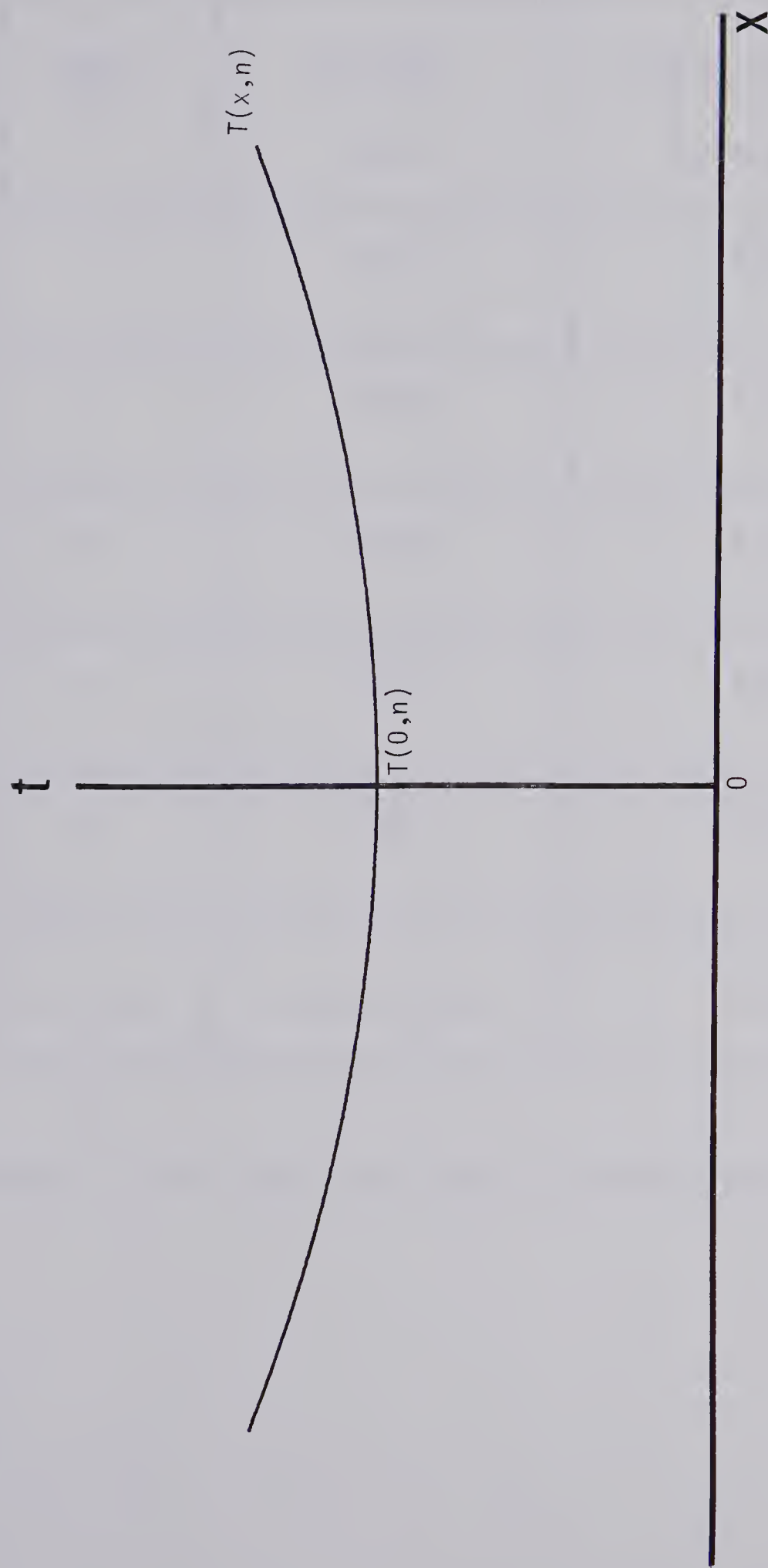
Figure 3.10: Travel time curve for a hypothetical horizontal reflector.

LAYER	THICKNESS (km)	INTERVAL VELOCITY (km/sec)
1	0.66	2.20
2	0.45	4.50
3	17.08	6.10
4	7.48	6.80
5	9.59	7.10
_____	_____	7.90

Figure 3.11: The crustal model used for normal moveout corrections.

STEPOUT

LAYER 1

LAYER 2

LAYER 3

18

8

0

8

18

t (sec)

6.4

6.5

8.6

8.65

11.25

11.3
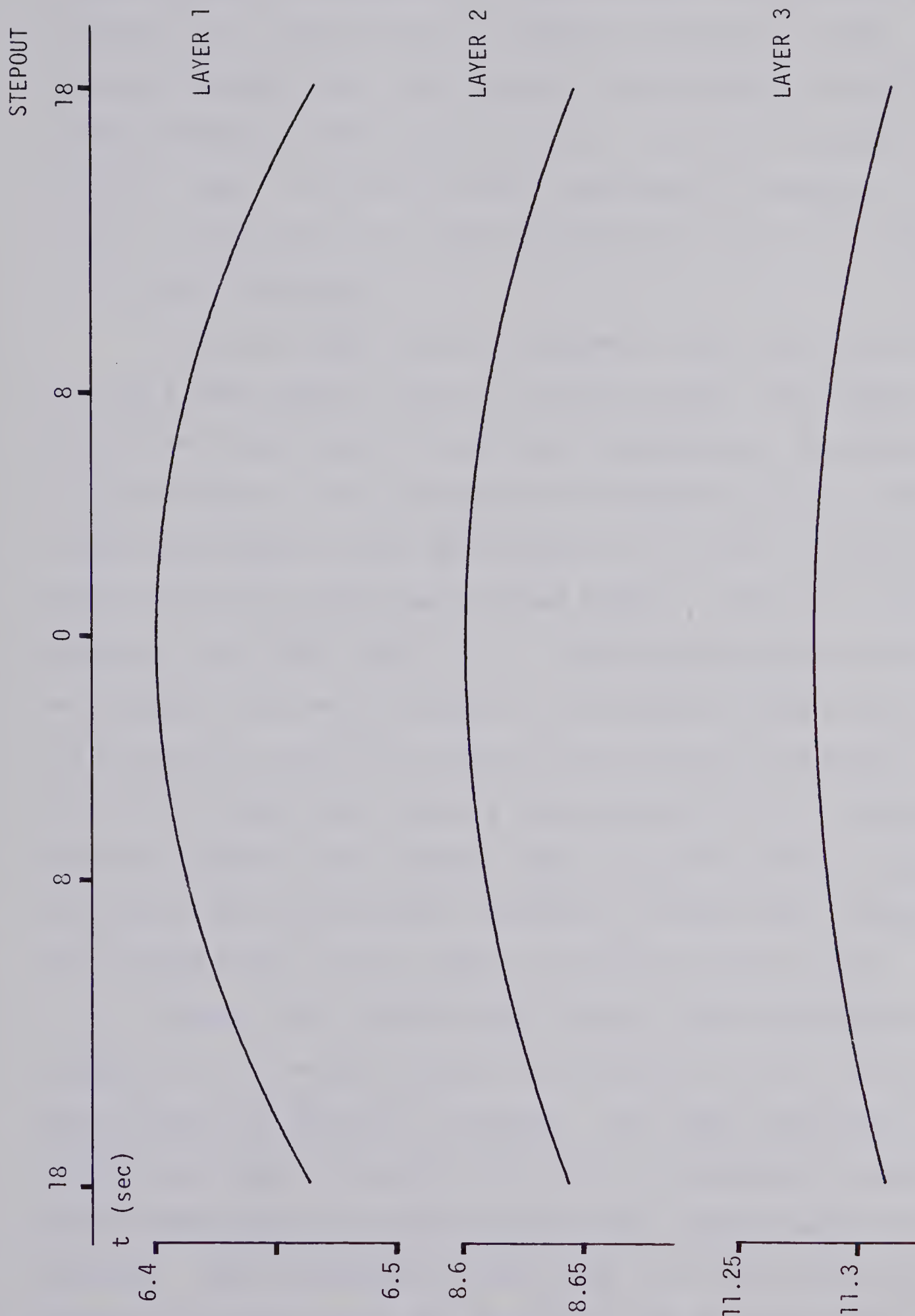
Figure 3.12: Travel time curves for the three deepest layers
found in figure 3.11.

times assuming interfaces at 0.004 seconds (the sampling
interval) for the 35 shot to detector distances. Next, for
each particular trace, the program interpolated an amplitude
corresponding to the travel time of a reflector at each
digital point. The final result simulated a series of
traces representing rays that appeared to have been recorded
with normal incidence.

Since the model did not assume a continuous velocity
increase with depth, some of the early times were double
valued for large shot to receiver separations. Therefore,
in this region, it was impossible to determine which reflec-
tion contributed to the amplitude of the trace, and thus
this part of the trace was zeroed (figure 3.13). In con-
junction with this, Mair *et al.* (1976) point out that off-
sets should not be so large as to introduce large variations
in reflection character due to varying reflection angle.
For the Manitoba data, only a few seconds had to be deleted.
With the Alberta data though, the high gain setting necessary
to record deep reflections resulted in almost five seconds
of clipped data, which I chose to delete at this time.

Figure 3.14 exhibits four traces before and after the
removal of the normal moveout for offsets of 4, 6, 18, 18,
and 30 shot to detector distances. The lower corrected
traces have been compressed throughout, the degree varying
with time along the record and with the shot to detector
spacing. For a spacing of four units, the trace does not
change very much after the correction has been applied.
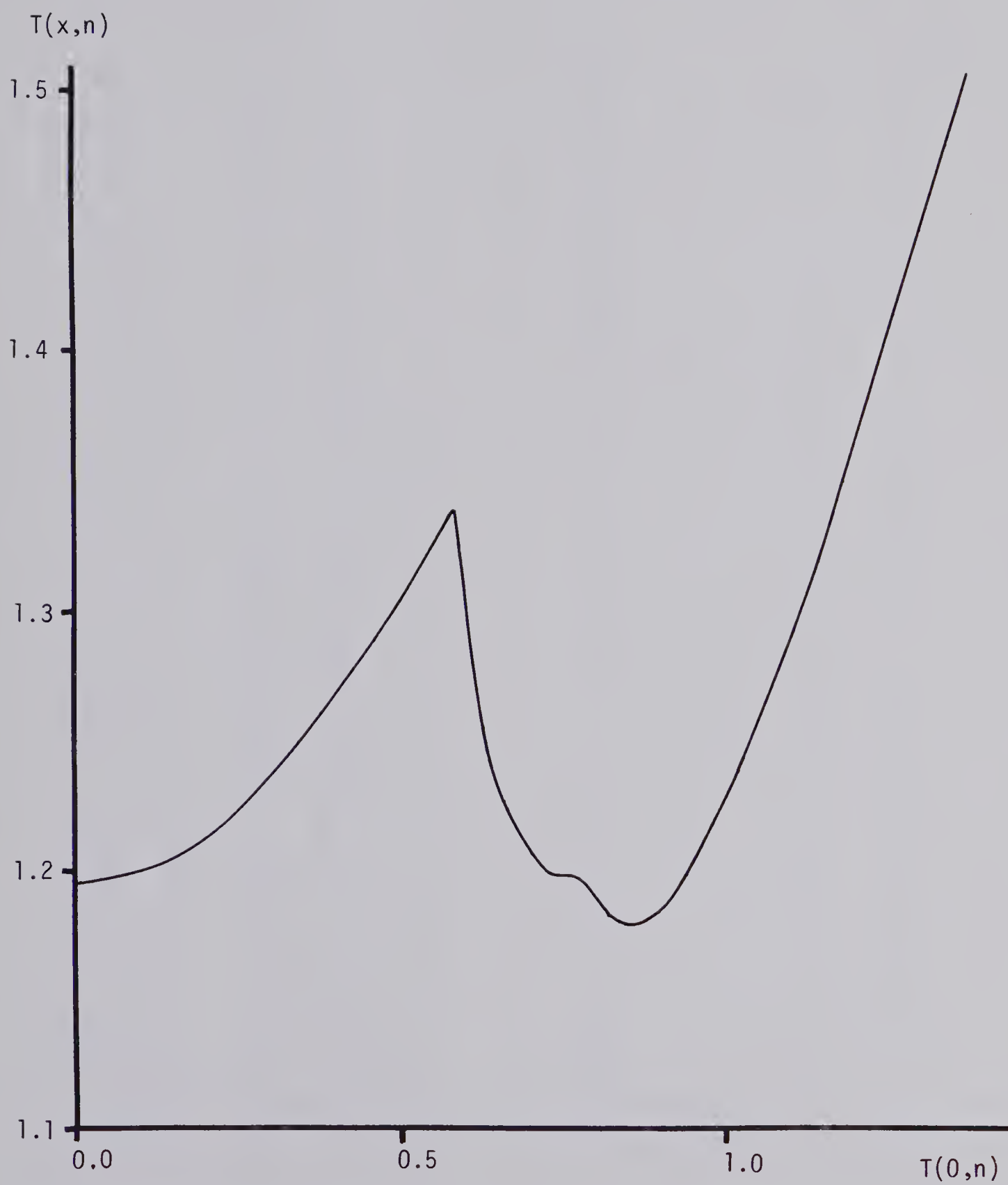
Figure 3.13: T(x,n) versus T(0,n) for a shot to receiver separation
of 2633 meters based on the model of figure 3.11.
Times are measured in seconds.

Figure 3.14:   Comparison of traces before and after the
               removal of normal moveout. The lower traces
               have been corrected. Note the possible
               reflections beneath the 'l's.

C.D.P. 172 1961-3450 (RAW)
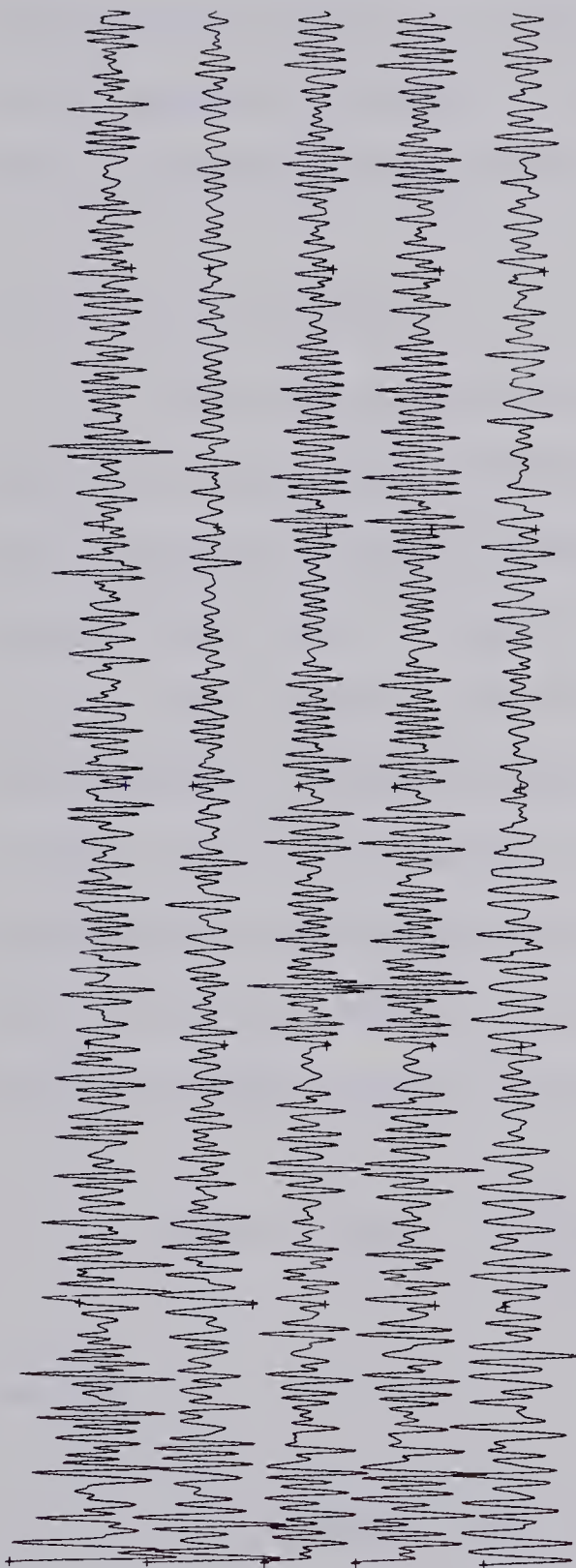
C.D.P. 172 1961-3450 (WITH NAN)
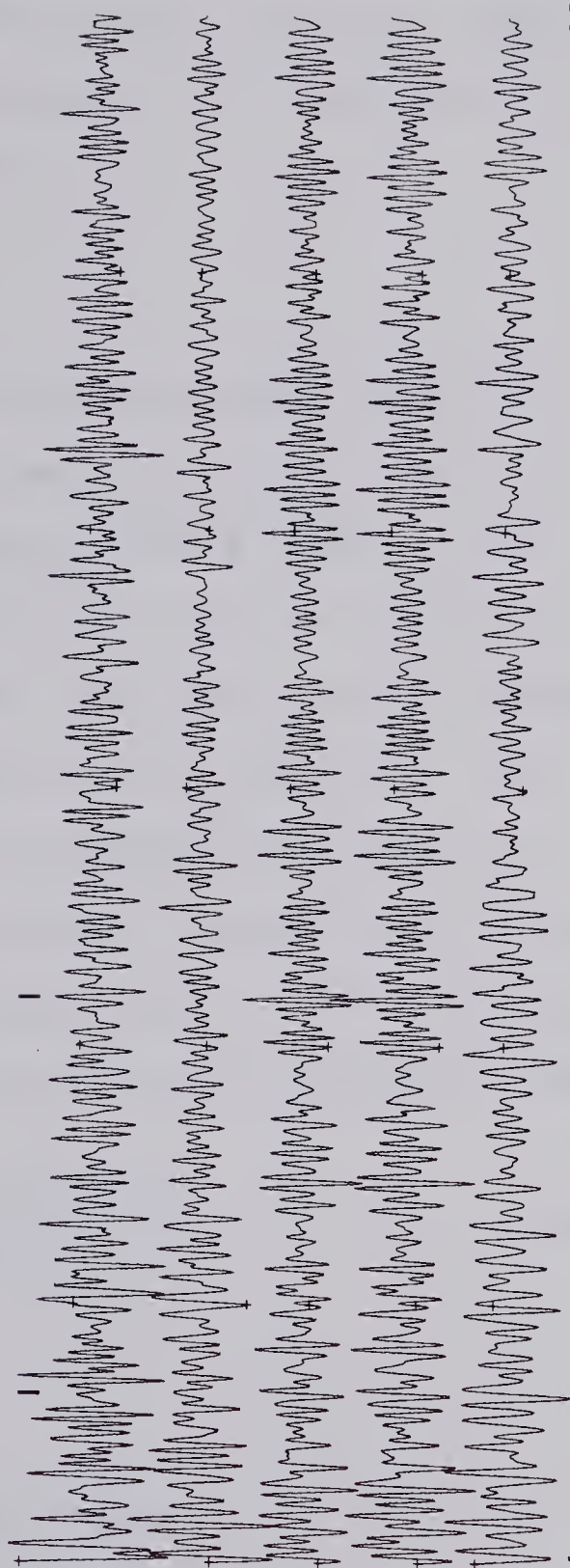
6

12

Time in seconds

However, for a spacing of 30 units, the early parts of the trace are greatly contracted, with the later sections being only somewhat compressed. At this time, any primary reflections present in the traces should line up. Figure 3.14 suggests possible reflections now in almost perfect time alignment (beneath the 'l's).

3.6. Normalization

With the data being collected on three different systems, each with a different gain setting, it was found that each trace had a different amplitude range. Thus, the next step in the analysis of the data was the normalization of the amplitudes of the traces. For this, it was decided to compute the average amplitude, for a particular time window, of one trace per group of traces belonging to a particular subsurface point, and make the rest of the traces in the group have this average amplitude. The normalization procedure may be expressed as follows (Clowes, 1966):

$$Y(i) = (X(i) - \bar{X}) \frac{\sum_{j=1}^{n} |Xs(j) - \bar{X}s|}{\sum_{j=1}^{n} |X(j) - \bar{X}|} \qquad 3.6.1$$

where

        Y   = normalized digital value

        X   = unnormalized digital value

        's' refers to the standard trace

        '-' refers to an average over the time window

Equation 3.6.1, as programmed by the author, works
as follows. The average value for the time window was
calculated for all traces. This mean was then removed
from all points in the particular trace. Then, the sum of
the absolute value of the deviations from the mean, within
the time window, was computed for each trace. The normal-
ized values were obtained by multiplying the mean removed
traces by the ratio of the sum of the deviations for the
standard trace to that for each of the other traces belong-
ing to a particular subsurface point. This not only
yielded normalized traces, but within the time window,
the D.C. average was removed.

3.7. Common Depth Point Stack

One of the main problems encountered in reflection
seismology is how to remove the noise while maintaining a
high reflection signal. To overcome this problem, Mayne
(1962) introduced a multiple coverage, common depth point
technique. This method is a stacking process which allows
multiple coverage of the same subsurface points (Dobrin,
1976; Telford *et al.*, 1976) utilizing different shot and
detector locations (figure 3.15). The accuracy of the
technique depends upon applying the correct time corrections
to each trace, both static and dynamic, so that the primary
reflections are properly stacked (Mayne, 1967). Stacking,
in this manner, results in the attenuation of random noise,
multiple reflections and reverberations (Marr *et al.*, 1967;
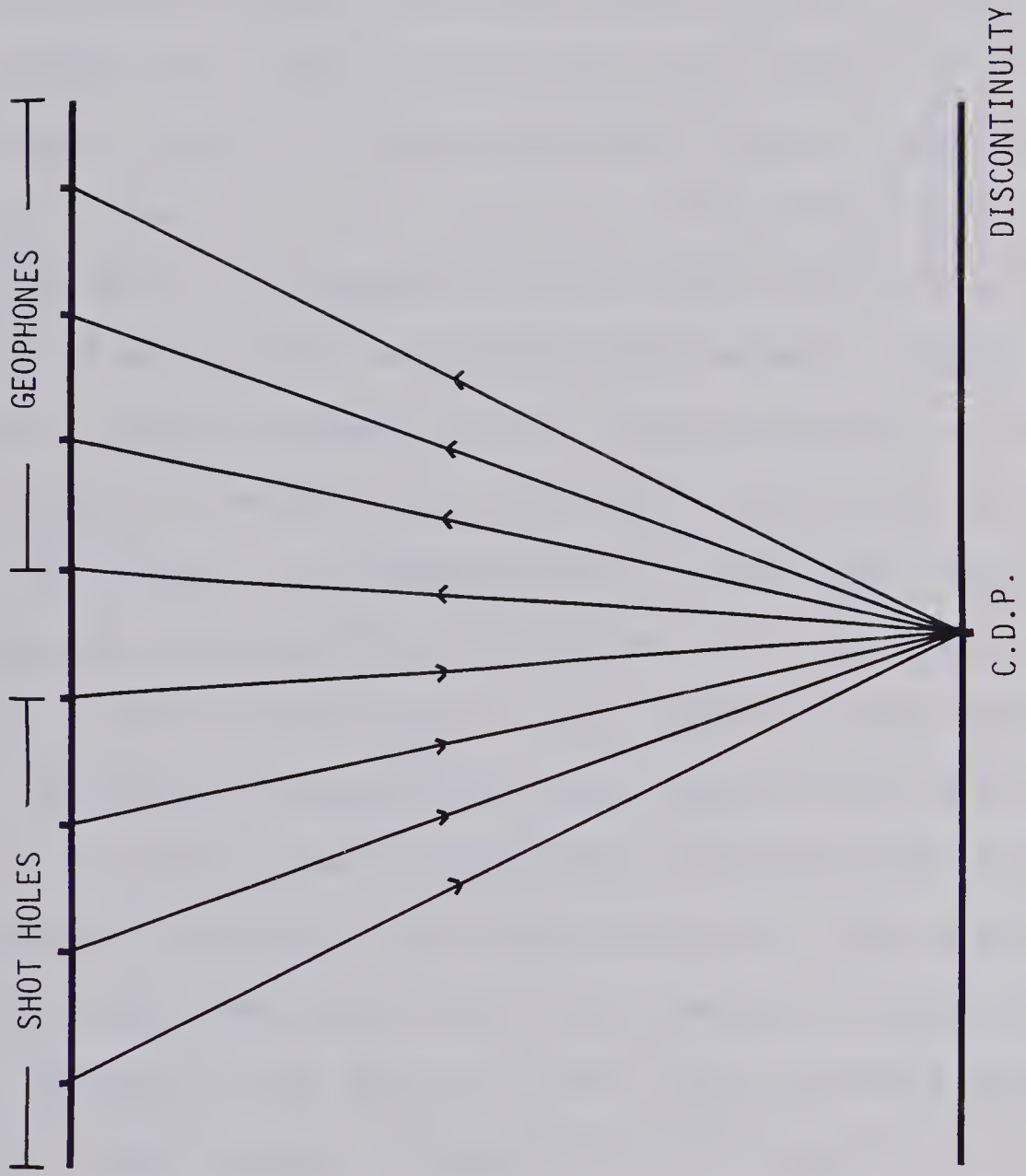
Figure 3.15: The common depth point technique used to obtain 400 percent coverage.

Courtier *et al*., 1967).

A trace weighting technique for improving the opera-
tion of the common depth point (C.D.P.) stack was suggested
by Brown *et al*. (1977). This process was designed for
vertical crustal reflection data; data in which the input
traces are recorded from the same shot and receiver posi-
tions. With different shot to receiver separations, as is
the case for C.D.P. data, the determination of the weighting
factors is extremely difficult due to variations in reflec-
tion amplitudes and frequencies between traces. White
(1977) also showed for low signal to noise ratios that the
errors in determining the weighting factors were very large.
Therefore, a weighted stack was not used. Any traces
which were obviously contaminated by noise were simply not
included in the stack. This would occur if the seismometer
output was dominated by local traffic, et cetera.

The average subsurface coverage used in the collec-
tion of the data was 400 percent, or four-fold (figure 2.6).
At this time, the static and dynamic corrections have been
applied to the data, but the static corrections may not
have been exact. Therefore, utilizing the cross correla-
tion program, all of the traces for a particular subsurface
point were cross correlated together in the vicinity of
possible reflections. Using these coefficients along with
plots of the various traces, I was able to refine the
static time corrections for all traces. A stacking program

was then written which allowed one to shift the traces
according to the revised statics. The operation of the
program may be mathematically expressed as

$$Y(j) = \frac{1}{n} \sum_{i=1}^{n} Xi(j) \qquad\qquad 3.7.1$$

where

        $Xi(j)$ = time corrected input traces

           n = number of input traces

        $Y(j)$ = output trace

    Figure 3.16 demonstrates the effectiveness of the
stacking process on two types of input signals. In both
cases, we observe an increase signal to noise ratio.
    Figures 3.17, 3.18 and 3.19 show the output of the
stacking program on three sections of the data. In the
shallow sections, for subsurface points 169 to 183, we can
see coherent energy at about 6.6 and 8.1 seconds. These
two energy bands can be seen quite clearly on figure 3.18,
but not very well at all on figure 3.19. In the deeper
sections, little bursts of coherent energy can be seen on
all of the plots, notably around 12.5 seconds. For all
cases, the pulses are still quite obscured by the noise,
with the phase velocity of the reflections being impossible
to determine. The bursts of coherent energy found at
various times throughout the sections are most probably

Figure 3.16: Application of the C.D.P. technique to test
data. In (a), we have two input channels
consisting of (1,1,0,0) and (1,0,1,0). The
signal is contained in sample one. On output,
we have (1,0.5,0.5,0), with a signal to
noise ratio of 2, and the noise being spread
out over two samples. Example (b) shows the
result of a five-fold stack on a spike input
pulse and coherent noise. The noise arrives
with an apparent velocity of five points per
trace.

a
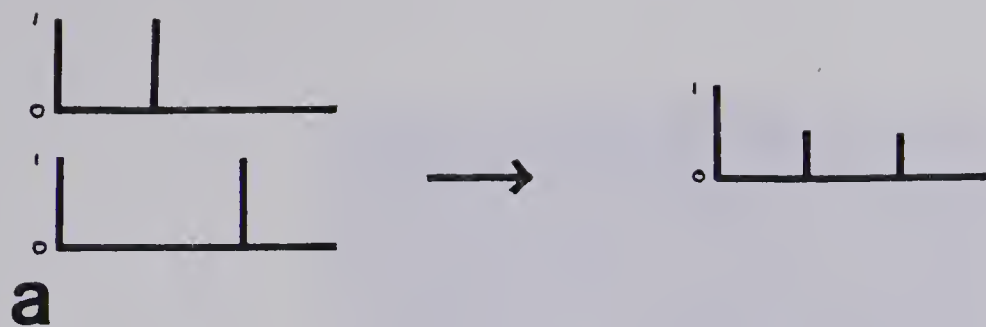
C.D.P. TEST DATA.

DISTANCE BETWEEN TRACES IS 0.146 KM

TIME IN SECONDS

| 6.40 | 6.59 | 6.78 | 6.97 | 7.15 | 7.34 |

INPUT PULSE
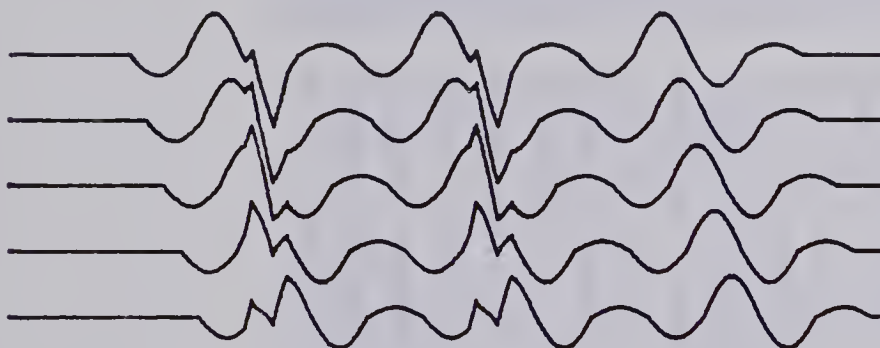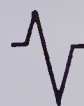
TIME IN SECONDS

| 6.40 | 6.59 | 6.78 | 6.97 | 7.15 | 7.34 |

b
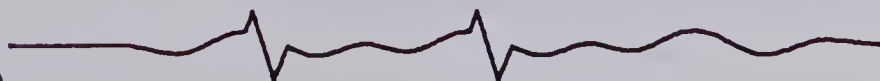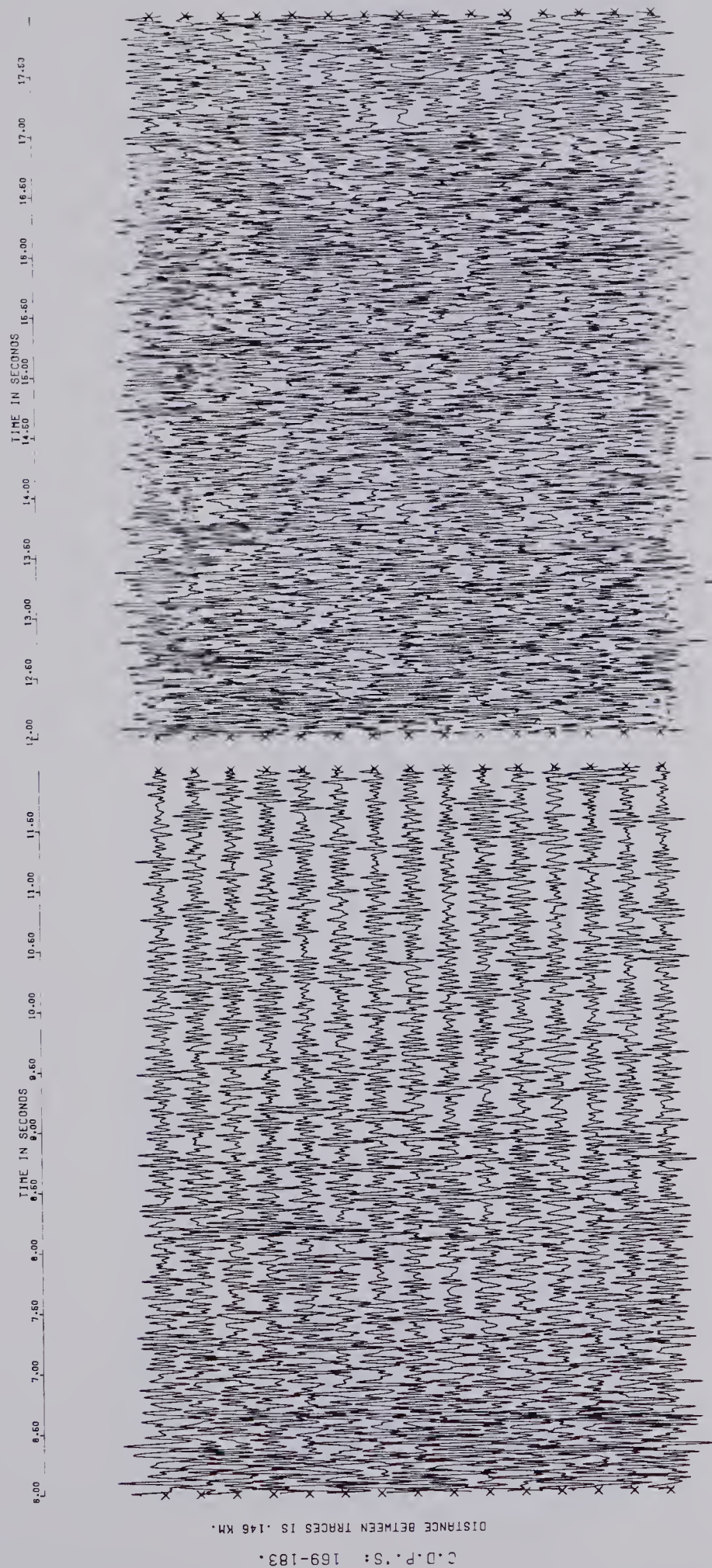
Figure 3.17: Common depth stack for subsurface points 169 to 183. The deep section (12 to 18 seconds) is amplified five times.
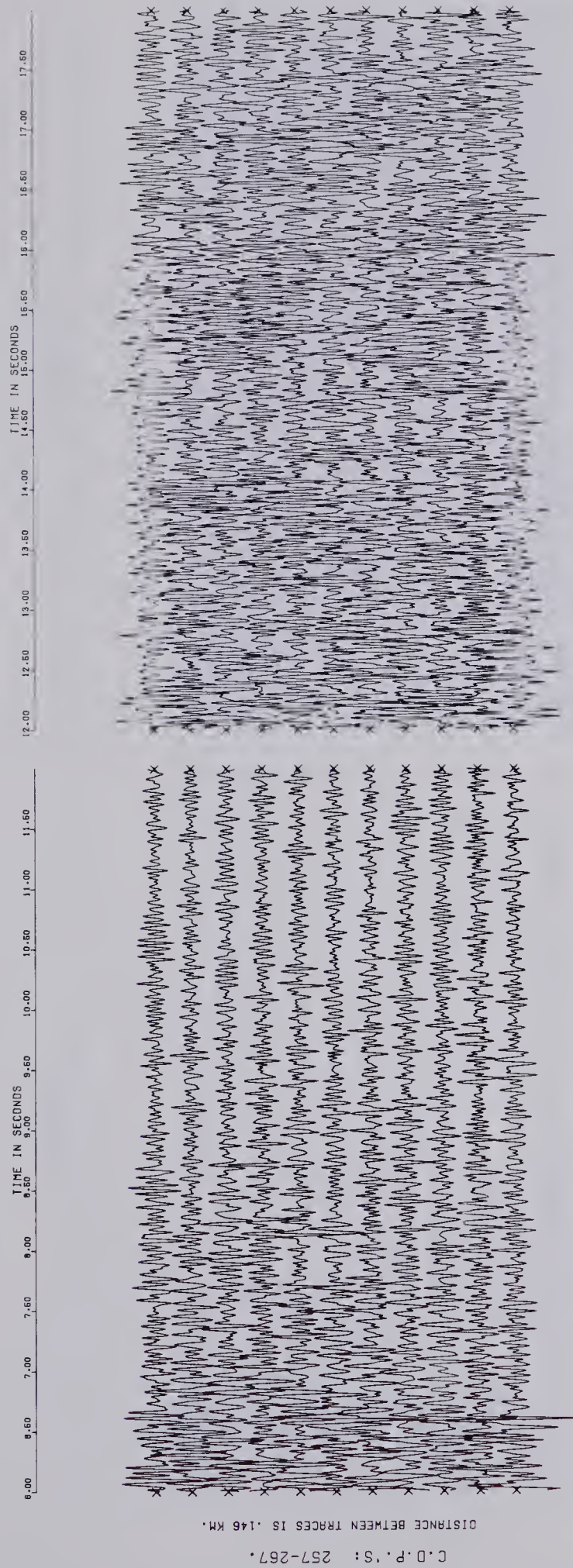
Figure 3.18: Common depth stack for subsurface points 257 to 267. The deep section is amplified 2.5 times.
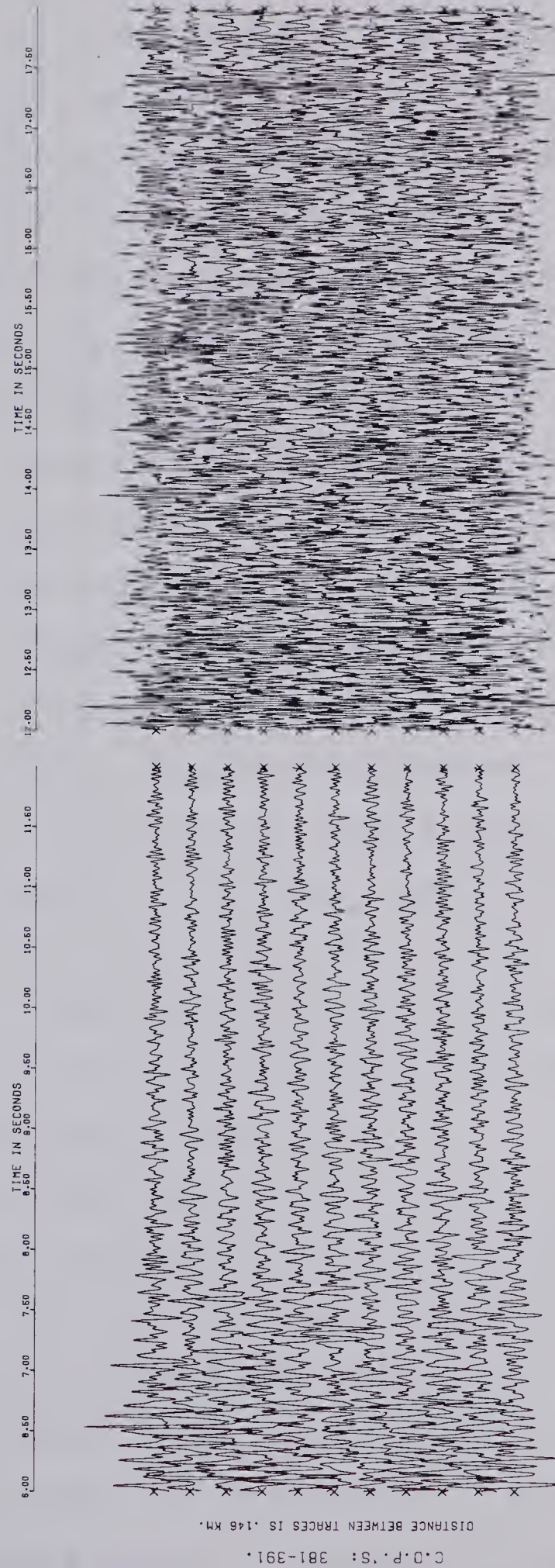
Figure 3.19: Common depth point stack for subsurface points 381 to 391. The deep section is amplified five times.

primary reflections, based on their amplitudes and the fact that multiples, being not in proper time alignment, would have been attenuated by the stack.

Figure 3.20 exhibits eleven traces corresponding to shot 144, one trace from each subsurface point from 257 to 267. On the plot, coherent energy appears to exist at about 6.6 seconds only. However, no distinct pulse can be clearly seen. In general, the record is much more noisy, and of far less value than the corresponding four-fold stack shown in figure 3.18.

To note the frequency of the main pulse, we made a power spectral estimate centered around the pulse at 6.6 seconds. Power spectral estimates were made for each sub-surface point, and the results were averaged. The time window was 0.2 seconds in length, with a taper being applied to 0.1 seconds of the data. Several thousand zeros were added to the signal to increase the resolution of the estimate. From figure 3.21, we note that the fre-quency of this main pulse is about 11 hertz, yielding a wavelength of about 590 meters.

The common depth point stack has been shown to be a powerful tool for enhancing primary reflections, provided the static and dynamic corrections are accurate. Random noise is attenuated as the square root of the number of input channels (Dobrin, 1976), while the coherent noise is attenuated as a function of its apparent velocity. However, as we can see from figures 3.18 through 3.20, primary
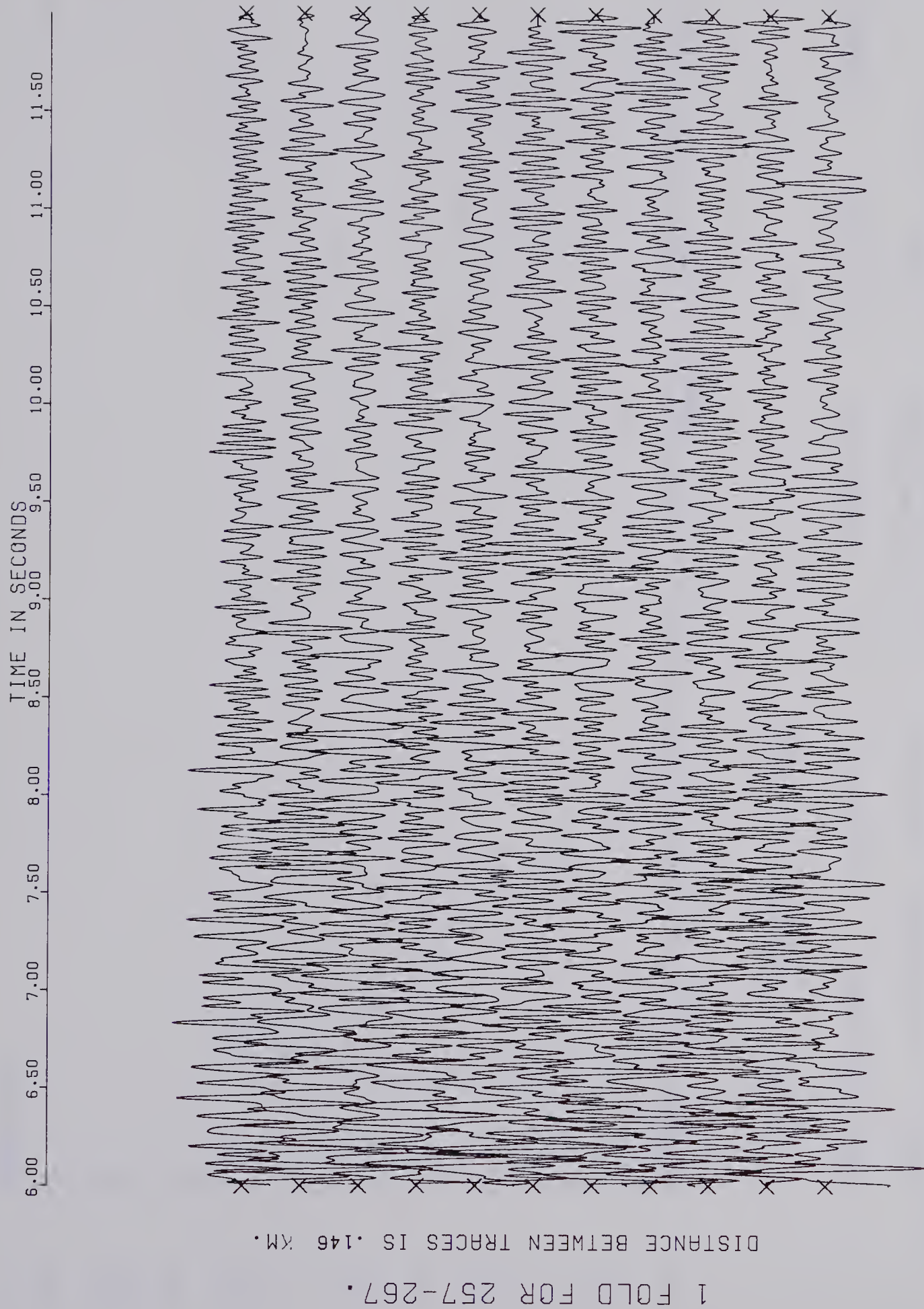
Figure 3.20: A one-fold stack for subsurface points 257 through 267.
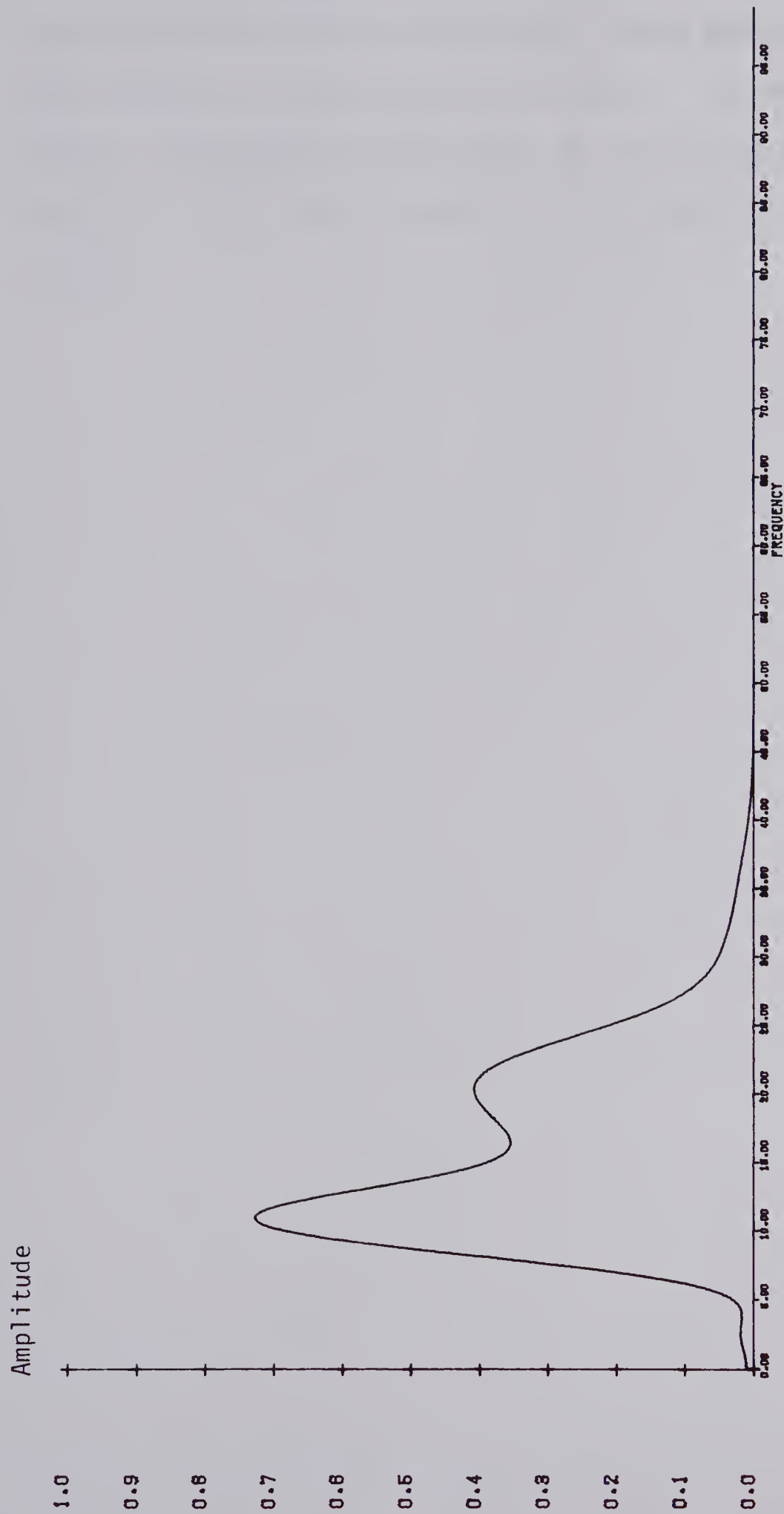
C.D.P.-POWER:6.6S.

AMPLITUDE MAX: 1.818E+07   MIN: 8.690E-02   MID VALUE: 9.088E+06

SCALE: 2.500E+06 UNITS/CM   NO. DATA POINTS: 2048

Figure 3.21: Average power of the 6.6 second pulse for subsurface points 257 through 267.

reflections are still somewhat obscure, and we would hope
to be able to enhance the signals even more. This will be
the subject of the following chapter. In order to apply
signal enhancement techniques to the stacked data, the
stacked traces were normalized with respect to one
another.

CHAPTER 4
MULTICHANNEL SIGNAL ENHANCEMENT TECHNIQUES

4.1. The Velocity Filter

Velocity filters are a class of two dimensional linear operators which are used to extract the desired signals from a background of coherent noise. The filter operates in the frequency and wave number space, and thus requires a spatial array of detectors (Kanasewich, 1975). In the design of the filter, it is assumed that both the signal and noise are perfectly coherent plane-waves, but arrive at the detectors with different apparent velocities. These filters have been applied in exploration seismology for many years, and have been termed pie-slice, fan, velocity or beam-forming filters.

The operation of a velocity filter may be stated quite briefly. By applying a two dimensional space-time operator in the frequency-spatial frequency domain, all events on a multichannel record, whose apparent velocities range from -V to +V are passed. Thus, the desired transfer function is

$$Y(f,k) = 1 \qquad \frac{-|f|}{V} \le K \le + \frac{|f|}{V} \qquad 4.1.1$$

$$= 0 \qquad \frac{-|f|}{V} > K > \frac{|f|}{V}$$

where K, the spatial frequency, is given by

$$K = \frac{|f|}{V} = \frac{\lambda}{2\pi} \hspace{4cm} 4.1.2$$

where λ is the wave number.

Figure 4.1 illustrates this ideal transfer function.

The impulse response of the filter is determined by the application of the two dimensional inverse Fourier transform on the transfer function (Kanasewich, 1975).

$$W(t,X) = \int_{-\infty}^{\infty} \int_{-\infty}^{\infty} Y(f,K) \ e^{2\pi i (ft - KX)} dKdf. \hspace{2cm} 4.1.3$$

The frequency limits are given by the Nyquist limits

$$\frac{-1}{2\Delta X} < K_N < \frac{1}{2\Delta X} \hspace{4cm} 4.1.4$$

$$\frac{-1}{2\Delta t} < f_N < \frac{1}{2\Delta t}$$

where ΔX is the detector spacing and Δt is the sampling interval. The time delay to the nth sample point is

$$Tn = n\Delta t \hspace{4cm} 4.1.5$$

and, the distance to the mth detector from the center of the recording array is

$$Xm = (m + \frac{1}{2})\Delta X \hspace{4cm} 4.1.6$$
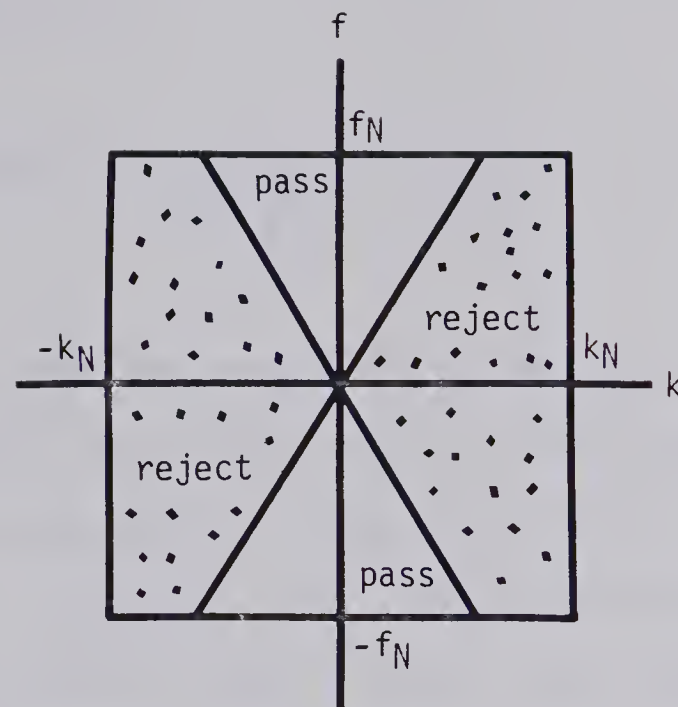
k=spatial frequency
k_N=Nyquist spatial frequency

f=frequency
f_N=Nyquist frequency

In the pass region, $Y(f,k)=1$
In the reject region, $Y(f,k)=0$

Figure 4.1: The velocity filter transfer function.

Utilizing equations 4.1.3 through 4.1.6, Embree *et al.* (1963) have shown that the impulse response of the filter may be expressed as

$$W(Tn,Xm) = \frac{1}{\pi^2 \left\{ \left(\frac{Xm}{\Delta X}\right)^2 - n^2 \right\}} \qquad 4.1.7$$

This impulse response is time and space symmetric, has zero-phase shift, and may be convolved with the original traces to produce a velocity filtered record (Kanasewich, 1975). However, this classical method is time consuming, as for N input traces, N/2 convolutions must be performed to produce an output trace. To reduce the computational time, Treitel *et al.* (1967) transformed the filter equations into the Z domain, and then made use of a recursive relation (Shanks, 1967) so that only one convolution is required for each output trace. Figure 4.2 depicts this algorithm, and is explained as follows. Each input trace from a given record containing an even number of equally spaced traces is subjected to two time shifts. From this pair of traces, a difference trace is evaluated, and the appropriately weighted difference traces are then summed. The resulting single output trace is then convolved with the filter operator producing the desired output trace. This algorithm is easily programmed, and computationally far less time consuming.

During the course of his Ph.D. thesis at the
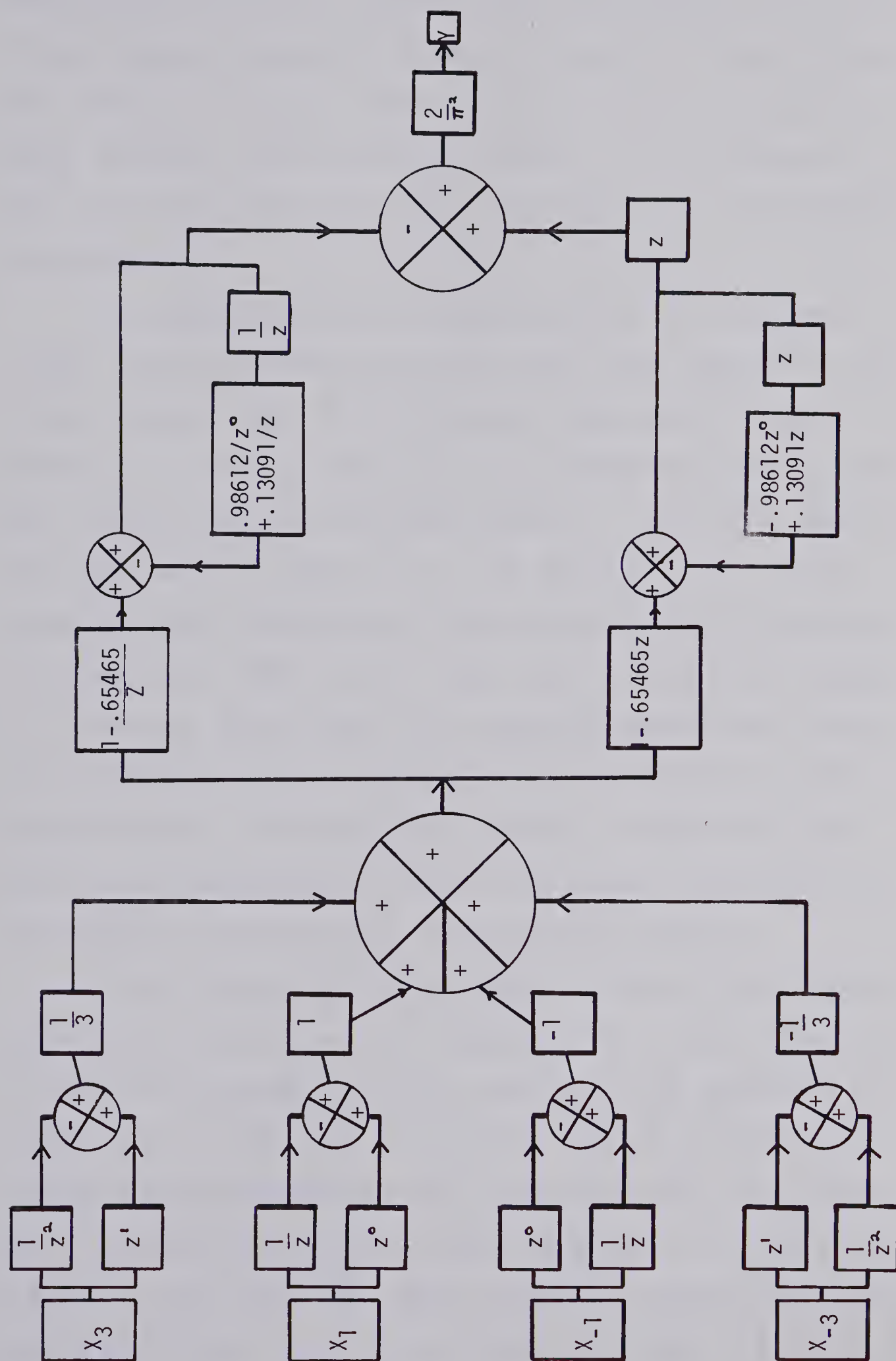
Figure 4.2: A four channel velocity filter (after Kanasewich,1975).

University of Alberta, Clowes (1969) developed a velocity filter program (appendix 3) which allowed a filter with an even number of traces. Due to the subsurface coverage being anywhere from 300 to 700 percent, it was decided that the application of a four trace fan-pass filter would be sufficient.

To demonstrate the effectiveness of the fan-pass filter, seven different dipping events with apparent velocities ranging from 12.2 kilometers persecond through an infinite apparent velocity to -12.2 kilometers per second were constructed in the input channels. These are shown in the upper part of figure 4.3. The three sets of traces below the input channels are the result of applying three different pass bands to the input data. From the diagram, it is obvious that events with apparent velocities within the specified range are passed without distortion, while those outside of the range are greatly attenuated. An event which propagates at one of the cutoff velocities is attenuated in amplitude by approximately one-half.

The velocity filter was then applied to the common depth point stacked data of figures 3.17 to 3.20. Velocity filtered seismograms for these data sets are contained in figures 4.4 to 4.7. In the shallow section of figure 4.4, a very strong reflection can be seen at about 6.6 seconds (A). This event can also be seen on figures 4.5 (B) and 4.6 (A). From the plots, this reflection appears to result from a horizontal layer in the Earth in figure 4.4 and 4.5,

Figure 4.3: Application of an eight channel velocity filter to synthetic data. Three different pass bands are applied to the data.

TIME IN SECONDS

0.00   0.63   1.27   1.90   2.54   3.17   3.81   4.44   5.08   5.71   6.35   6.98   7.62

PULSE: TEST SUITE 1

DISTANCE BETWEEN TRACES IS .146 KM.

VELOCITY FILTERED DATA

TIME IN SECONDS

0.00   0.63   1.27   1.90   2.54   3.17   3.81   4.44   5.08   5.71   6.35   6.98   7.62

$V1_{APP}$ IS 36.6 K/S
$V2_{APP}$ IS 12.2 K/S

$V1_{APP}$ IS -36.6 K/S
$V2_{APP}$ IS 36.6 K/S

$V1_{APP}$ IS -12.2 K/S
$V2_{APP}$ IS -36.6 K/S

Figure 4.4: Application of a four channel velocity
             filter to the stacked data for subsurface
             points 169 to 183. The deeper section (12 to
             18 seconds) is amplified five times. Coherent
             energy may be seen above A, B, C, and D.

Figure 4.5: Application of a four channel velocity filter to the stacked data for subsurface points 257 to 267. The deep section is amplified 2.5 times.

Figure 4.6: A four channel velocity filter as applied to the
stacked data for subsurface points 381 to 391. The
deep section is amplified five times.

and from a westerly dipping layer in figure 4.6. A westerly dipping event at about 8.1 seconds is strongly seen on figures 4.4 (B) and 4.5 (A), but is somewhat obscure on figure 4.6 (B). Other coherent phases of lesser amplitude are seen throughout the filtered sections, but these are likely due to random noise producing a coherent line up of energy, or is what is left of multiple reflections after attenuation in the C.D.P. stack.

In the deeper regions of the velocity filtered sections, coherent energy can be seen at about 12.5 seconds (pulse C) on all of figures 4.4 through 4.6. From the pie-slice, this event is dipping to the east on figures 4.5 and 4.6, and to the west on figure 4.4. Other deeper events appear to exist on the section, notably around 14 seconds (pulse D).

Figure 4.7 exhibits the results of velocity filtering the traces belonging to shot 144 (figure 3.20), that is, using only one-fold coverage. The traces were taken from subsurface points 257 to 267, whose velocity filtered section may be seen in the first half of figure 4.5. The good quality reflections at 6.6 (B) seconds is still enhanced, while the dipping event at 8.1 (A) seconds is only partially brought out. Other coherent phases can be seen at 9.3 and 11.6 seconds. These events can also be located on figure 4.5, but they are of far less amplitude. Thus, it is believed that these two events are the result of multiply reflected energy from a shallower horizon.
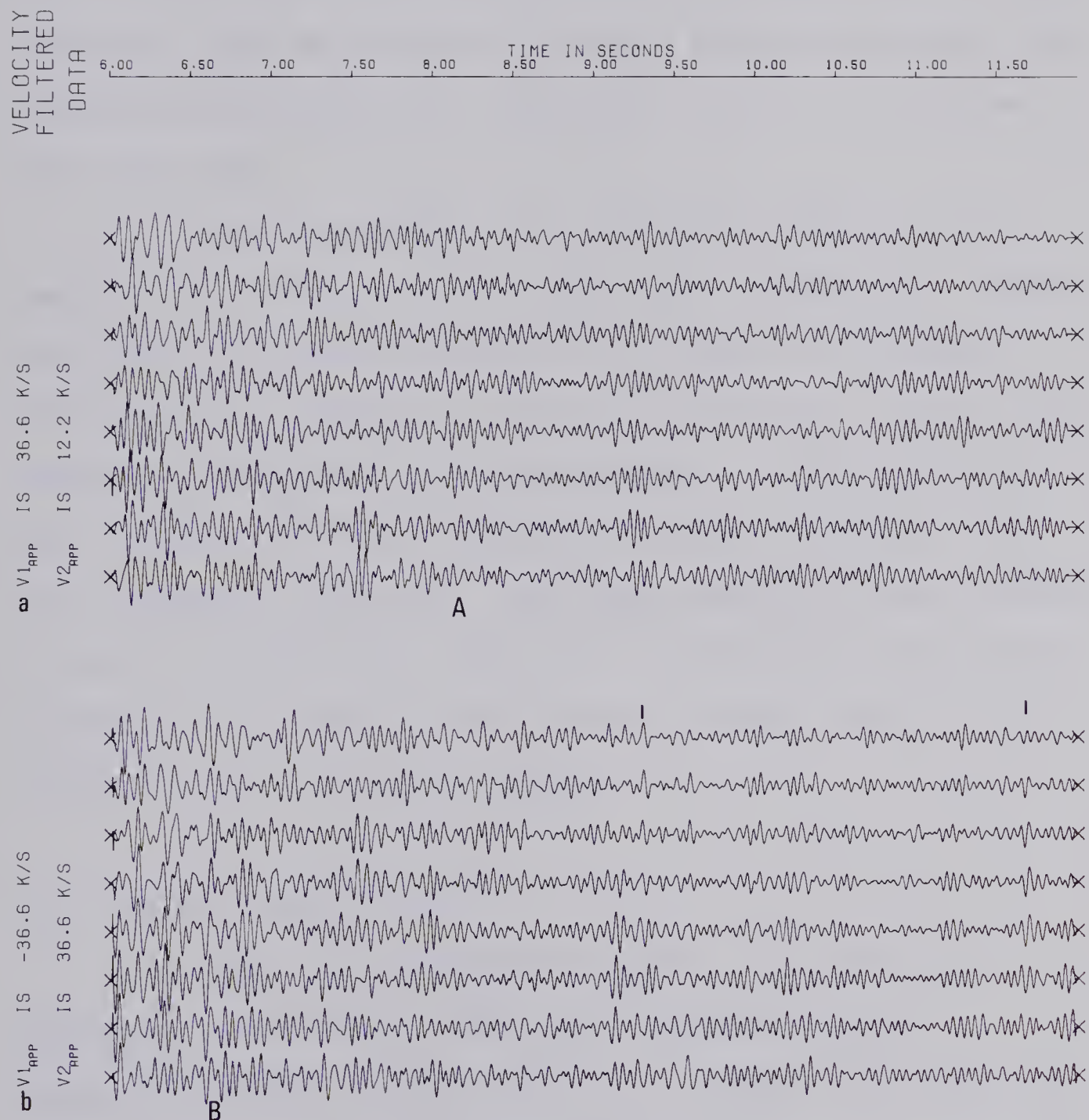
Figure 4.7: The velocity filtered section for the data of figure
3.20. Reflected events are seen at A and B, with possible
multiple reflections beneath the two 'I's.

When stacked with other traces of varying shot to detector distances, they are not quite in time alignment, and are thus severely attenuated. However, when taken alone, multiple reflections along adjacent traces would appear to have arrived with some apparent velocity across the spread. Therefore, when we velocity filtered the data section, the multiple reflections were enhanced, and are of relatively high amplitude.

The fan-pass filter can clearly be seen to have improved the quality of the reflection seismograms. Reflected events occurring around 6.6, 8.1 and 12.5 seconds, which had been obscured by noise on the C.D.P. stacks, were enhanced greatly on all three sections. With this technique, not only are the primary reflections enhanced, but their apparent velocities, and thus the dips of the horizons are easily determined. Therefore, through the use of this technique, it should be fairly easy to detail the crustal structure of a particular region.

4.2   The N-th Root stack

A method of non-linear velocity filtering was developed by Muirhead (1968), and expanded upon by Kanasewich *et al*. (1973), which they termed the N-th root stack. Basically, the filter involves the extraction of the N-th root of each element in all of the traces, where N is any positive integer. The traces are then summed and raised back up to the N-th power. The filter was shown to

be effective in removing random noise, with the effective-
ness increasing with the number of channels. For a delta
function noise spike, the rejection varies approximately
as K^{-N}, where K is the number of channels. Unlike linear
filters, one cannot obtain an impulse response or a
transfer function. Also, the output of the filter is dis-
torted to some degree.

The N-th root stacking filter may be mathematically
expressed as

$$Yiv = Riv|Riv|^{N-1} \qquad 4.2.1$$

where

$$Riv = \frac{1}{\sum_{j=1}^{K} W(j)} \sum_{j=1}^{K} \frac{X(i+\tau_j),j}{|X(i+\tau_j),j|} \left[\frac{GW(j)}{G(j)} |X(i+\tau j),j| \right]^{1/N} \qquad 4.2.2$$

with

Yiv = single channel output

X(i),j = ith data point on the jth channel

N = any positive integer

K = number of channels

G = common gain for normalization

G(j) = gain of the jth channel

W (j) = weighting coefficient for the jth channel

Also, we have

$$\tau_j = \frac{D_j}{V} \hspace{4cm} 4.2.3$$

where

D_j = distance from array center to jth detector

V = apparent velocity of the wave

In the case of normalized common depth point data, these equations reduce to

$$Yiv = \left[\frac{1}{K} \sum_{j=1}^{K} \frac{X(i+\tau_j),j}{|X(i+\tau_j),j|} |X(i+\tau_j),j|^{1/N} \right]$$

$$\times \left[\frac{1}{K} \sum_{j=1}^{K} \frac{X(i+\tau_j),j}{|X(i+\tau_j),j|} |X(i+\tau_j),j|^{1/N} \right]^{N-1}$$

$$4.2.4$$

Thus, we are attempting to enhance particular reflections with particular apparent velocities. If N=1, we obtain a linear 'delay and sum' velocity filter.

Figure 4.8 demonstrates the operation of the filter. The upper part of the figure consists of three examples, each with two input channels. One of the channels (channel 1) contains only signal, whereas channel 2 contains both signal and noise. For only pure signal (case a), it is passed without distortion. In case b, where only noise is present, the effect of increasing the power of the stack is evident. Example c has 90 units of noise added to the signal to make up channel 2, and again we note the effect
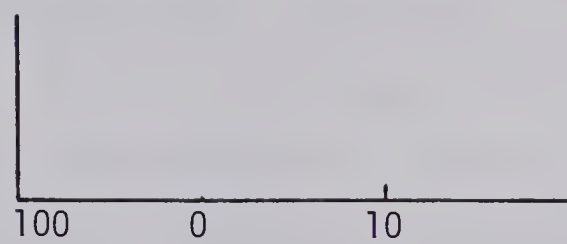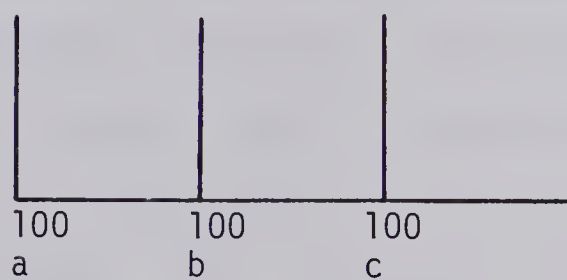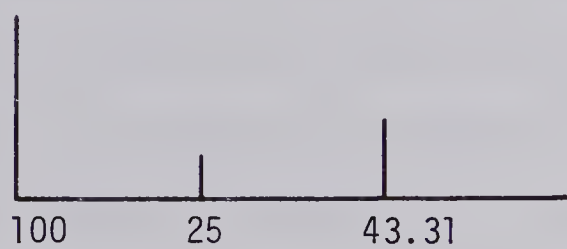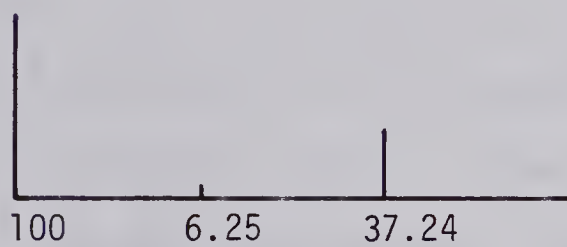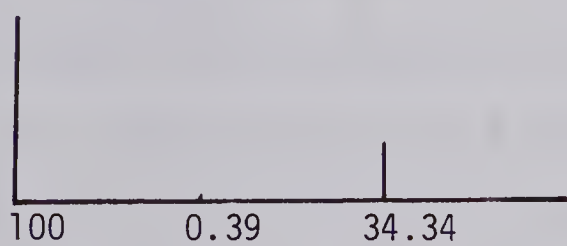
Figure 4.8: The N-th stack as applied to spike model data.

of increasing the power of the stack in reducing the noise.

Figure 4.9 demonstrates the effect of the filter on a synthetic pulse. The input consists of five channels each comprising two input signals. The signals are some-what distorted due to the effect of a slanting noise field arriving with an apparent velocity of five digital points per channel. As we can see, the two input signals are reproduced, with some distortion, with the noise field being totally eliminated. This indicates that this filter may be used to determine the apparent velocities of the arrivals, and thus the dips of the underlying layers.

A program was written which would perform an eight root stack (appendix 3) using the normalized common depth point data as input (shallow sections). The number of channels to use in the stack was chosen to be four (the same as used in the fan-filter), and stepouts were chosen to range from -4 to +4 digital points. The output of this program on the C.D.P. traces 169 to 183 is seen in figure 4.10. We see that strong arrivals occur at stepouts equal to zero and three, for reflections at 6.6 (A) and 8.1 (B) seconds. The signals are a bit distorted, but the noise is so well destroyed that the exact timing of the reflection is possible. For stepout equal to zero, the slight jump of the pulse between output channels 8 and 9 is very noticeable, and very accurately timed. This jump can also be seen on the velocity filter plots (figure 3.17), but not quite so clearly.

EIGHTH ROOT STACK.

DISTANCE BETWEEN TRACES IS 0.146 KM
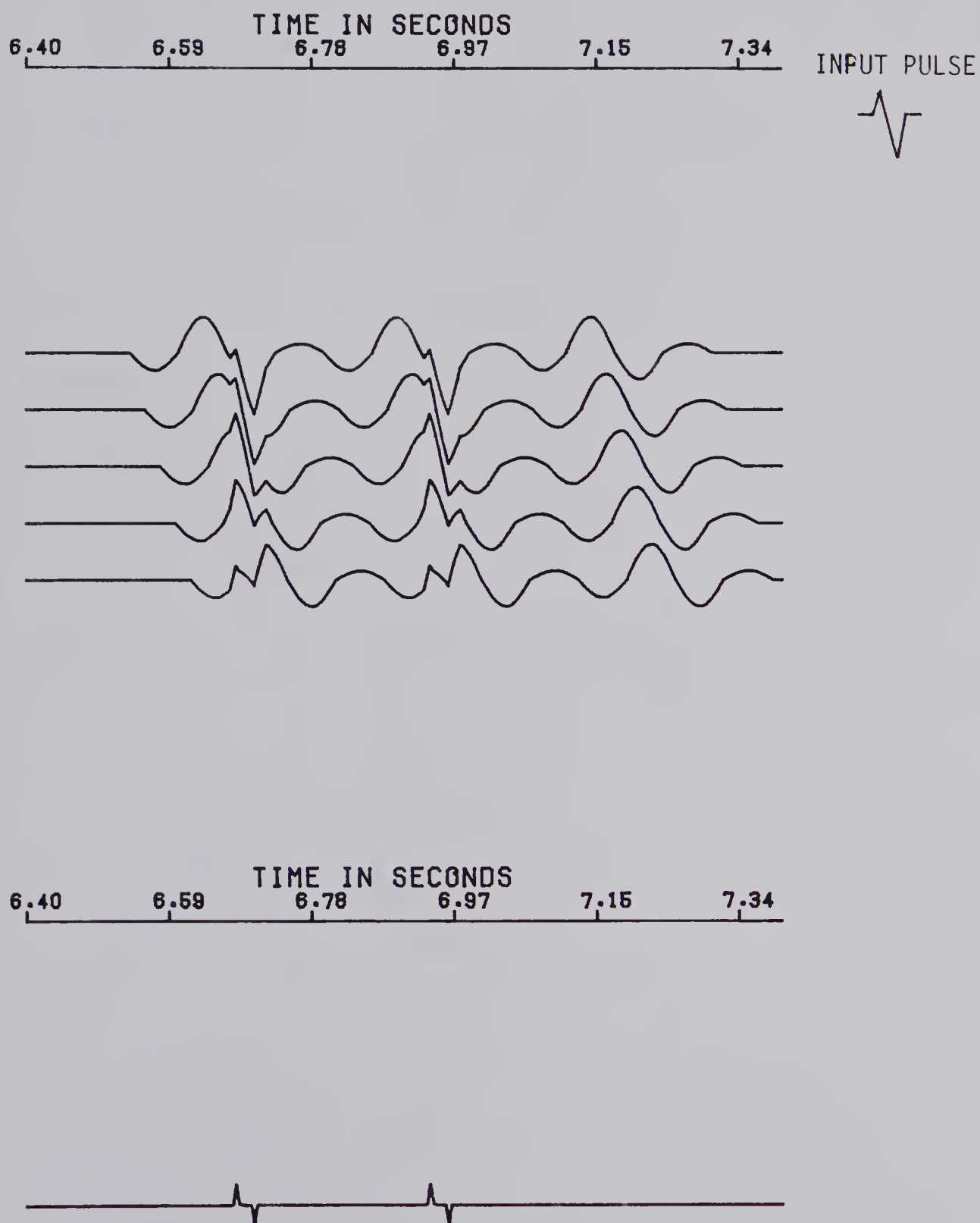
Figure 4.9: Application of an eighth root stack to a spike input pulse
and coherent noise. The noise arrives with an
apparent velocity of five points per trace.
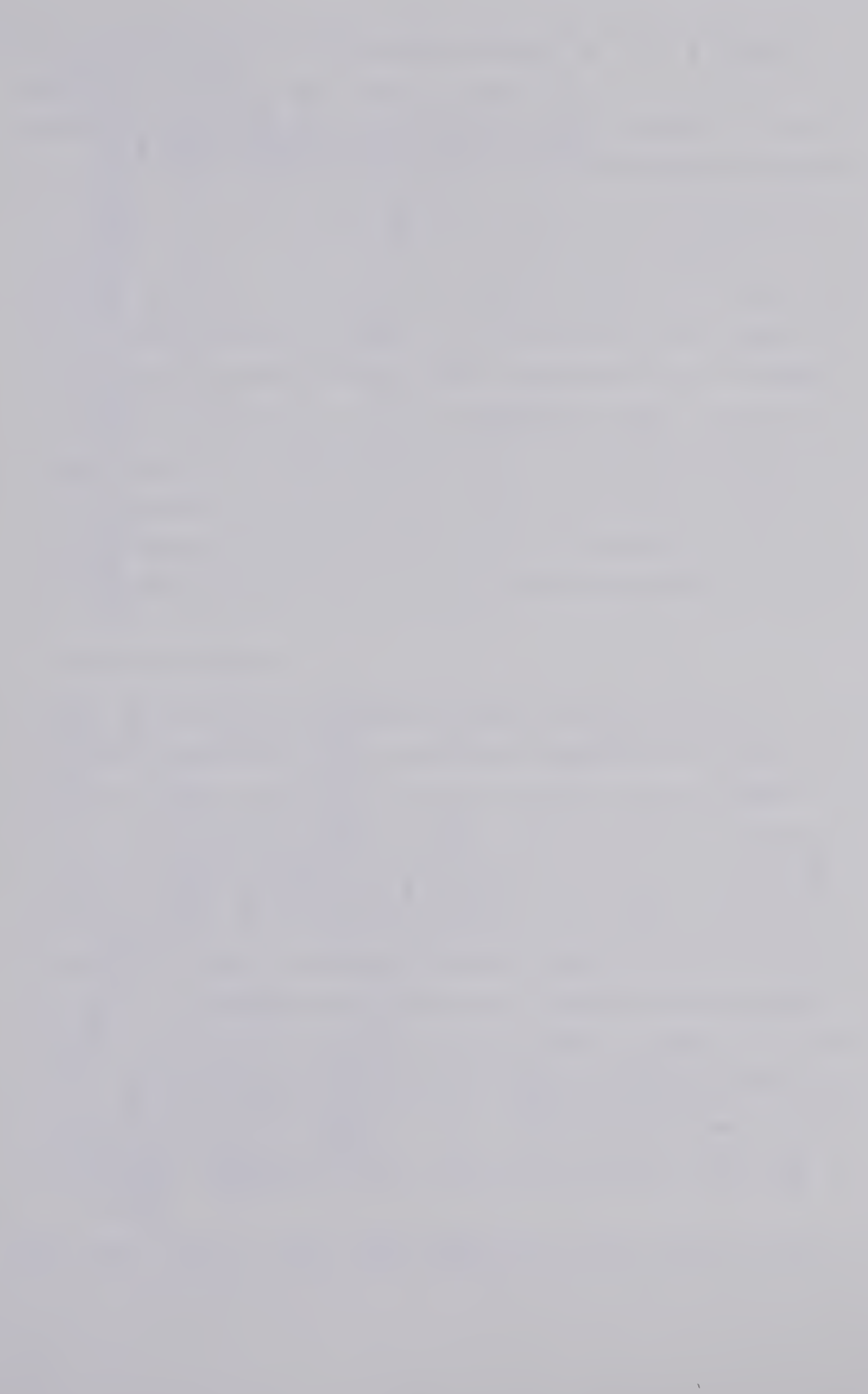
Figure 4.10:   An eight root stack of the stacked data for
               subsurface points 169 to 183.   Coherent
               energy may be seen above A and B.

a NTHROST STACK C.D.P. 189-193 STEPOUT=0

A

b NTHROST STACK C.D.P. 189-193 STEPOUT=3

B
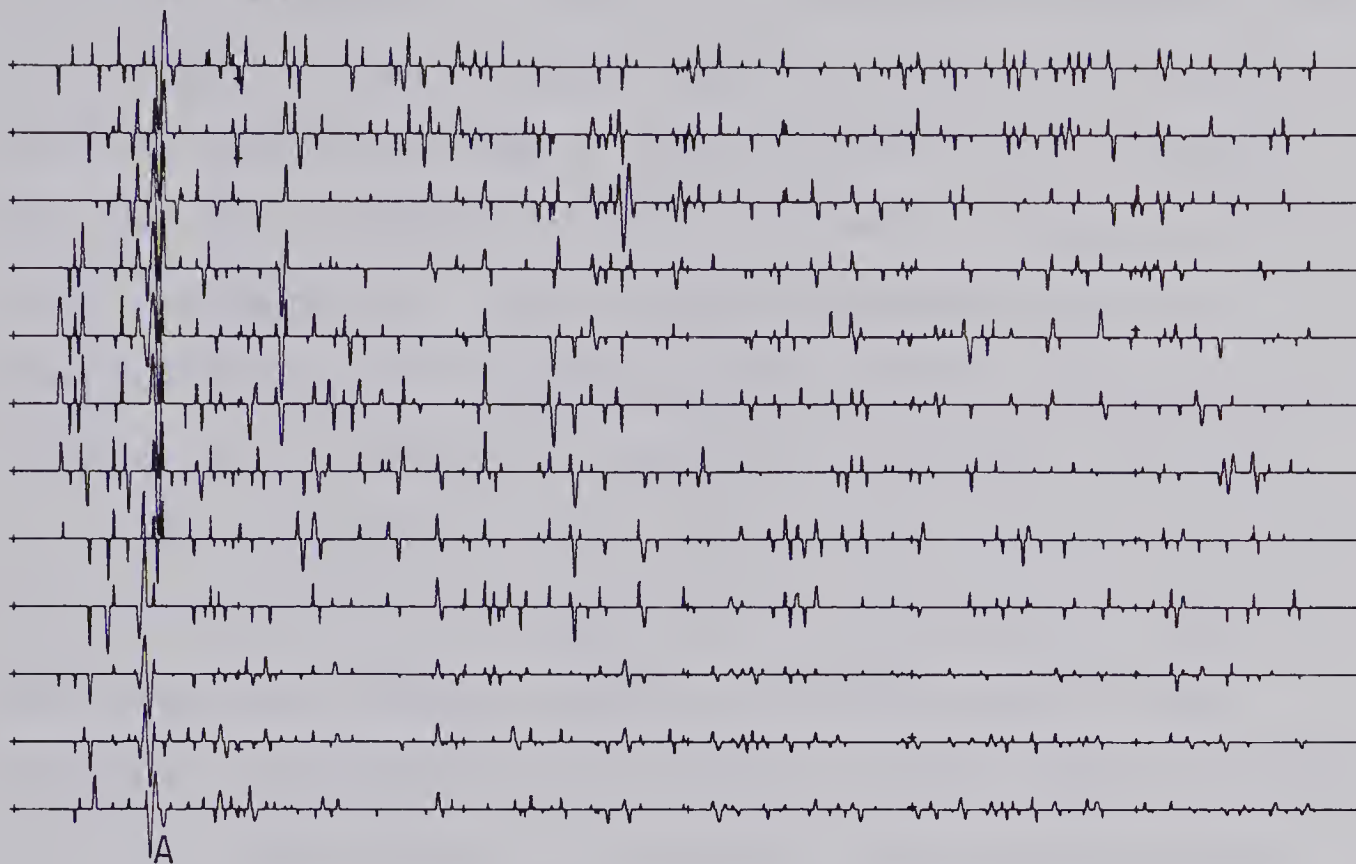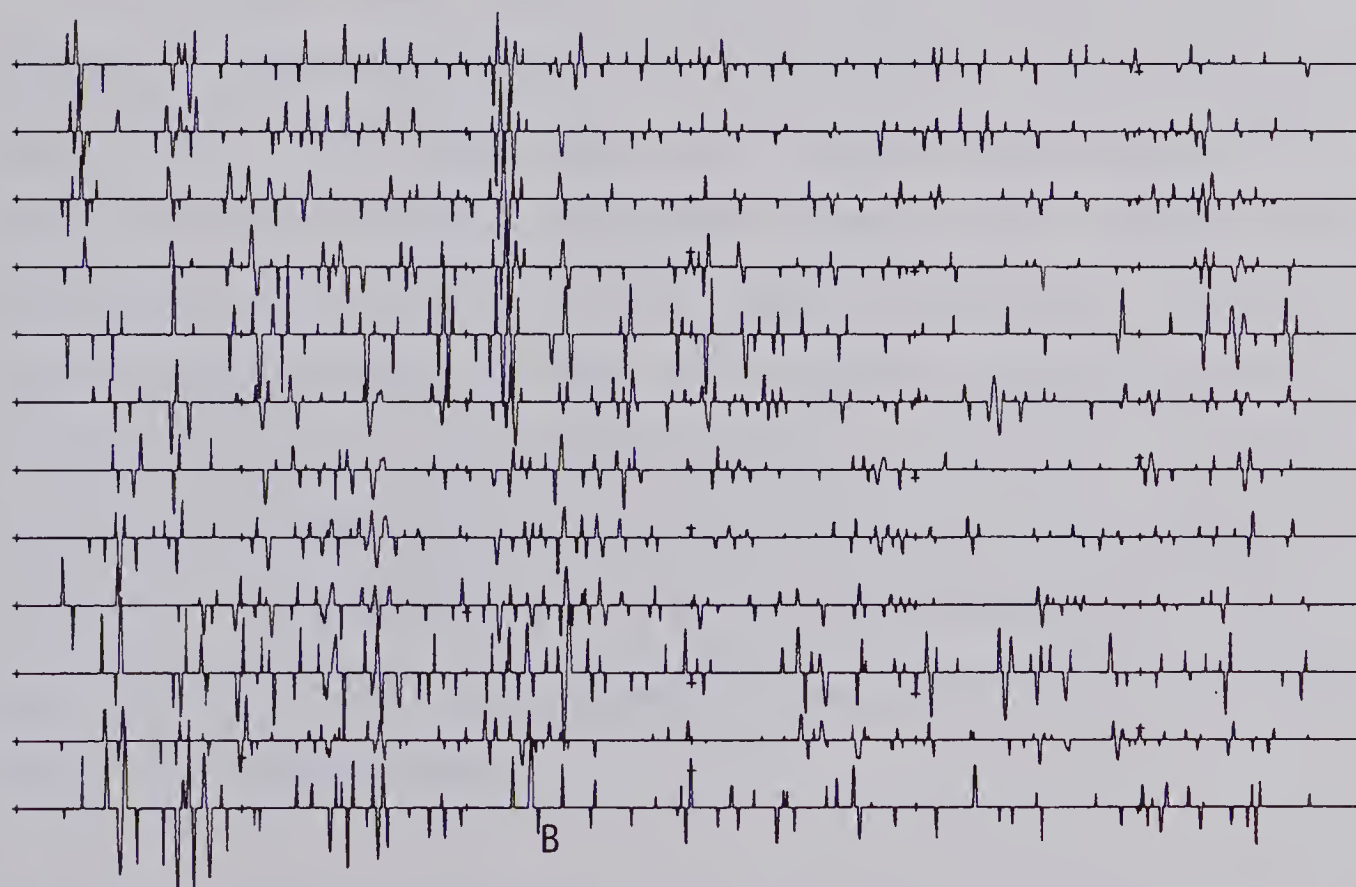
TIME IN SECONDS

6.00   6.50   7.00   7.50   8.00   8.50   9.00   9.50   10.00   10.50   11.00   11.50

The output of the filter for subsurface points 257 to 267 may be seen in figure 4.11, and may be compared with the velocity filtered output seen in figure 3.18. Again, for zero stepout we have a strong arrival at 6.6 seconds (A); and for a stepout of three, we have a strong arrival at 8.1 seconds (B). These events are quite clear in figure 3.18, but the remaining noise which is also seen in figure 3.18 is much more reduced by the eight root stack.

For subsurface points 381 to 391, the action of the filter may be seen in figure 4.12. With stepout equal to three, we have coherent energy at 6.7 (A) and 8.3 (B) seconds. The pulse at 6.7 seconds is quite clear on figure 3.19, but the event at 8.3 seconds is barely noticeable.

The N-th root stack, multichannel filter is very useful in enhancing seismic reflection data. The effective-ness of the filter increases with increasing power of the stack, and the filter effectively removes both random noise and noise arriving with finite apparent velocity. In the case of the fan-pass filter, the apparent velocity of the arriving wave may be determined within a certain pass band. However, with the N-th root stacking filter, the apparent velocity of the arrivals may be determined exactly. This great resolution is very important when dealing with reflec-tions from dipping beds.

4.3. Multichannel Adaptive Filter Theory

The two main types of adaptive multichannel filters
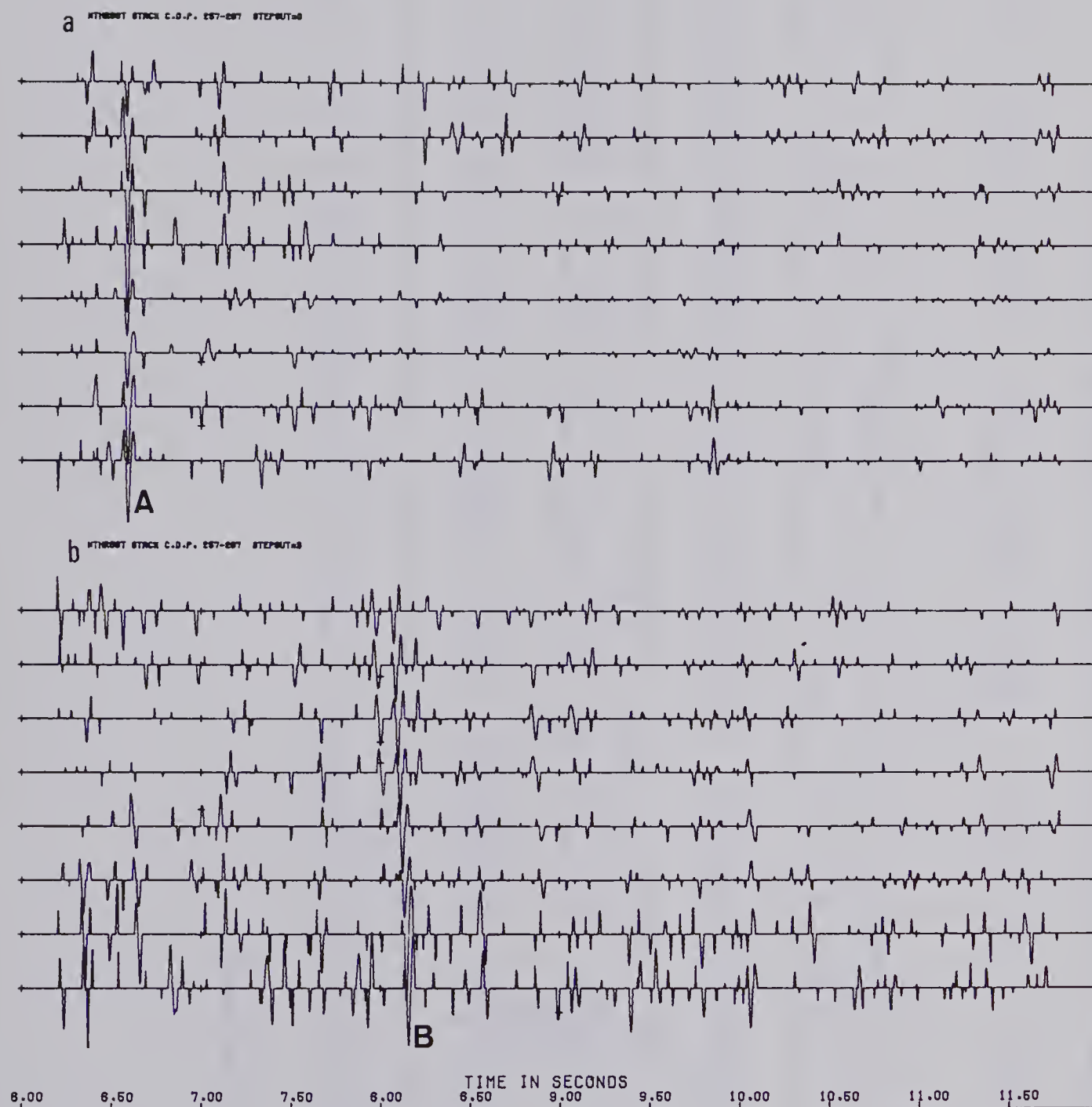
Figure 4.11: The eight root stack as applied to the stacked data for subsurface points 257 to 267.
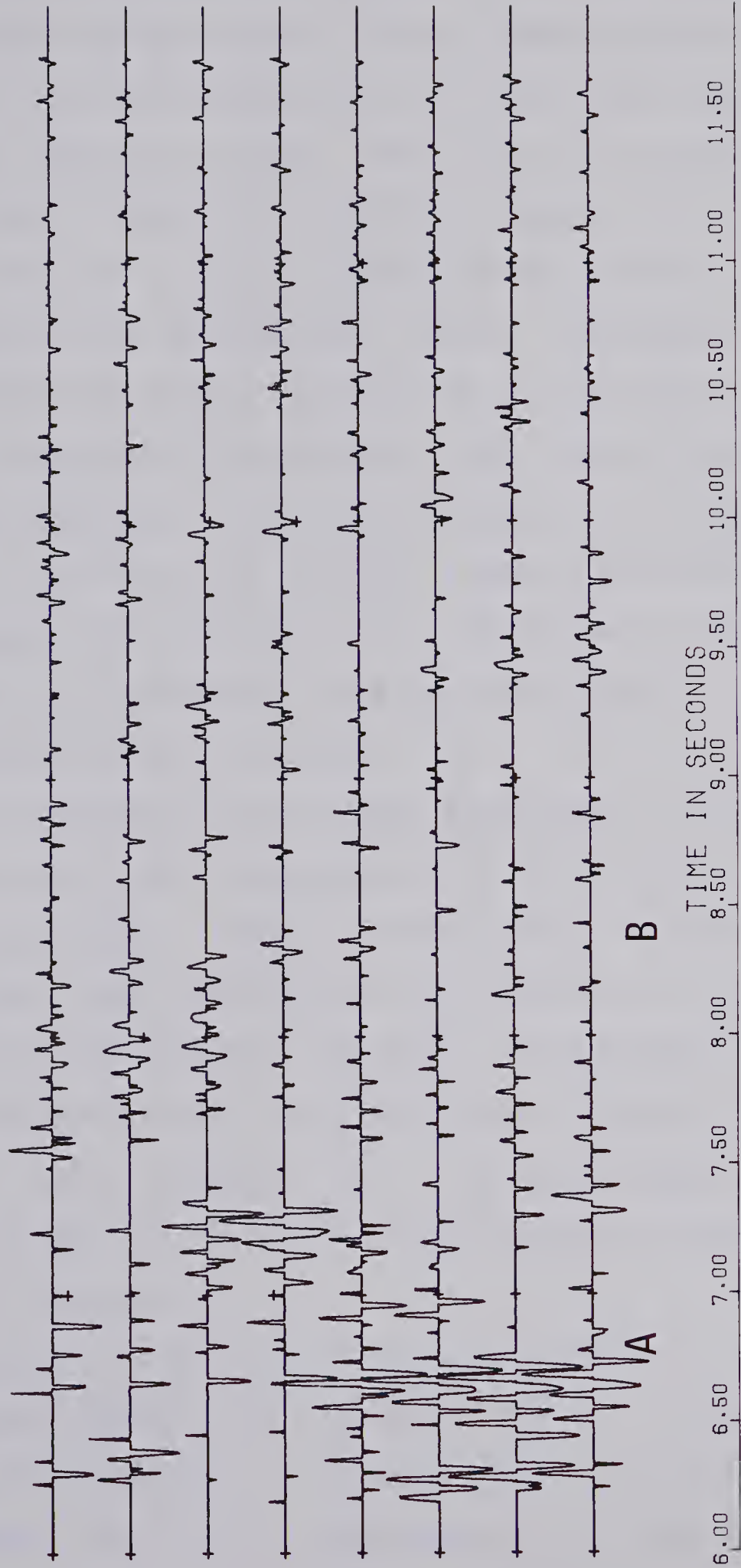
Figure 4.12: Application of an eight root stacking filter on the stacked data for subsurface points 381 to 391.

applied to reflection seismic information are the maximum
likelihood filter and the Wiener filter. Adaptive multi-
channel filters are constructed from the input data, which
is often common depth point data. Utilizing the autocor-
relation and cross correlation statistics between the
input traces, the Wiener filter compresses the unknown
signal to a delta function (Mercado, 1973). Therefore,
primary reflected energy will be noted by a significant
peak in the zero lag cross correlation term. On the other
hand, maximum likelihood filters are constructed to detect
coherent signal arriving with infinite apparent velocity
across the spread, and to minimize the output power of the
traces. Random noise and noise arriving with finite
apparent velocity are thus reduced.

Maximum likelihood filters were developed to analyze
data obtained from nuclear blast detectors in Arizona and
Montana (Mercado, 1978). The multichannel data is first
studied for event free time windows near intervals of sig-
nal. Through various digital techniques, the coherent
signals are adjusted to have the proper time alignment.
Then, using the noise interval, the filter is designed,
and subsequently applied to a time window containing both
the signal and the noise.

Multichannel filtering is a process that makes use
of data recorded digitally on K channels, $X_1(t),...,X_K(t)$,
where each $X_i(t)$ represents one channel of seismic data.
A digital seismic trace may be represented by a finite

series of real numbers which are samples of the seismic
energy being recorded at a constant time interval Δt.

The autocorrelation of each $X_i(t)$ is defined to be

$$r_\tau = \frac{1}{N} \{X_i(t) \cdot X_i(t-\tau)^T\} \qquad \tau = 0, \pm 1, \pm \ldots \qquad 4.3.1$$

where N is the number of samples of $X_i(t)$ and '·' indicates
inner product and 'T' means transpose.

The cross correlation between any two seismic
channels $X_i(t)$ and $X_j(t)$ is defined to be

$$g_\tau = \frac{1}{N} \{X_i(t) \cdot X_j(t-\tau)^T\} \qquad \tau = 0, \pm 1, \pm \ldots \qquad 4.3.2$$

In the multichannel case, we can represent the multichannel
data by a column vector $X(t)$ (Wiggins *et al.*, 1965)

$$X(t) = (X_1(t), \ldots, X_K(t))^T. \qquad 4.3.3$$

The multichannel autocorrelation function now
becomes

$$r_\tau = \frac{1}{N} \{X(t) * X(t-\tau)^T\} \qquad \tau = 0, \pm 1, \pm \ldots \qquad 4.3.4$$

where '*' indicates matrix multiplication. These coeffi-
cients satisfy (Robinson, 1967)

$$r-\tau = r_\tau^T \qquad 4.3.5$$

The multichannel filter is represented by the coefficients $\bar{f}(0),\ldots,\bar{f}(\tau)$, where each $\bar{f}(i)$ is a $K\times1$ matrix. The multichannel signal is the input to the filter with the resulting single channel output, $O(t)$. To obtain the output, one must convolve the input, $X(t)$, with the filters.

$$O(t) = X(t)\overset{T}{*} \bar{f}(0) + \ldots + X(t-\tau)\overset{T}{*} \bar{f}(\tau). \qquad 4.3.6$$

Using appendix 1, equation 4.3.6 may be rewritten as

$$O(t) = X_1(t-\tau)*f_1(\tau) + \ldots + X_K(t-\tau)*f_K(\tau) \qquad 4.3.7$$

where each $f_j(\tau)$ is a $(\tau+1)\times1$ matrix.

If the filter is to pass coherent signal between input channels undistorted, then the sum of the filters must be a delta function (Mercado, 1978).

$$f_1(\tau) + \ldots + f_K(\tau) = \delta(\tau) \qquad 4.3.8$$

or

$$f_1(\tau) = \delta(\tau) - f_2(\tau) - \ldots - f_K(\tau). \qquad 4.3.9$$

Substituting 4.3.9 into 4.3.7,

$$O(t) = X_1(t-\tau)*\{\delta(\tau)-f_2(\tau)-\ldots-f_K(\tau)\}+\ldots+X_K(t-\tau)*f_K(\tau)$$

$$= X_1(t)-X_1(t-\tau)*f_2(\tau)-\ldots-X_1(t-\tau)*f_K(\tau)+\ldots$$

$$+X_K(t-\tau)*f_K(\tau)$$

$$= X_1(t)+[X_2(t-\tau)-X_1(t-\tau)]*f_2(\tau)+\ldots$$

$$+[X_K(t-\tau)-X_1(t-\tau)]*f_K(\tau). \qquad 4.3.10$$

Therefore,

$$O(t) = X_1(t)+\Delta_2(t-\tau)*f_2(\tau)+\ldots+\Delta_K(t-\tau)*f_K(\tau) \qquad 4.3.11$$

where $\Delta_i(t-\tau) = X_i(t-\tau) - X_1(t-\tau)$.

The output power is given by $O(t)^T*O(t)$, and the minimization of this power will yield the least-squares solution for $f_2(\tau),\ldots,f_K(\tau)$ (see appendix 2 for details regarding the three channel case). The resulting simultaneous equations necessary to obtain the filter coefficients are of the form,

$$\begin{bmatrix} r_0 & r_1 & \cdots & r_\tau \\ r_{-1} & r_0 & \cdots & r_{\tau-1} \\ & \vdots & & \vdots \\ r_{-\tau} & & \cdots & r_0 \end{bmatrix} \begin{bmatrix} \bar{f}(0) \\ \cdot \\ \cdot \\ \cdot \\ \bar{f}(\tau) \end{bmatrix} = - \begin{bmatrix} g_0 \\ \cdot \\ \cdot \\ \cdot \\ g_\tau \end{bmatrix} \qquad 4.3.12$$

where the first matrix is the multichannel autocorrelation matrix of the differences traces $\Delta_2(t-\tau),\ldots,\Delta_K(t-\tau)$. From equation 4.3.5, we note that this matrix is Toeplitz in form. Each of the elements, r_τ, is a $(K-1) \times (K-1)$ matrix. The matrix elements $\bar{f}(o),\ldots,\bar{f}(\tau)$ are $(K-1) \times 1$ matrices representing the filter, and the matrix elements $g_0,\ldots,g_\tau$ are $(K-1) \times 1$ cross correlation terms between the first channel, $X_1(t)$, and $\{\Delta_2(t-\tau),\ldots,\Delta_K(t-\tau)\}$.

The solution of this set of simultaneous equations gives the coefficients $\bar{f}(o),\ldots,\bar{f}(\tau)$, which are related to $f_2(\tau),\ldots,f_K(\tau)$ by

$$\bar{f}(j) = f_2(j),\ldots,f_K(j) \qquad j=0,\ldots,\tau \qquad 4.3.13$$

Thus, using equation 4.3.11, we are able to obtain a filtered output channel. A three channel maximum likelihood filter program was written based on appendix 2.

Figure 4.13 demonstrates the action of a two channel maximum likelihood filter on a simple spike model. A simple stack of the channels yields a 2 to 1 signal to noise ratio (SNR). If we apply a three filter operator to the channels, as depicted in the figure, we obtain an output channel with a 4 to 1 signal to noise ratio. We also note that the noise has now been spread over four samples.

At first, an attempt was made to calculate $\bar{f}(o)$, $\ldots,\bar{f}(\tau)$ based on an algorithm of Wiggins (1965) which makes

Let $X1(t) = 1,1,0,0,0,0$

$X2(t) = 1,0,1,0,0,0$

$\Delta2(t) = X2(t)-X1(t) = 0,-1,1,0,0,0$

Therefore,

$$\bar{\Delta}^T * \bar{\Delta} = \begin{bmatrix} 0 & -1 & 1 & 0 & 0 & 0 \\ 0 & 0 & -1 & 1 & 0 & 0 \\ 0 & 0 & 0 & -1 & 1 & 0 \end{bmatrix} \begin{bmatrix} 0 & 0 & 0 \\ -1 & 0 & 0 \\ 1 & -1 & 0 \\ 0 & 1 & -1 \\ 0 & 0 & 1 \\ 0 & 0 & 0 \end{bmatrix} = \begin{bmatrix} 2 & -1 & 0 \\ -1 & 2 & -1 \\ 0 & -1 & 2 \end{bmatrix}$$

$$[X1(t)^T * \bar{\Delta}]^T = \bar{\Delta}^T * X1(t) = \begin{bmatrix} 0 & -1 & 1 & 0 & 0 & 0 \\ 0 & 0 & -1 & 1 & 0 & 0 \\ 0 & 0 & 0 & -1 & 1 & 0 \end{bmatrix} \begin{bmatrix} 1 \\ 1 \\ 0 \\ 0 \\ 0 \\ 0 \end{bmatrix} = \begin{bmatrix} -1 \\ 0 \\ 0 \end{bmatrix}$$

Now,

$$\bar{\Delta}^T * \bar{\Delta} * \bar{f} = -[X1(t)^T * \bar{\Delta}]^T$$

Thus,

$$\begin{bmatrix} 2 & -1 & 0 \\ -1 & 2 & -1 \\ 0 & -1 & 2 \end{bmatrix} \begin{bmatrix} f2(0) \\ f2(1) \\ f2(2) \end{bmatrix} = \begin{bmatrix} 1 \\ 0 \\ 0 \end{bmatrix} \rightarrow \begin{array}{l} f2(0)=3/4 \\ f2(1)=1/2 \\ f2(2)=1/4 \end{array}$$

Therefore,

$$O(t) = X1(t) + \Delta2(t-\tau)*f2(\tau) = \begin{bmatrix} 1 \\ 1 \\ 0 \\ 0 \\ 0 \\ 0 \end{bmatrix} + \begin{bmatrix} 0 & 0 & 0 \\ -1 & 0 & 0 \\ 1 & -1 & 0 \\ 0 & 1 & -1 \\ 0 & 0 & 1 \\ 0 & 0 & 0 \end{bmatrix} \begin{bmatrix} 3/4 \\ 1/2 \\ 1/4 \end{bmatrix} = \begin{bmatrix} 1 \\ 1/4 \\ 1/4 \\ 1/4 \\ 1/4 \\ 0 \end{bmatrix}$$

Figure 4.13: The two channel maximum likelihood filter as applied to a spike model.

use of the multichannel autocorrelation matrix being in Toeplitz form. Utilizing an inversion scheme, based on this algorithm, found in Robinson (1967), a program was written to do maximum likelihood filtering. However, this technique did not work at all, and is likely the result of many of the columns in the autocorrelation matrix nearly being equivalent (degenerate matrix). This fact was also noted by Mercado (1978). Attempts at writing higher degree maximum likelihood filter programs were also made (four and five channels), but these also met with failure. Again, this is likely a result of near dependency amongst the columns of the autocorrelation matrix.

Thus, it was found that a three channel maximum likelihood filter was best programmed. The algorithm for solving the simultaneous equations of equation 4.3.12 is contained in the IMSL library of the University of Alberta's computing center, and the complete program is located in appendix 3.

Figure 4.14 shows a test function for the program, and the resulting output. As we can see, the slanting noise events are almost totally annihilated, whereas the coherent signal is well enhanced and accurately reproduced. The filter operator is 40 points in length.

The application of the 40 points, three channel maximum likelihood filter on real data may be seen in figure 4.15. For this section, I chose the eleven sub-surface points 169 to 179, whose C.D.P. stack may be seen

3-CHANNEL FILTER.

DISTANCE BETWEEN TRACES IS 0.146 KM
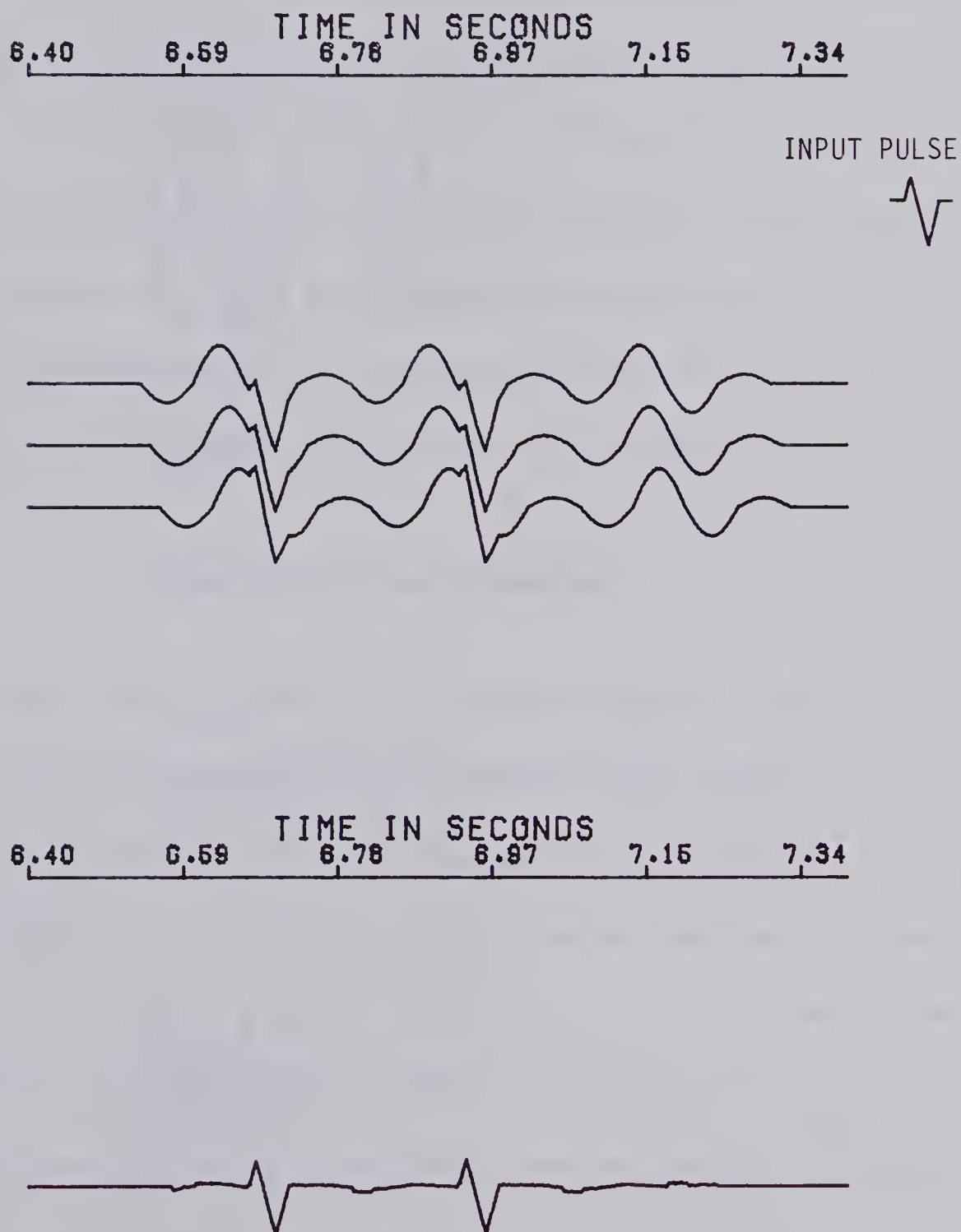
Figure 4.14: A three channel maximum likelihood filter applied to
a spike input pulse and coherent noise. The noise arrives
with an apparent velocity of three points per trace. The
output is amplified five times.
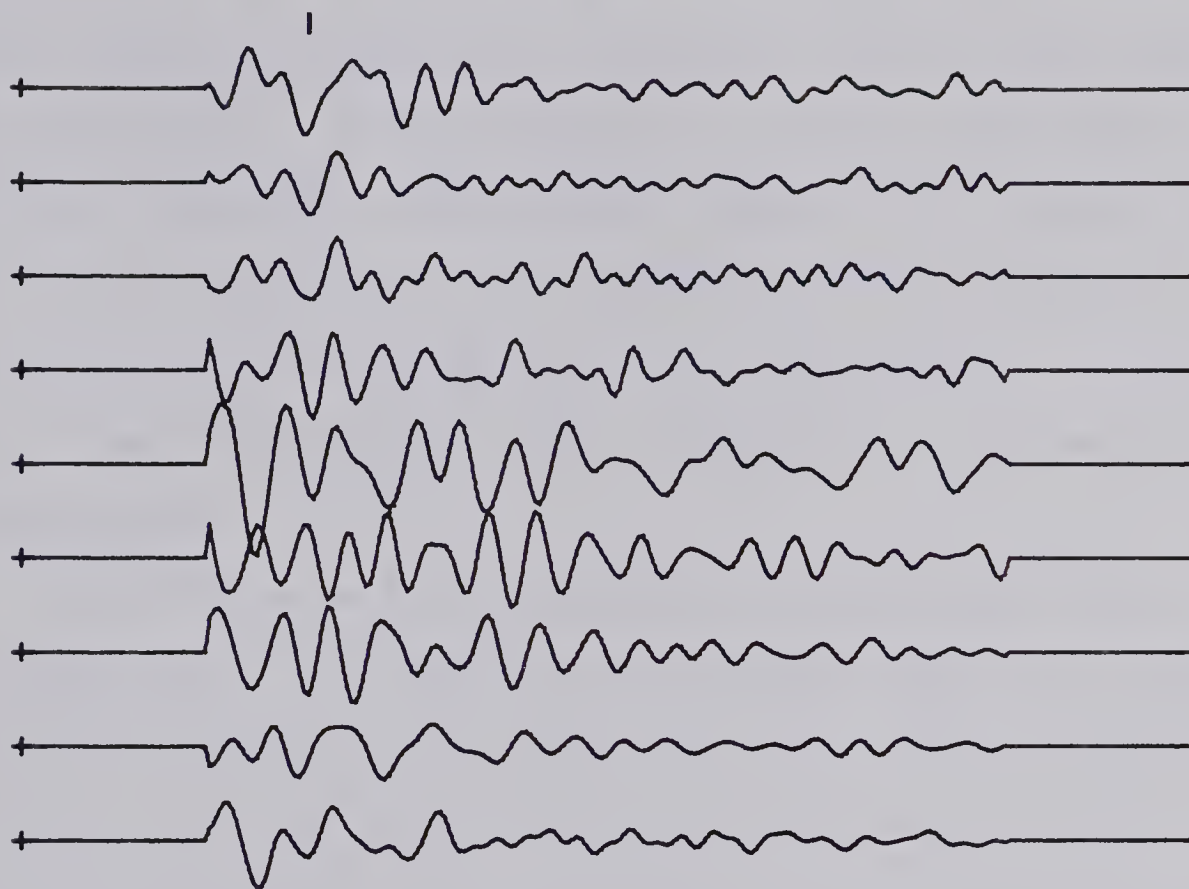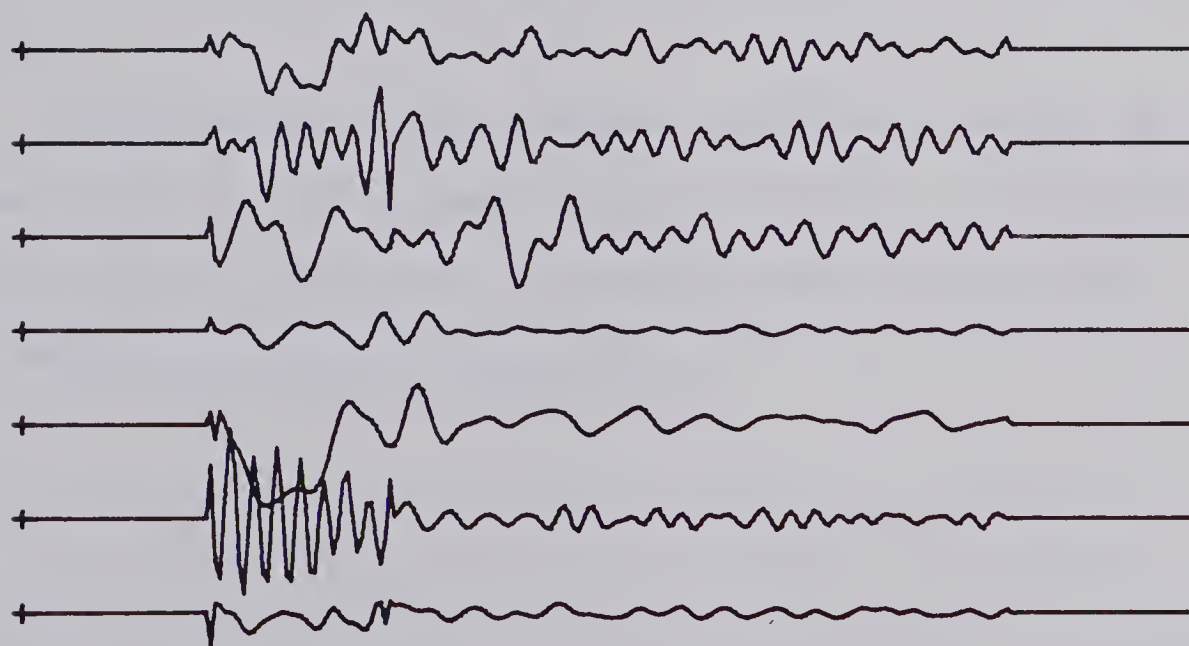
Figure 4.15: Application of a three channel maximum likelihood filter on the data for subsurface points 169 to 183. Coherent energy may be seen beneath the 'I' in the upper half.

in figure 3.17 (shallow section). The top part of the figure exhibits the output after one pass with the filter, and the lower part exhibits the output after another pass with the filter. In the figure, we see that the noise is quite well reduced. The coherent pulse at 6.6 seconds has been enhanced somewhat, but it also has been distorted. The slight step in the pulse is also noticeable. A third pass of the filter on the data resulted in a depreciation of the output.

The filter was also applied to the stacked data corresponding to the shallow section for subsurface points 257 to 267 (figure 3.18), with the result being displayed in figure 4.16. A highly distorted pulse may be seen around 6.6 seconds which corresponds to the input pulse. On the whole, the output is not very good, and further application of the filter to the data did not improve it any more.

Application of the maximum likelihood filter to real seismic data was not deemed very successful. Reflecting events were not enhanced very much, and in some cases, were distorted beyond recognition.
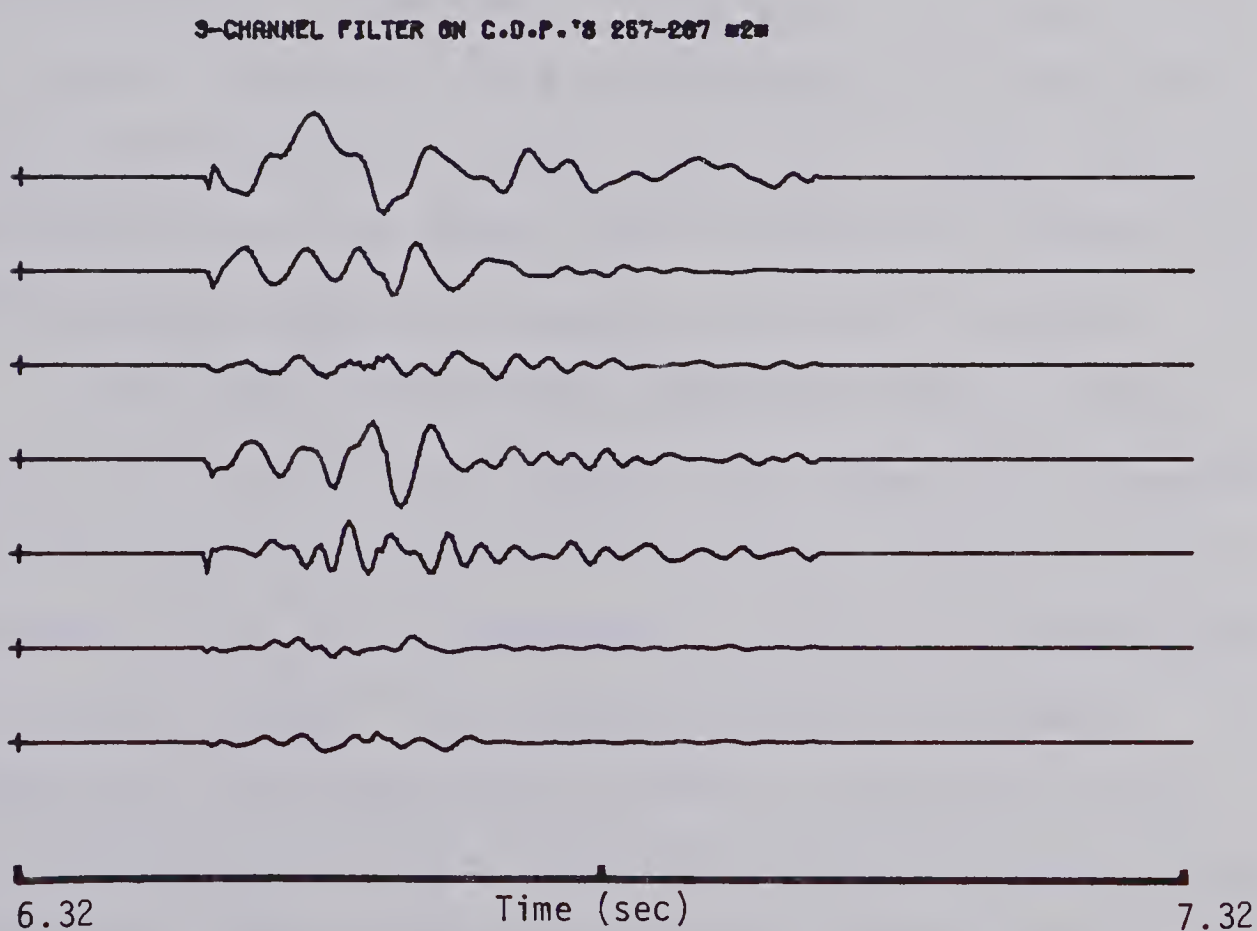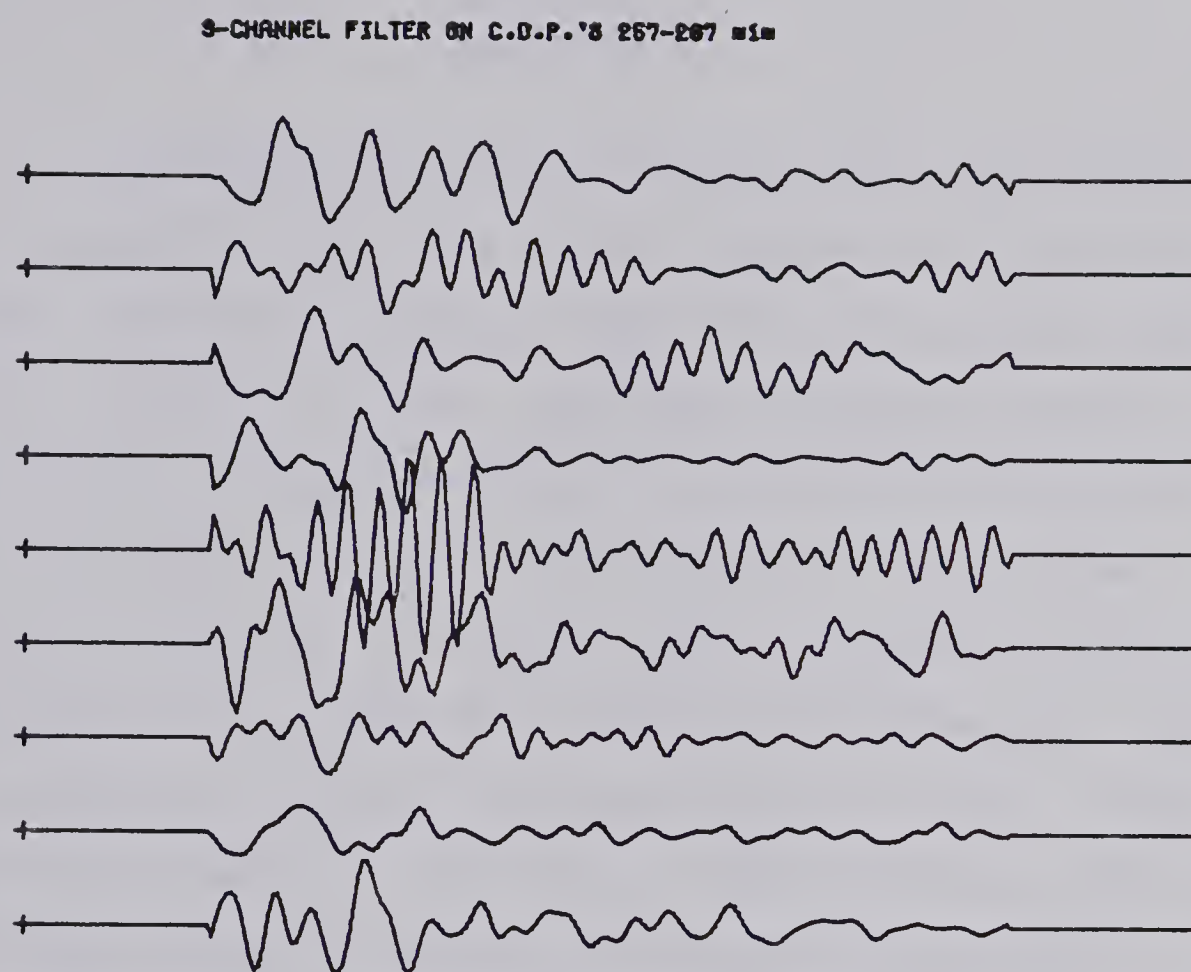
Figure 4.16: Application of a three channel maximum likelihood filter on the stacked data for subsurface points 257 to 267.

CHAPTER 5
CONCLUSIONS

Seismograms recorded in southeastern Saskatchewan and southwestern Manitoba clearly indicate the existence of near vertical incidence, deep reflecting events from within the Earth's crust. Our own reflection profile was obtained along three lines in southwestern Manitoba over a distance of about 72 kilometers. The data was recorded digitally on magnetic tape. Through the use of the University of Alberta's Amdahl 470V/6 computer, static and dynamic corrections were applied to the data. Power spectral analysis of the various traces indicates that the reflected energy is contained between the frequencies of 10 and 30 hertz. Therefore, a zero-phase band-pass filter with cutoff frequencies of 8 and 40 hertz was applied to the data to improve its overall quality. A major reflection recorded at a two-way travel time of about 6.6 seconds was found to have a dominant frequency of about 11 hertz.

Using cross correlation curves and various plots, primary reflections were brought into proper time alignment for three sections of subsurface points. Traces for each subsurface point were subsequently stacked and investigated for coherent energy. To further enhance any primary reflections, the techniques of velocity filtering, N-th root stacking and maximum likelihood filtering were applied to the data. Both velocity filtering and N-th root stacking enhanced well all reflections, with maximum likelihood

filtering having very little success. To produce eight velocity filtered traces (each six seconds in length) from eleven input channels on the Amdahl 470V/6 took approximately 4.8 seconds, while the corresponding eight root stack time was about 1.5 seconds.

Maximum likelihood filtering was not found to be a very useful technique. Accurate inversion of the large autocorrelation matrices is very difficult and very expensive. To compute nine output traces (each one second in length) from eleven input channels requires roughly 13.5 seconds of computer time. Also, it was found that the filter is very unstable when the noise is not coherent. Thus, this technique should not be used in the analysis of data where random noise predominates.

This thesis illustrates that the reflection method, with its increased resolution, can add substantially to the knowledge of the crust. Suggestions for future studies of this type include:

(1) Use of tapered arrays and multiple holes to to increase the quality of the reflection seismograms. Also, a better site selection for the geophones and stringers (not near power lines or on gravel roads) would increase the quality of the records.

(2) Multiple reflections did not seem to be a problem, but were noticed on some sections. The increase from 400 to 1200 percent coverage

would probably eliminate these and enhance the continuity of primary reflected energy.

(3)   A velocity analysis could be used to determine exactly the velocities necessary to remove the normal moveout (NMO) associated with the records. This is not a vital step in the analysis since even for spread lengths of up to ten kilometers, the effect of variations in velocities on NMO, for long ray paths, is very small. However, it would simplify the steps necessary to bring primary reflections into proper time alignment.

(4)   Band-pass and velocity filtering can be used before stacking to remove various forms of noise (for example, ground roll). With a twelve-fold stack, the multiple reflections should be well attenuated eliminating any need for deconvolution. An eight root stack subsequently applied to the stacked data should now well enhance any primary reflections.

On the velocity filtered sections obtained in this study, three main reflecting horizons can be seen; one at about 6.6 seconds, one at 8.1 seconds, and one at 12.5 seconds. An approximate average velocity down to these horizons may be determined by using the structure model of figure 3.12, and the following equation from Taner and Koehler (1969).

$$V_a(n) = \frac{2\sum_{K=1}^{n} d(K)}{T(o,n)}$$

5.1.1

where the parameters are the same as those of secton 3.5.
Using equation 5.1.1, we get average velocities to the
three layers of about 5.7, 5.9 and 6.2 kilometers per
second respectively. From figure 5.1, the approximate
dip angle to each of these horizons is

$$\alpha = \sin^{-1}\left[\frac{V_a(n)\ \Delta T}{2X}\right]$$

5.1.2

Figures 5.2 through 5.4 exhibit the resultant
migrated crustal sections with the approximate dips shown.
In order to confirm the continuity of these horizons, they
must be located on many more sections along the three
lines. If the reflections are from a transition zone
instead of a sharp velocity discontinuity, the events may
not correlate over great distances (see section 1.2).

These models can be compared with the preliminary
refraction model for the east side of the Churchill-
Superior boundary (figure 5.5). The shallow layers seen
in the refraction profile were not observed due to limita-
tions in our recording instrumentation. The upper two
layers in the reflection models were not detected by the
refraction method, possibly due to wide spacing in the shot
to receiver locations, but our deep reflector at 12.5
seconds coincides quite closely with the third layer, and
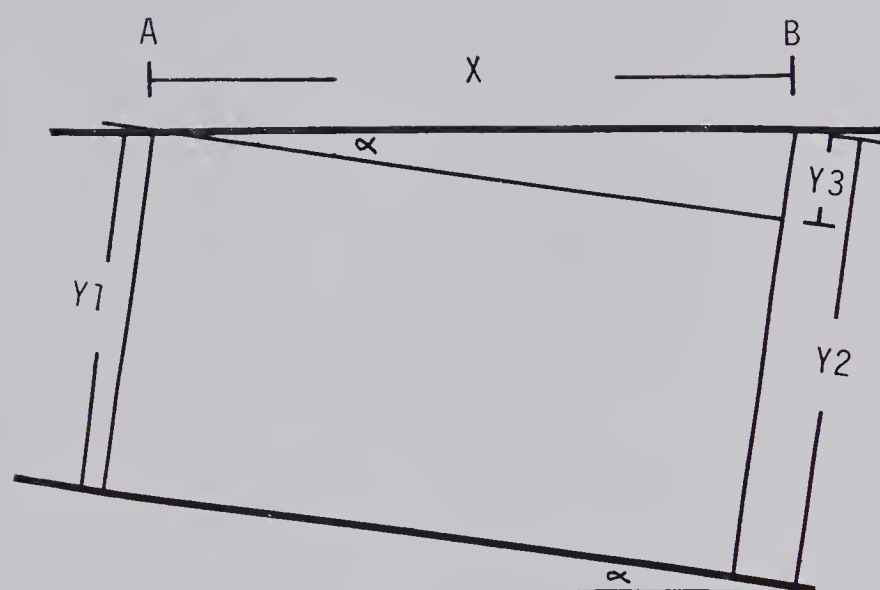
α = dip of the reflector

T1= two way travel time to the reflector below A

T2= two way travel time to the reflector below B

Therefore,

Y1= distance travelled by the wave below A

$$= \frac{Vav * T1}{2}$$

Y2= distance travelled by the wave below B

$$= \frac{Vav * T2}{2}$$

Y3= Y2-Y1

$$= \frac{Vav}{2} * (T2-T1) = \frac{Vav * \Delta T}{2}$$

Figure 5.1: The expression for the dip angle for a reflector
where the average velocity down to the layer is
constant.
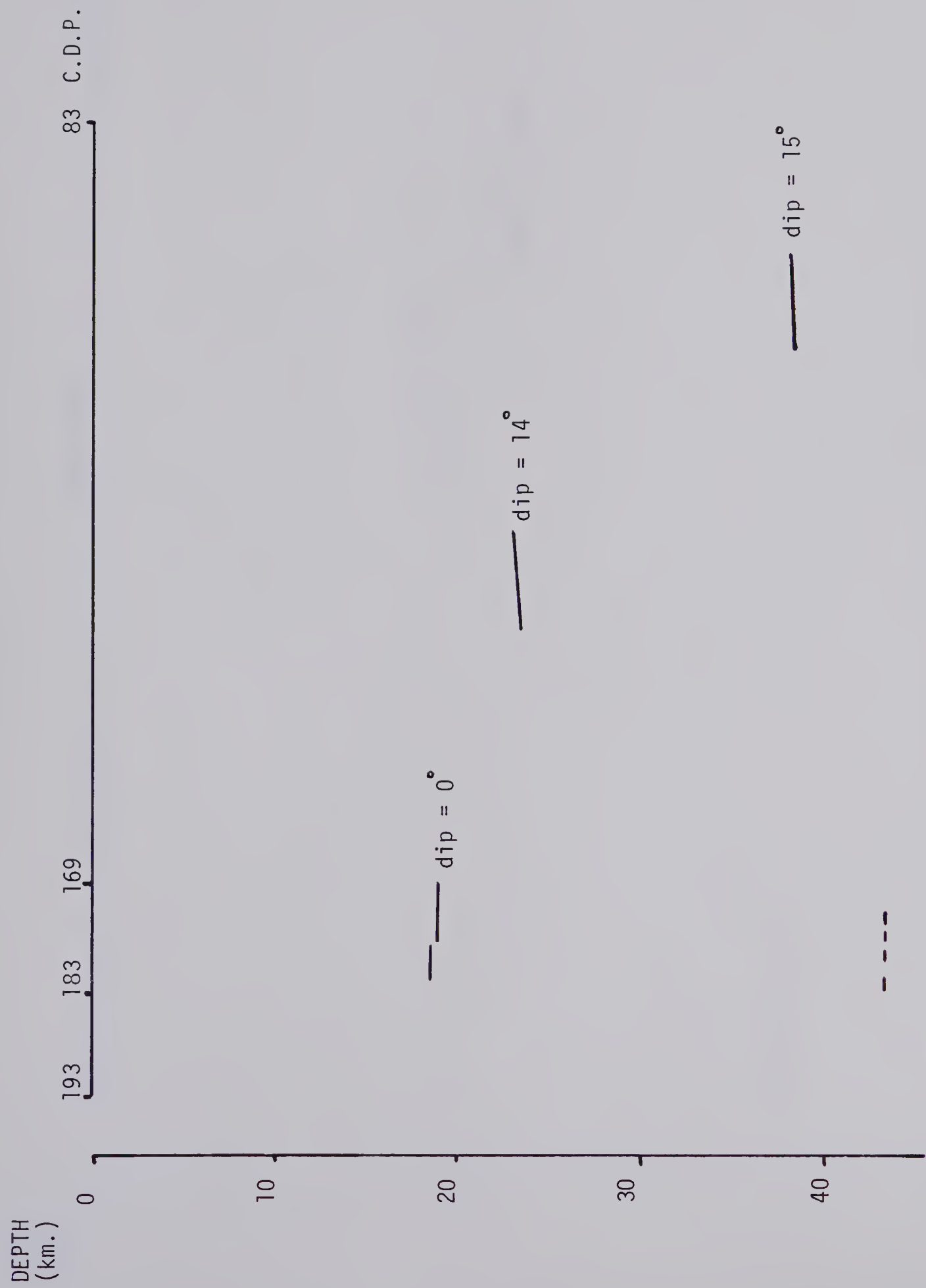
Figure 5.2: Deep crustal model as derived from subsurface points 169 to 183.
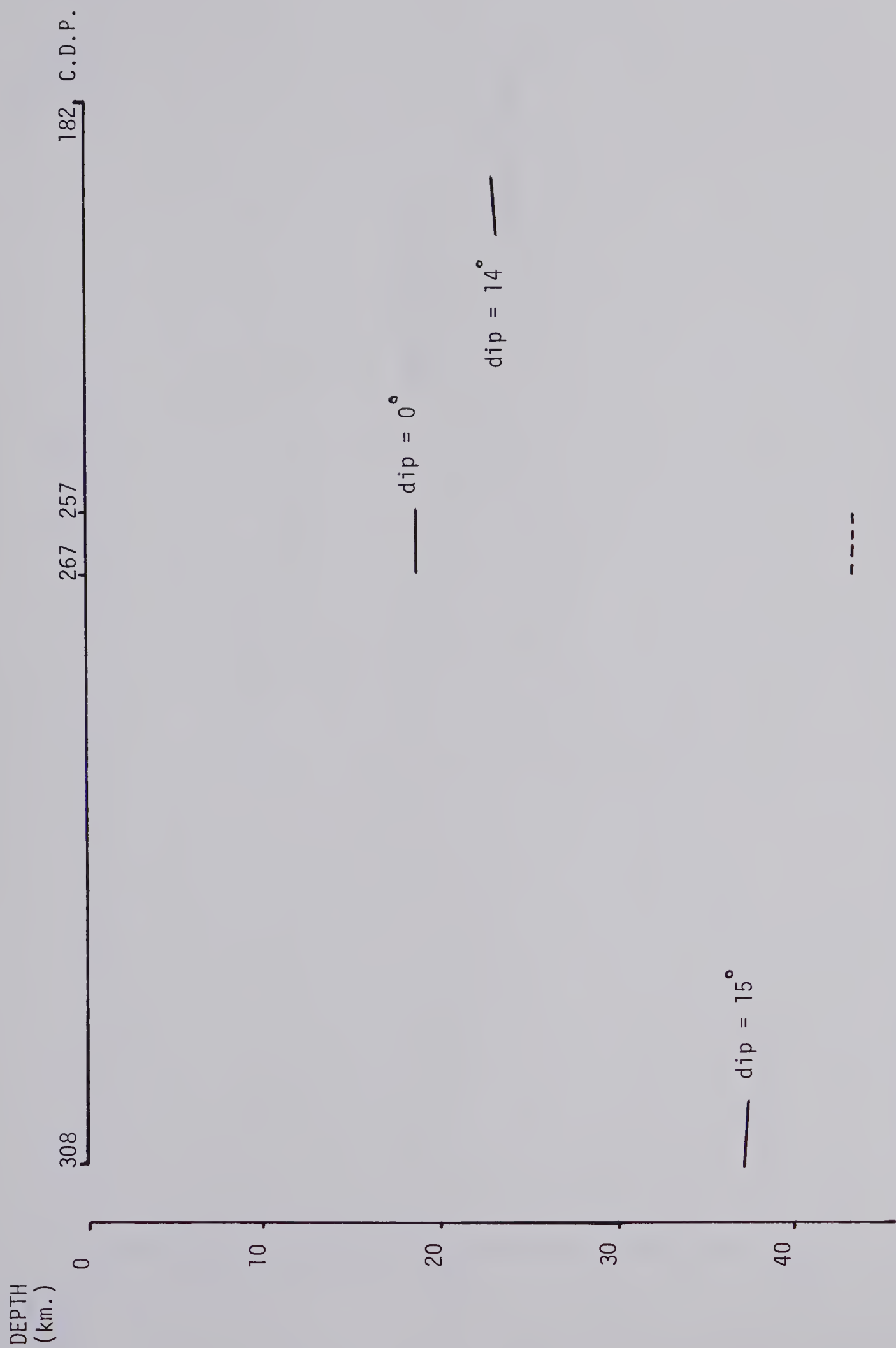
Figure 5.3: Deep crustal model as derived from subsurface points 257 to 267.
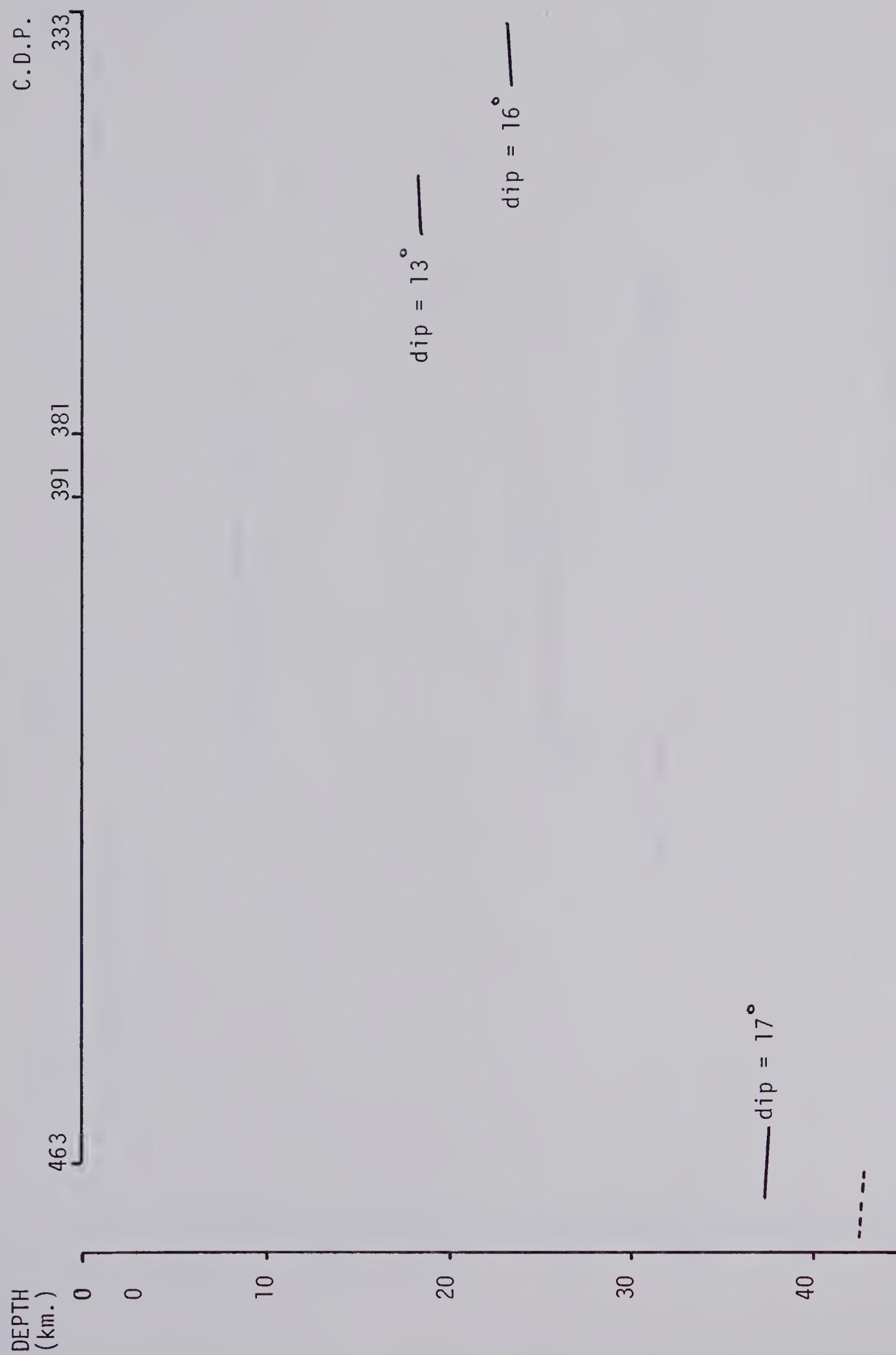
Figure 5.4: Deep crustal model as derived from subsurface points 381 to 391.
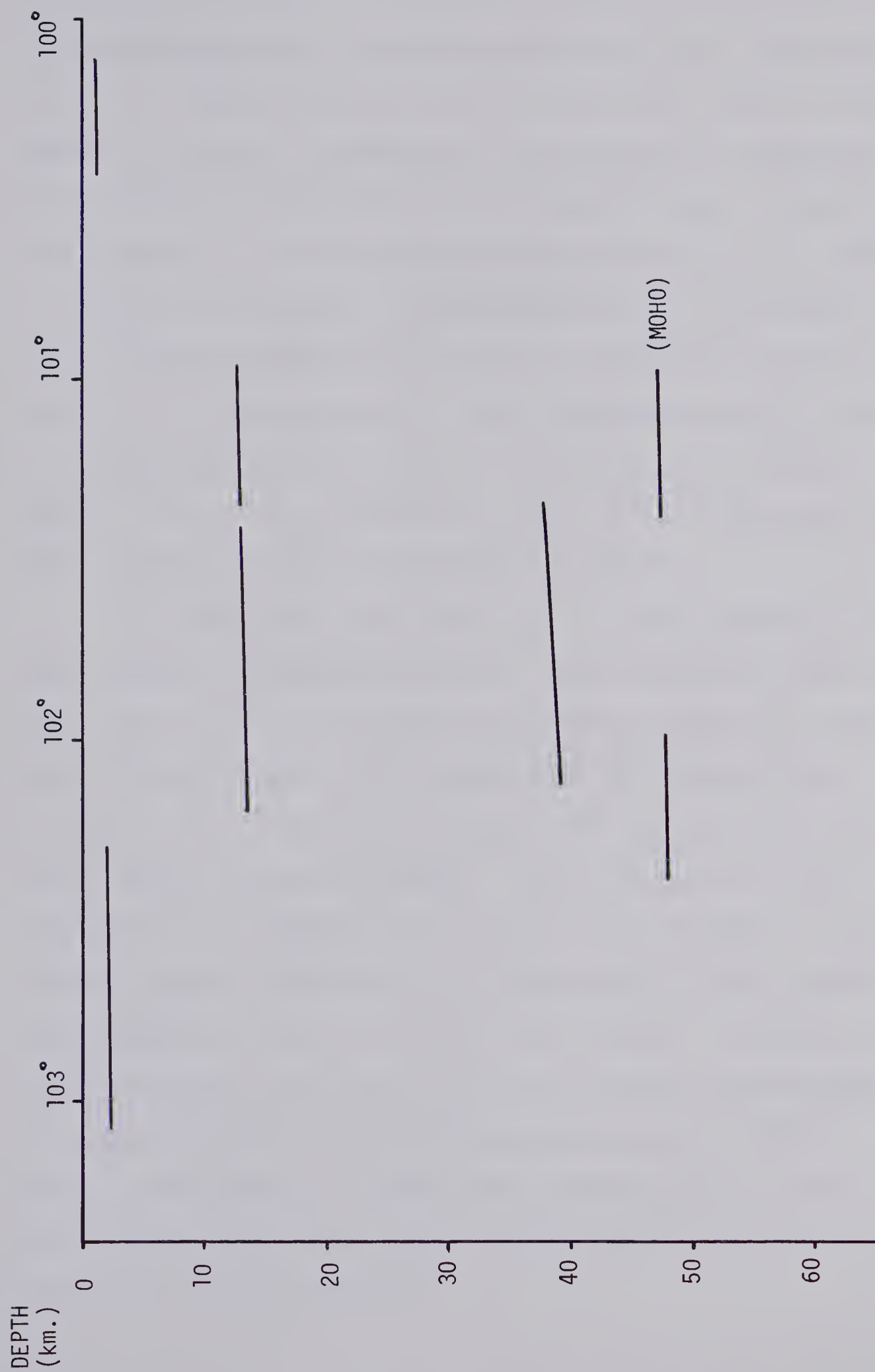
Figure 5.5: Preliminary findings of the east-west refraction profile (after Green,1977).

the energy at about 14.0 seconds coincides approximately with the Mohorovicic discontinuity seen in the refraction profile. The refraction profile across the boundary zone seems to indicate a boundary at 100.9 degrees longitude corresponding to the break in the second layer. Across this boundary, the Mohorovicic discontinuity is at a depth of about 46 kilometers. Unfortunately, this structure break occurs at the very end of our reflection profile, and thus in order to see it, the reflection profile should be repeated over this region. Since the field program appears likely to be funded in 1979, it is recommended that this interesting area be studied in detail.

In conclusion, the velocity filtered sections clearly enhanced all reflections within a specified pass band, but only limits could be placed on the phase velocity. With the N-th root stack, only events with the proper time alignment for a specified stepout were passed, with all other events being eliminated. The technique is very dependent upon amplitude and proper time alignment of the various traces, which when all are correct, make accurate computations of phase velocity very simple. The N-th root stack has been successfully used to enhance low frequency refraction seismic records (Kanasewich *et al.*, 1973). However, this thesis is the first demonstration of the value of the N-th root stack in the signal enhancement of reflection seismic profiles.

BIBLIOGRAPHY

Al-Chalabi, M., 1973. Series approximation in velocity
      and traveltime computations. Geophys. Prosp., 21,
      pp. 783-795.

Allsopp, D.F., Burke, M.D. and Cumming, G.L., 1972. A
      digital recording system. Bull. Seis. Soc. Am.,
      62, pp. 1641-1647.

Angenheister, G. and Pohl, J., 1971. Deep crustal
      reflections on a 17 kilometer digital reflection
      profile in south Germany (Nordlinger, Ries).
      Observ. Royal Belgique Commun., 12th Assem. Gen.
      Comm. Seism. Eur., Series A, no. 13, pp. 173-176.

Bartelsen, H., Meissner, R. and Murawski, H., 1976.
      Seismic reflection measurements along the geotra-
      verse Rhenoherzynicum. Publication no. 85 from
      the Institute of Geophysics, Kiel, F.R.G.

Bath, M. and Tryggvason, E., 1962. Deep seismic reflec-
      tion experiments at Kiruna. Geof. Pura Appl., 51,
      pp. 79-90.

Bell, C.K., 1971a. History of the Churchill-Superior
      boundary. Geol. Assoc. Can. Spec. Pap. 9, pp. 5-10.

Bell, C.K., 1971b. Boundary geology, upper Nelson River
      area, Manitoba and northwestern Ontario. Geol.
      Assoc. Can. Spec. Pap. 9, pp. 11-39.

Brown, R.J., Friesen, G.H., Hall, D.H. and Stephenson,
      O.G., 1977. Weighted vertical stacking in crustal
      seismic reflection studies on the Canadian Shield.
      Geophy. Prosp., 25, pp. 251-268.

Burwash, R.A., Baadsgaard, H. and Peterman. Z.E., 1962.
      Precambrian K-Ar dates from western Canada
      sedimentary basin. J. Geophys. Res., 67, no. 4,
      pp. 1617-1625.

Claerbout, J.F., 1976. Fundamentals of geophysical data
      processing with applications to petroleum prospecting.
      McGraw Hill Book Company, New York, pp. 1-23.

Clowes, R.M., 1966. Deep crustal seismic reflections at
      near-vertical incidence. M.Sc. thesis, Edmonton:
      University of Alberta, Department of Physics.

Clowes, R.M., 1969. Seismic reflection investigations of crustal structure in southern Alberta. Ph.D. thesis, Edmonton: University of Alberta, Department of Physics.

Clowes, R.M., Kanasewich, E.R. and Cumming, G.L., 1968. Deep crustal seismic reflections at near vertical incidence. Geophysics, 33, pp. 441-451.

Clowes, R.M. and Kanasewich, E.R., 1970. Seismic attenuation and the nature of reflecting horizons within the crust. J. Geophys. Res., 75, pp. 6693-6705.

Cooley, J.W. and Tukey, J.W., 1965. An algorithm for the machine calculation of complex Fourier series. Math. Comp., 19, pp. 297-301.

Courtier, W.H. and Mendenhall, H.L., 1967. Experiences with multiple coverage seismic methods. Geophysics, 32, pp. 230-258.

Cranstone, D.A. and Turek, A., 1975. Geological and geochronological relationships of the Thompson nickel belt, Manitoba. Can. J. Earth Sci., 13, pp. 1058-1069.

Cumming, G.L. and Chandra, N.N., 1975. Further studies of reflections from the deep crust in southern Alberta. Can. J. Earth Sci., 12, pp. 539-557.

Dewey, J.F. and Burke, K.C.A., 1973. Tibetan, Variscan and Precambrian basement reactivation: Products of continental collision. J. Geol., 81, pp. 683-692.

Dickins, D.G., 1973. Least-squares inverse filtering of seismic reflection data. M.Sc. thesis, Edmonton: University of Alberta, Department of Physics.

Dix, C.H., 1955. Seismic velocities from surface measurements. Geophysics, 20, pp. 68-86.

Dix, C.H., 1965. Reflection seismic crustal studies. Geophysics, 30, pp. 1068-1084.

Dobrin, M.B., 1976. Introduction to geophysical prospecting. McGraw-Hill Inc., New York.

Dohr, G. and Fuchs, K., 1967. Statistical evaluation of deep crustal reflections in Germany. Geophysics, 32, pp. 951-967.

Dohr, G.P. and Meissner, R., 1975. Deep crustal reflections in Europe. Geophysics, 40, pp. 25-39.

Embree, P., Burg, J.P. and Backus, M.M., 1963. Wide-band velocity filtering - the pie-slice process. Geophysics, 28, pp. 948-974.

Ganley, D.C., 1973. A seismic reflection crustal model near Edmonton, Alberta. M.Sc. thesis, Edmonton: University of Alberta, Department of Physics.

Ganley, D.C. and Cumming, G.L., 1974. A seismic reflection model of the crust near Edmonton, Alberta. Can. J. Earth Sci., 11, pp. 101-109.

Gibb, R.A., 1968a. The densities of Precambrian rocks of northern Manitoba. Can. J. Earth Sci., 5, pp. 433-438.

Gibb, R.A., 1968b. A geological interpretation of the Bouguer anomalies adjacent to the Churchill-Superior boundary in northern Manitoba. Can. J. Earth Sci., 5, pp. 439-453.

Goldich, S.S., Lidiak, E.G., Hedge, C.E. and Walthall, F.G., 1966. Geochronology of the midcontinent region, United States: 2. Northern region. J. Geophys. Res., 71, pp. 5389-5408.

Goodwin, A.M., 1972. The Superior Province in variations in tectonic styles in Canada. R. Price and R. Douglas (eds.) Toronto: Geological Association of Canada, pp. 527-623.

Green, A.G. and Stephenson, O.G., 1977. Cooperative near vertical incident reflection and refraction/wide angle reflection seismic surveys across the Superior-Churchill boundary zone in southern Canada. University of Manitoba.

Gurbuz, B.M., 1970. A study of the earth's crust and upper mantle using travel times and spectrum characteristics of body waves. Bull. Seism. Soc. Am., 60, pp. 1921-1935.

Jacobs, J.A., Russel, R.D. and Wilson, J.T., 1974. Physics and Geology. McGraw Hill Book Company, New York, pp. 54-99.

James, D.E. and Steinhart, J.S., 1966. Structure beneath continents: A critical review of explosion studies 1960-1965, in The earth beneath the continents,

J.S. Steinhart and T.J. Smith (eds.). Washington: American Geophysical Union, pp. 293-333.

Junger, A., 1951. Deep basement reflections in Big Horn County, Montana. Geophysics, 16, pp. 499-505.

Kanasewich, E.R., 1975. Time sequence analysis in geophysics. University of Alberta Press, Edmonton.

Kanasewich, E.R. and Cumming, G.L., 1965. Near vertical incidence seismic reflections from the Conrad discontinuity. J. Geophys. Res., 70, pp. 3441-3446.

Kanasewich, E.R., Hemmings, C.D. and Alpaslan, T., 1973. N-th root stack non-linear multichannel filter. Geophysics, 38, pp. 327-338.

Kornik, L.J. and Maclaren, A.S., 1966. Aeromagnetic study of the Churchill-Superior boundary in northern Manitoba. Can. J. Earth Sci., 3, pp. 547-557.

Lee, J., 1977. Multilayer gravity inversion using Fourier transforms. M.Sc. thesis, Edmonton: University of Alberta, Department of Physics.

Lindseth, R.O., 1967. The nature of digital seismic processing. J. Can. Soc. Exp. Geophys., 3, pp.31-111.

Mair, J.A. and Lyons, J.A., 1976. Seismic reflection techniques for crustal structure studies. Geophysics, 41, pp. 1272-1290.

Marr. J.D. and Zagst, E.F., 1967. Exploration horizons from new seismic concepts of CDP and digital processing. Geophysics, 32, pp. 207-224.

Mateker Jr., E.J., 1965. A treatise on some aspects of modern exploration seismology. Courtesy of Pan American Petroleum Company.

Mayne, W.H., 1962. Common reflection point horizontal data stacking techniques. Geophysics, 27, pp.927-938.

Mayne, W.H., 1967. Practical considerations in the use of common reflection point techniques. Geophysics, 32, pp. 225-229.

Meissner, R., 1966. An interpretation of the wide angle measurements in the Bavarian molasse basin. Geophys. Prosp., 15, pp. 598-617.

Mercado, E.J., 1973. Multichannel adaptive filter
    theory and applications to reflection seismology.
    Proc. 1st Int. Joint Conf. on Pattern Recognition,
    IEEE Computer Soc., pp. 464-491.

Mercado, E.J., 1978. Maximum likelihood filtering of
    reflection seismograph data. Geophysics, 43,
    pp. 497-513.

Mintrop, L., 1949. On the stratification of the earth's
    crust according to seismic studies of a large
    explosion and earthquakes. Geophysics, 14, pp.321-336.

Muirhead, K.J., 1968. Eliminating false alarms when
    detecting seismic events automatically. Nature,
    217, pp. 533-534.

Narans Jr., H.D., Berg Jr., J.W. and Cook, K.L., 1961.
    Sub-basement seismic reflections in northern Utah.
    J. Geophys. Res., 66, pp. 599-603.

Oliver, J., Dobrin, M., Kaufman, S., Meyer, R. and
    Phinney, R., 1976. Continuous seismic reflection
    profiling of the deep basement, Hardeman County,
    Texas. Geol. Soc. Am. Bull., 87, pp. 1537-1546.

Papazachos, B.C., Comninakis, P.E. and Drakopoulos, J.C.,
    1966. Preliminary results of an investigation of
    crustal structure in southeastern Europe. Bull.
    Seism. Soc. Am., 56, pp. 1241-1268.

Pennington, R.H., 1970. Introductory computer methods
    and numerical analysis. Macmillan Company,
    New York.

Perkins, W.E. and Phinney, R.A., 1971. A reflection
    study of the Wind River uplift, Wyoming.
    Geophysical Monograph Series, 14, pp. 41-50.

Robinson, E.A., 1967. Multichannel time series analysis
    with digital computer programs. Holden-Day, Inc.,
    San Francisco.

Schriever, W., 1952. Reflection seismograph prospecting -
    how it started. Geophysics, 17, pp. 936-942.

Shanks, J.L., 1967. Recursion filters for digital
    processing. Geophysics, 32, pp. 33-51.

Smithson, S.B. and Shire, P.N., 1975. Field measurements
    of compressional wave velocities in common crystal-
    line rocks. Earth Planetary Science Letters, 27,
    pp. 170-176.

Smithson, S.B. and Brown, S.K., 1977. A model for lower
     continental crust. Earth Planetary Science Letters,
     25, pp. 134-144.

Sollogub, V.B. and Prosen, D., 1973. Crustal structure
     of central and southeastern Europe by data of
     explosion seismology. Tectonophysics, 20, pp. 1-33.

Steinhart, J.S. and Meyer, R.P., 1961. Explosion studies
     of continental structure. Carnegie Inst. Wash.
     Publ. 622, Washington: The Kirby Lithographic
     Company, Inc.

Taner, M.T. and Koehler, F., 1969. Velocity spectra-
     digital computer derivation and applications of
     velocity functions. Geophysics, 34, pp. 859-881.

Telford, W.M., Geldhart, L.P., Sheriff, R.E. and Keys, D.A.,
     1976. Applied Geophysics, Cambridge University
     Press, Cambridge, pp. 218-434.

Treitel, S., Shanks, J.L. and Frasier, C.W., 1967. Some
     aspects of fan filtering. Geophysics, 32, pp.789-800.

White, R.E., 1977. The performance of optimum stacking
     filters in the presence of uncorrelated noise.
     Geophys. Prosp., 25, pp. 165-178.

Wiggins, R.A. and Robinson, E.A., 1965. Recursive
     solution to the multichannel filtering problem.
     J. Geophys. Res., 70, pp. 1885-1891.

Zverev, S.M. (ed.), 1967. Problems in deep seismic
     sounding. New York: Consultants Bureau.

APPENDIX 1
MULTICHANNEL FILTER OUTPUT EQUATIONS

The output of a multichannel filter may be expressed as (equation 4.3.6)

$$O(t) = X(t)^T * \bar{f}(o) + \ldots + X(t-\tau)^T * \bar{f}(\tau)$$

$$
\begin{vmatrix} X_1(o) & \ldots & X_K(o) \\ \cdot & & \cdot \\ \cdot & & \cdot \\ \cdot & & \cdot \\ X_1(N) & \ldots & X_K(N) \end{vmatrix}
\begin{vmatrix} f_1(o) \\ \cdot \\ \cdot \\ \cdot \\ f_K(o) \end{vmatrix}
+ \ldots +
\begin{vmatrix} X_1(-\tau) & \ldots & X_K(-\tau) \\ \cdot & & \cdot \\ \cdot & & \cdot \\ \cdot & & \cdot \\ X_1(N-\tau) & \ldots & X_K(N-\tau) \end{vmatrix}
\begin{vmatrix} f_1(\tau) \\ \cdot \\ \cdot \\ \cdot \\ f_K(\tau) \end{vmatrix}
$$

where

O(t) = single channel output trace

$X_i(t)$ = ith input channel

K = number of input channels

$f_i(\tau)$ = filter for lag τ

Equation A.1.1 may be expressed as

$$
O(t) =
\begin{vmatrix} X_1(1)f_1(o) + \ldots + X_K(o)f_K(o) \\ \cdot \\ \cdot \\ \cdot \\ X_1(N)f_1(o) + \ldots + X_K(N)f_K(o) \end{vmatrix}
+ \ldots +
\begin{vmatrix} X_1(-\tau)f_1(\tau) + \ldots + X_K(-\tau)f_K(\tau) \\ \cdot \\ \cdot \\ \cdot \\ X_1(N-\tau)f_1(\tau) + \ldots + X_K(N-\tau)f_K(\tau) \end{vmatrix}
$$

$$
= \begin{vmatrix}
X_1(0)f_1(0)+\ldots+X_K(0)f_K(0)+\ldots+X_1(-\tau)f_1(\tau)+\ldots+X_K(-\tau)f_K(\tau) \\
\vdots \\
X_1(N)f_1(0)+\ldots+X_K(N)f_K(0)+\ldots+X_1(N-\tau)f_1(\tau)+\ldots+X_K(N-\tau)f_K(\tau)
\end{vmatrix}
$$

A.1.2

Rewriting equation A.1.2, we obtain

$$
0(t) = \begin{vmatrix}
X_1(0)f_1(0)+\ldots+X_1(-\tau)f_1(\tau)+\ldots+X_K(0)f_K(0)+\ldots+X_K(-\tau)f_K(\tau) \\
\vdots \\
X_1(N)f_1(0)+\ldots+X_1(N-\tau)f_1(\tau)+\ldots+X_K(N)f_K(0)+\ldots+X_K(N-\tau)f_K(\tau)
\end{vmatrix}
$$

A.1.3

This may be expressed as

$$
0(t) = \begin{vmatrix}
X_1(0) & \ldots & X_1(-\tau) \\
 & \cdot & \\
 & \cdot & \\
 & \cdot & \\
X_1(N) & \ldots & X_1(N-\tau)
\end{vmatrix}
\begin{vmatrix}
f_1(0) \\
\cdot \\
\cdot \\
\cdot \\
f_1(\tau)
\end{vmatrix}
+\ldots+
\begin{vmatrix}
X_K(0) & \ldots & X_K(-\tau) \\
 & \cdot & \\
 & \cdot & \\
 & \cdot & \\
X_K(N) & \ldots & X_K(N-\tau)
\end{vmatrix}
\begin{vmatrix}
f_K(0) \\
\cdot \\
\cdot \\
\cdot \\
f_K(\tau)
\end{vmatrix}
$$

A.1.4

APPENDIX 2

THREE CHANNEL MAXIMUM LIKELIHOOD FILTER

The following discussion of the three channel
maximum likelihood filter is based largely on two references
(Mercado, 1973; 1978). The author has simply tried to
clarify some of the steps in the derivation.

If we let the three input channels be denoted by
$X_1(t)$, $X_2(t)$ and $X_3(t)$, then the single channel output
$O(t)$ is the convolution of the input traces with the
filters $f_1(\tau)$, $f_2(\tau)$ and $f_3(\tau)$. Mathematically, we have

$$O(t) = X_1(t-\tau)*f_1(\tau)+X_2(t-\tau)*f_2(\tau)+X_3(t-\tau)*f_3(\tau)$$

A.2.1

Since the filter is to pass coherent signal
arriving with infinite apparent velocity, the filters must
satisfy

$$f_1(\tau)+f_2(\tau)+f_3(\tau) = \delta(\tau) \qquad\qquad A.2.2$$

or

$$f_1(\tau) = \delta(\tau)-f_2(\tau)-f_3(\tau) \qquad\qquad A.2.3$$

Substituting equation A.2.3. into A.2.1

$$O(t) = X_1(t-\tau)*[\delta(\tau)-f_2(\tau)-f_3(\tau)]+X_2(t-\tau)*f_2(\tau)+X_3(t-\tau)*f_3(\tau)$$

$$= X_1(t-\tau)*\delta(\tau)-X_1(t-\tau)*f_2(\tau)-X_1(t-\tau)*f_3(\tau)+X_2(t-\tau)*f_2(\tau)$$

$$+X_3(t-\tau)*f_3(\tau)$$

$$= X_1(t)+[X_2(t-\tau)-X_1(t-\tau)]*f_2(\tau)+[X_3(t-\tau)-X_1(t-\tau)]*f_3(\tau)$$

A.2.4

Now, let

$$\Delta i(t-\tau) = X_i(t-\tau)-X_1(t-\tau) \qquad i = 2,3 \qquad\qquad A.2.5$$

Substituting A.2.5 into A.2.4,

$$O(t) = X_1(t)+\Delta_2(t-\tau)*f_2(\tau)+\Delta_3(t-\tau)*f_3(\tau) \qquad\qquad A.2.6$$

We would now like to obtain the least-squares solution for $f_2(\tau)$ and $f_3(\tau)$ that will minimize the output power. The output power is given by

$$P = O(t)^T*O(t)$$

$$= [X_1(t)+\Delta_2(t-\tau)*f_2(\tau)+\Delta_3(t-\tau)*f_3(\tau)]^T*[X_1(t)+$$

$$\Delta_2(t-\tau)*f_2(\tau)+\Delta_3(t-\tau)*f_3(\tau)]$$

$$= [X_1(t)^T + f_2^T(\tau) * \Delta_2(t-\tau)^T + f_3(\tau)^T * \Delta_3(t-\tau)^T] * [X_1(t) +$$

$$\Delta_2(t-\tau) * f_2(\tau) + \Delta_3(t-\tau) * f_3(\tau)]$$

$$= X_1(t)^T * X_1(t) + X_1(t)^T * \Delta_2(t-\tau) * f_2(\tau) + X_1^T(\tau) * \Delta_3(t-\tau) * f_3(\tau)$$

$$+ f_2^T(\tau) * \Delta_2(t-\tau)^T * X_1(t) + f_2^T(\tau) * \Delta_2(t-\tau)^T * \Delta_2(t-\tau) * f_2(\tau)$$

$$+ f_2^T(\tau) * \Delta_2(t-\tau)^T * \Delta_3(t-\tau) * f_3(\tau) + f_3^T(\tau) * \Delta_3(t-\tau)^T * X_1(t)$$

$$+ f_3^T(\tau) * \Delta_3(t-\tau)^T * \Delta_2(t-\tau) * f_2(\tau) + f_3^T(\tau) * \Delta_3(t-\tau)^T * \Delta_3(t-\tau) * f_3(\tau)$$

$$A.2.7$$

For vectors A and B, and matric C; the product A*C*B is a scalar, and thus, $A*C*B = B^T*C^T*A^T$. Using this, equation A.2.7 simplifies to

$$P = X_1(t)^T * X_1(t) + 2X_1(t)^T * \Delta_2(t-\tau) * f_2(\tau) + 2X_1^T(t) * \Delta_3(t-\tau) * f_3(\tau)$$

$$+ f_2^T(\tau) * \Delta_2(t-\tau)^T * \Delta_2(t-\tau) * f_2(\tau) + 2f_2^T(\tau) * \Delta_2(t-\tau)^T * \Delta_3(t-\tau) * f_3(\tau)$$

$$+ f_3^T(\tau) * \Delta_3(t-\tau)^T * \Delta_3(t-\tau) * f_3(\tau) \qquad A.2.8$$

Using arguments analogous to those found in appendix 1, we have

$$\Delta_2(t-\tau) * f_2(\tau) + \Delta_3(t-\tau) * f_3(\tau) = \bar{\Delta}\bar{f} \qquad A.2.9$$

where $\bar{\Delta}$ is the two channel convolution matrix of $\Delta_2(t)$ and $\Delta_3(t)$

$$\bar{\Delta} = \begin{bmatrix} \Delta_2(0) & \Delta_3(0) & \cdots & \Delta_2(-\tau) & \Delta_3(-\tau) \\ \cdot & \cdot & & \cdot \\ \cdot & \cdot & & \cdot \\ \cdot & \cdot & & \cdot \\ \Delta_2(N) & \Delta_3(N) & \cdots & \Delta_2(N-\tau) & \Delta_3(N-\tau) \end{bmatrix} \quad \text{A.2.10}$$

and,

$$\bar{f} = \begin{bmatrix} f_2(0) \\ f_3(0) \\ \cdot \\ \cdot \\ \cdot \\ f_2(\tau) \\ f_3(\tau) \end{bmatrix}$$

Therefore, equation A.2.8 may be compactly written as

$$P = X_1(t)^T * X_1(t) + 2X_1(t)^T * \bar{\Delta} * \bar{f} + \bar{f}^T * \bar{\Delta}^T * \bar{\Delta} * \bar{f} \quad \text{A.2.12}$$

The minimization of the power and the least-squares solution for $\bar{f}$ is accomplished by differentiating P with respect to $\bar{f}$, and setting the result equal to zero.

$$\frac{\partial P}{\partial \bar{f}} = \frac{\partial(X_1(t)^T * X_1(t))}{\partial \bar{f}} + \frac{2\partial(X_1(t)^T * \bar{\Delta} * \bar{f})}{\partial \bar{f}} + \frac{\partial(\bar{f}^T * \bar{\Delta}^T * \bar{\Delta} * \bar{f})}{\partial \bar{f}}$$

$$= 0 + 2X_1(t)^T * \bar{\Delta} + 2\bar{f}^T * \bar{\Delta}^T * \bar{\Delta} \quad \text{A.2.13}$$

Therefore,

$$2(X_1(t)^T * \bar{\Delta})^T + 2\bar{\Delta}^T * \bar{\Delta} * \bar{f} = 0 \qquad \text{A.2.14}$$

This leads to

$$\bar{\Delta}^T * \bar{\Delta} * \bar{f} = -(X_1(t)^T * \bar{\Delta})^T \qquad \text{A.2.15}$$

that is,

$$\bar{f} = -(\bar{\Delta}^T * \bar{\Delta})^{-1} (X_1(t)^T * \bar{\Delta})^T \qquad \text{A.2.16}$$

At this point, we may note that equation A.2.16 is the filter equation for the Wiener filters. The main advantage of the maximum likelihood filter over the Wiener filter is that for N input channels, N filters must be calculated for Wiener filtering whereas only N-1 filters have to be calculated for maximum likelihood filtering.

APPENDIX 3
LISTINGS OF COMPUTER PROGRAMS

A3.1   The Velocity Filter

The velocity filter program used in this thesis was
initially written by Clowes (1969) as part of his Ph.D.
thesis, and later revised by the author for analysis of
the data collected in southwestern Manitoba. This
program velocity filters seismic data according to the
algorithm located in section 4.1.

For use in the program, the input channels can have
a maximum of 1500 points, and they must be stored in trace
mode on magnetic tape. This input data is read off of
the tape through the use of the system routine READ. To
plot out the input and output traces, a call must be made
to the subroutine Plotvf, which makes use of the Calcomp
plotter subroutines.

```
C        THE VELOCITY FILTER PROGRAM
         REAL *4 SUM(3000),Y(3000),Z(3000),TS(64),RB(1500)
         COMMON/STORAG/XDATA(15,3000)
C        XDATA...THE MATRIX OF INPUT CHANNELS
         COMMON/STORE/XFILT(12,2500),SEPT,SCALE,COPS,RECNO(5)
        1,CENTER,NTAU,NS,TSTART
C        XFILT...THE MATRIX OF OUTPUT CHANNELS
         INTEGER PTSTAR,ROWST,CENTER,START,CENT(5),TAU(5)
         INTEGER*2 LEN
         XPOS=2.0
         YPOS=29.0
         NTR PT=0
   100 FORMAT(16I5)
   101 FORMAT(8F10.0)
   103 FORMAT(5A4)
         READ(5,100) ISTOP
C        ISTOP...IF 999,THE TEST PULSE IS USED.
C                IF 100,THE INPUT TAPE IS USED.
         READ(5,100) M,NTR,NOUT,JPLOT,PTSTAR,NPEND,NS,NL
C        JPLOT...IF 0,NO PLOT IS DONE
C                IF 1,INPUT AND OUTPUT TRACES ARE PLOTTED.
C        NTR.....NUMBER OF INPUT TRACES
C        M.......NUMBER OF TRACES TO BE USED IN THE FAN PASS
C                OPERATION
C                (M MUST BE EVEN)
C        NOUT....NUMBER OF OUTPUT TRACES
         READ(5,101) SEPT,COPS,SCALE,TSTART
C        TSTART...START TIME FOR AXIS IN PLOT
C        SCALE....SCALING FACTOR TO BE USED IN THE PLOT
C        SEPT.....SEPARATION BETWEEN TRACES IN THE PLOT
C        COPS.....NUMBER OF POINTS PER SECOND.
         READ(5,100) (CENT(I),I=1,NS),(TAU(I),I=1,NS)
C        CENT(I)...THE MOVEOUT IN POINTS PER TRACE ABOUT
C                  WHICH THE PASSBAND IS CENTERED.
C        TAU(I)....THE MOVEOUT IN POINTS PER TRACE OF THE
C                  CUTOFF VELOCITY
C        NS........NUMBER OF PASSBANDS TO EXECUTE
         IF (JPLOT.EQ.1) CALL PLOTS
         IF(ISTOP.EQ.999) GO TO 130
         NPTS=(NPEND-PTSTAR)+1
C        NPTS...NUMBER OF POINTS IN THE INPUT TRACES
         READ(5,103) RECNO
C        RECNO...TITLE FOR THE PLOT
C
C READ IN THE DATA WITH PTSTAR=1
C
         DO 8 I=1,NTR
         CALL READ(RB,LEN,0,LX,8)
         DO 8 J=1,NPTS
```

```
      8 XDATA(I,J)=RB(J)
        IF(ISTOP.EQ.100) GO TO 150
C
C DO THE TEST FUNCTION
C
    130 CALL PULSE(TS)
        NPTS=NPEND-PTSTAR+1
        TSTART=0.0
        READ(5,103) RECNO
    150 IF (JPLOT.EQ.1)CALL PLOTVF(NTR,NPTS,1,NOUT,PTSTAR,0,
       1NTR PT, XPOS,YPOS)
C PLOT THE INPUT TRACES
        DO 65 KF=1,NS
        CENTER=CENT(KF)
        NTAU=TAU(KF)
        L=M-1
        MC=L*IABS(CENTER)
        NEND=NPEND-(L+1)*NTAU/2
        START=PTSTAR+(L-1)*NTAU/2
        IF (CENTER.LT.0) START=START+MC
        IF (CENTER.GT.0) NEND=NEND-MC
C THE STARTING AND ENDING TIMES HAVE BEEN SHIFTED SO
C THAT ONLY POINTS BETWEEN PTSTAR AND NPEND WILL BE
C USED WHEN THE DATA POINTS ARE TIME SHIFTED.
        A=0.65465
        B=0.98612
        C=0.13091
        D=0.2026424
        ROWST=0
     20 ROWST=ROWST+1
        DO 10 I=1,NL
     10 SUM(I)=0.0
        DO 50 K=START,NEND
        NSN=K-PTSTAR+1
        IROW=ROWST
        DO 40 J=1,M
        JA=J-1
        MU=2*JA-L
        MUDE=(MU-1)*NTAU/2
        MUAD=(MU+1)*NTAU/2
        JB=CENTER*JA
        ICOL1=K-MUDE+JB
        ICOL2=K+MUAD+JB
        DIFF=(XDATA(IROW,ICOL1)-XDATA(IROW,ICOL2))/MU
        SUM(NSN)=SUM(NSN)+DIFF
     40 IROW=IROW+1
     50 CONTINUE
        NST1=START-PTSTAR+1
        NEN1=NEND-PTSTAR+1
C SUM HAS BEEN FILLED WITH THE WEIGHTED SUM OF THE
```

```
C TIME SHIFTED TRACES
C
      DO 55 I=1,NL
      Y(I)=0.0
      Z(I)=0.0
   55 XFILT(ROWST,I)=0.0
      DO 60 K=NST1,NEN1
      NA=K-1
      NB=K-2
      Y(K)=SUM(NA)-A*SUM(NB)+B*Y(NA)-C*Y(NB)
      NN=NEN1-K+NST1
      NC=NN+1
      ND=NN+2
   60 Z(NN)=SUM(NN)-A*SUM(NC)+B*Z(NC)-C*Z(ND)
      DO 70 I=NST1,NEN1
   70 XFILT(ROWST,I)=D*(Z(I)-Y(I))
C THE TRACES HAVE BEEN FILTERED.
      IF (ROWST.LT.NOUT) GO TO 20
      IF (JPLOT.EQ.1) CALL PLOTVF(ROWST,NPTS,2,NOUT,1,KF,
     1NTR PT,XPOS,YPOS)
C PLOT THE OUTPUT TRACES
   65 CONTINUE
      IF (JPLOT.EQ.0) GO TO 120
      CALL PLOT (XPOS,YPOS-28.0,-3)
      CALL PLOT(0.0,0.0,999)
  120 STOP
      END




      SUBROUTINE PLOTVF(NTP,NPTS,INDEX,NOUT,NPSTAR,KF,
     ;NTR PT,XPOS,YPOS)
      COMMON/STORAG/XDATA(15,3000)
      COMMON/STORE/XFILT(12,2500),SEPT,SCALE,COPS,RECNO(5)
     1,CENTER,NTAU,NS,TSTART
      INTEGER CENTER
      NPEND=NPSTAR+NPTS-1
      T=2.0/COPS
      XLEN=FLOAT(NPTS)*T
      ABSINT=0.5
      MNTR=MOD(NTR PT,2)
      GO TO (20,30),INDEX
   20 DO 27 J=1,NTP
      DO 22 JA=NPSTAR,NPEND
   22 XDATA(J,JA)=XDATA(J,JA)/SCALE
   27 CONTINUE
      CALL PLOT (XPOS,YPOS,-3)
      CALL PLOT (0.0,-1.0,-3)
      CALL AXIS (0.0,0.0,'TIME IN SECONDS',+15,XLEN,0.0,
```

```
      1TSTART,ABSINT,10.0)
       YD=3.5+5.5*SEPT
       CALL SYMBOL (-1.0,-YD,0.2,RECNO,90.0,20)
       YDADD=YD+0.50
       CALL SYMBOL(-0.5,-YDADD,0.15,'DISTANCE BETWEEN TRACES
      1 IS .146 KM.',90.0,35)
       GO TO 39
   30  DO 10 J=1,NTP
       DO 5 JA=NPSTAR,NPEND
    5  XFILT(J,JA)=XFILT(J,JA)/SCALE
   10  CONTINUE
       IF(MNTR.NE.0) GO TO 36
   33  CALL PLOT (-XLEN,0.0,-3)
   36  IF (KF.NE.1) GO TO 39
       CALL PLOT (0.0,-2.0,-3)
       CALL AXIS (0.0,0.0,'TIME IN SECONDS',+15,XLEN,0.0,
      1TSTART,ABSINT,10.0)
       CALL SYMBOL (-1.0,-0.7,.20,'VELOCITY',90.0,8)
       CALL SYMBOL (-0.7,-0.7,0.20,'FILTERED',90.0,8)
       CALL SYMBOL (-.3,-.4,0.20,'DATA',90.0,4)
   39  IF (KF.EQ.0) GO TO 44
       YD=2.1+FLOAT(NOUT-1)*SEPT
       FNUM1=((CENTER-NTAU)/COPS)
       IF (FNUM1.NE.0.) GO TO 40
       VEL1=1.0
       GO TO 41
   40  VEL1=0.293/FNUM1
   41  FNUM2=((CENTER+NTAU)/COPS)
       IF (FNUM2.NE.0.) GO TO 42
       VEL2=1.0
       GO TO 43
   42  VEL2=0.293/FNUM2
   43  CALL SYMBOL(-1.0,-YD,.15,'V1',90.0,2)
       CALL SYMBOL(-0.9,-YD+.25,.10,'APP',90.0,3)
       CALL WHERE (XP,YP,FCTR)
       YP=YP+0.2
       CALL SYMBOL(-1.0,YP,.15,' IS ',90.0,4)
       CALL WHERE (XP,YP,FCTR)
       YP=YP+0.2
       CALL NUMBER (-1.0,YP,.15,VEL1,90.0,1)
       CALL WHERE (XP,YP,FCTR)
       YP=YP+0.2
       CALL SYMBOL (-1.0,YP,.15,'K/S',90.0,3)
       CALL SYMBOL (-0.5,-YD,.15,'V2',90.0,2)
       CALL SYMBOL (-0.4,-YD+.25,.10,'APP',90.0,3)
       CALL WHERE (XP,YP,FCTR)
       YP=YP+0.2
       CALL SYMBOL (-0.5,YP,.15,' IS ',90.0,4)
       CALL WHERE (XP,YP,FCTR)
       YP=YP+0.2
```

```
      CALL NUMBER (-0.5,YP,.15,VEL2,90.0,1)
      CALL WHERE (XP,YP,FCTR)
      YP=YP+0.2
      CALL SYMBOL (-0.5,YP,.15,'K/S',90.0,3)
   44 DO 80 J=1,NTP
      MJ=MOD(J,2)
      IF (J.NE.1) GO TO 45
      CALL PLOT (0.0,-2.0,-3)
      GO TO 46
   45 IF (MJ.EQ.0) GO TO 60
      CALL PLOT (-XLEN,-SEPT,-3)
   46 CALL SYMBOL (0.0,0.0,.15,04,0.0,-4)
      GO TO (47,49),INDEX
   47 CALL PLOT (0.0,XDATA(J,NPSTAR),3)
      DO 48 JA=NPSTAR,NPEND
      TSCALE=T*FLOAT(JA-NPSTAR+1)
   48 CALL PLOT (TSCALE,XDATA(J,JA),2)
      GO TO 75
   49 CALL PLOT (0.0,XFILT(J,NPSTAR),3)
      DO 50 JA=NPSTAR,NPEND
      TSCALE=T*FLOAT(JA-NPSTAR+1)
   50 CALL PLOT (TSCALE,XFILT(J,JA),2)
      GO TO 75
   60 CALL PLOT (XLEN,-SEPT,-3)
      CALL SYMBOL (0.0,0.0,.15,04,0.0,-4)
      GO TO (61,64),INDEX
   61 CALL PLOT(0.0,XDATA(J,NPEND),3)
      DO 62 JA=NPSTAR,NPEND
      TSCALE=-T*FLOAT(JA-NPSTAR+1)
      JCC=NPEND-JA+NPSTAR-1
      IF (JCC.LT.NPSTAR) JCC=NPSTAR
   62 CALL PLOT (TSCALE,XDATA(J,JCC),2)
      GO TO 75
   64 CALL PLOT (0.0,XFILT(J,NPEND),3)
      DO 65 JA=NPSTAR,NPEND
      TSCALE=-T*FLOAT(JA-NPSTAR+1)
      JCC=NPEND-JA+NPSTAR-1
      IF (JCC.LT.NPSTAR) JCC=NPSTAR
   65 CALL PLOT(TSCALE,XFILT(J,JCC),2)
   75 CALL PLOT (TSCALE,0.0,3)
      CALL SYMBOL (TSCALE,0.0,.15,04,0.0,-4)
   80 CONTINUE
      GO TO (81,84), INDEX
   81 DO 83 J=1,NTP
      DO 82 JA=NPSTAR,NPEND
   82 XDATA(J,JA)=XDATA(J,JA)*SCALE
   83 CONTINUE
      GO TO 92
   84 DO 90 J=1,NTP
      DO 85 JA=NPSTAR,NPEND
```

```
    85 XFILT(J,JA)=XFILT(J,JA)*SCALE
    90 CONTINUE
    92 IF (KF.NE.NS) GO TO 100
       IF (MNTR.EQ.0) GO TO 95
       XPOS=XLEN+5.0
       GO TO 97
    95 XPOS=5.0
    97 YPOS=11.0+FLOAT(3*NTP+8)*SEPT
   100 NTR PT=NTP
       RETURN
       END




       SUBROUTINE PULSE(TS)
       COMMON/STORAG/XDATA(15,3000)
       REAL TS(64)
       PI=3.1415926
       DO 6 I=1,16
       JR=I-1
       TS(I)=-0.5*SIN(PI/16*JR)
     6 CONTINUE
       DO 7 I=17,32
       JP=I-17
       TS(I)=SIN(PI/16*JP)
     7 CONTINUE
       DO 8 I=33,48
       JQ=I-33
       TS(I)=-0.75*SIN(PI/16*JQ)
     8 CONTINUE
       DO 9 I=49,64
       JC=I-49
       TS(I)=0.25*SIN(PI/16*JC)
     9 CONTINUE
C      DO 1 I=1,64
C      JR=I-1
C      TS(I)=EXP(-PI/16.*JR)*SIN(0.5*PI*JR)
C    1 CONTINUE
       DO 2 J=1,11
       DO 2 I=1,3000
     2 XDATA(J,I)=0.0
       L=0
       DO 3 I=1,7
       II=I-1
       IB=(200*I)+1+(II*64)
       L=L+1
       DO 4 J=1,11
       JA=(L-4)*2
       JS=J-1
```

```
      JN=JS*JA
      IT=IB-JN
      NN=IT+63
      DO 5 JT=IT,NN
      JL=(JT-IT)+1
    5 XDATA(J,JT)=TS(JL)
    4 CONTINUE
    3 CONTINUE
      RETURN
      END
```

A3.2.   The N-th Root Stack

This program computes the eight root stack for a
given set of input seismic traces according to the theory
found in section 4.2.   A maximum of 15 input channels is
allowed, and each trace must comprise 1500 data points.
These input traces must be located on a magnetic tape
with a block length of 6000 bytes, and are read with the
aid of the system routine READ.   To accommodate different
stepouts in the stack, the first and last 50 points of
the output trace are set equal to zero.   The resulting
output traces are then written onto magnetic tape via the
system routine WRITE.

```
C       THE 8TH-ROOT STACKING PROGRAM
        INTEGER *2 LEN,LEB
        REAL *4 RB(1500),Y(1500),YY(1500),X(15,1500)
C       RB...A SEISMIC CHANNEL FROM THE INPUT TAPE
C       X....THE MATRIX OF INPUT CHANNELS
C       YY...AN OUTPUT CHANNEL TO BE WRITTEN ONTO TAPE
  100 FORMAT(16I5)
        READ(5,100) M,NTR,NS
C       M......NUMBER OF TRACES TO BE USED IN THE STACK.
C       NTR...NUMBER OF INPUT TRACES
C       NS-1..NUMBER OF POSITIVE STEPOUTS
        LEB=6000
        NSS=(2*NS)-1
        ML=-NS
        NOUT=(NTR-M)+1
C       NOUT..NUMBER OF OUTPUT TRACES
C READ IN THE DATA.
C
        DO 1 I=1,NTR
        CALL READ(RB,LEN,0,LX,8)
        DO 1 J=1,1500
    1 X(I,J)=RB(J)
C DO NSS EIGTH ROOT STACKS.
        DO 8 IR=1,NSS
        N1=1
        N2=M
        ML=ML+1
        DO 2 I=1,NOUT
        LQ=50
        DO 3 J=1,1500
    3 Y(J)=0.0
        NN=0
        DO 4 JQ=N1,N2
        NN=NN+1
        DO 5 JC=51,1450
        LQ=LQ+1
        IF(X(JQ,LQ).EQ.0.0) GO TO 5
        Y(JC)=Y(JC)+(ABS(X(JQ,LQ))**0.125)*X(JQ,LQ)/
      ;(ABS(X(JQ,LQ)))
    5 CONTINUE
        LQ=(ML*NN)+50
    4 CONTINUE
        DO 6 JC=1,1500
        IF(Y(JC).EQ.0.0) YY(JC)=0.0
        IF(YY(JC).EQ.0.0) GO TO 6
        YY(JC)=(ABS(Y(JC)/FLOAT(M))**8)*Y(JC)/(ABS(Y(JC)))
    6 CONTINUE
        CALL WRITE(YY,LEB,0,LY,1)
C WRITE THE OUTPUT ON TAPE
        WRITE(6,100) N1,N2,LQ,ML
```

```
      N1=N1+1
      N2=N2+1
2     CONTINUE
8     CONTINUE
      STOP
      END
```

A3.3.   The Three Channel Maximum Likelihood Filter

This program computes a three channel maximum likelihood filter according to the theory found in appendix 2. A maximum of eleven input channels may be used, each with a block length of 1000 bytes. The input traces must be stored in trace mode on magnetic tape, and are read with the system routine READ. All output traces are written onto tape through the routine WRITE.

To obtain the filter coefficients, equation 4.3.12 must be solved, which is of the form

$$AX = B \hspace{4cm} A3.3.1$$

The solution to this set of linear equations is obtained through the IMSL library routine LEQTIF. The subroutine is called by

```
CALL LEQTIF(A,M,N,N,B,IDGT,WKAREA,IER)
```

where

A = input autocorrelation matrix of dimension $N \times N$.

B = input cross correlation matrix of dimension $N \times 1$. On output, the solution X replaces B.

WKAREA = work area of dimension N.

IDGT = decimal places of accuracy in the elements
    of A and B.

IER = an error parameter

Two other IMSL library routines used in the program are VMULFP and VMULFM. VMULEP computes the matrix product $A*B^T$ through the call

        CALL VMULFP (A,B,L,M,N,L,N,C,L,IER)

where

        A = input matrix of dimension L × M

        B = input matrix of dimension N × M

        C = output matrix of dimension L × N

        IER = error parameter

        VMULFM computes the matrix product A^T*B by

        CALL VMULFM (A,B,L,M,N,L,C,M,IER)

where

        A = input matrix of dimension L × M

        B = input matrix of dimension L × N

        C = output matrix of dimension M × N

        IER = error parameter

        Other subroutines used in this program are Trans (transpose a matrix), Macron, Multi and Plit (plotting routine).

```
C         THE 3-CHANNEL MAXIMUM LIKELIHOOD FILTER
          REAL *4  DQ(40,250),DELT(2,250),RB(250),B(80,1),
         ;XX(250),DEL1(2,125),DEL2(2,125),WKAREA(80),A(80,80),
         ;XXX(2,250),TS(64),R(15),X1(125),C1(2,2),OTT(250),
         ;G1(2,1),G2(2,1),FF(40,1),C2(2,2),C22(2,2),CT(250,1)
          INTEGER *2 LEN,LEB
          COMMON/STORAG/X(11,250)
          COMMON/STORE/OT(9,250),N,NOUT,RECORD(5),RY(250)
C         X....THE MATRIX OF INPUT CHANNELS
C         OT...THE MATRIX OF OUTPUT CHANNELS
   100 FORMAT(16I5)
   101 FORMAT(4F10.0)
   102 FORMAT(6F15.5)
   103 FORMAT('0',10X,'FILTER COEFFS. ARE: '/)
   111 FORMAT(5A4)
   211 FORMAT('0',10X,5A4/)
   212 FORMAT('0',10X,'SCALE CHOSEN ',F8.1/)
          READ(5,100) INDEX,JPLOT
C         INDEX...IF 100,USE THE TEST PULSE
C         JPLOT...IF 100,A PLOT IS MADE
          READ(5,100) N,NC,NS,NF,NS1,NF1,NLAG,ISE,NSQ,NFQ
C         N....NUMBER OF INPUT CHANNELS
C         NC...3 FOR A 3-CHANNEL FILTER
C         NS...DIGITAL STARTING POINT FOR EACH TRACE
C         NF...DIGITAL END POINT FOR EACH TRACE
C         NS1..DIGITAL STARTING POINT FOR DESIGNING THE FILTER
C         NF1..DIGITAL END POINT FOR DESIGNING THE FILTER
          READ(5,101) TLN,CSEP,SCL,HT
C         TLN...LENGTH OF THE PLOT
C         CSEP..SEPARATION BETWEEN CHANNELS IN THE PLOT
C         SCL...SCALE FACTOR USED IN THE PLOT
C         HT....HEIGHT FACTOR USED IN THE PLOT
          READ(5,111) RECORD
C         RECORD...TITLE OF THE PLOT
          LEB=1000
          NOFS=NLAG+1
          NB=NC-1
          NOFS2=NB*NOFS
C CALCULATE THE NUMBER OF POINTS PER TRACE
          NTS=(NF-NS)+1
          NINT=NTS-1
          NTT=(NF1-NS1)+1
C CALCULATE THE NUMBER OF POINTS USED TO THE DETERMINE THE
C FILTERS
          SUBLN=TLN/(FLOAT(NINT))
          NOUT=N-NB
C         NOFS...NUMBER OF OPERATOR POINTS
C         NOUT...NUMBER OF OUTPUT TRACES
          XPOS=2.0
          YPOS=29.0
```

```
      BS2=-1.0
      DO 91 JJ=1,NOUT
      DO 91 J=1,NTS
   91 OT(JJ,J)=0.0
C CALCULATE RY FOR THE PLOT
      DO 20 I=1,NTS
   20 RY(I)=FLOAT(I-1)*SUBLN
      IF(JPLOT.EQ.100) CALL PLOTS
      IF(JPLOT.EQ.100) CALL FACTOR(.8)
      IF(INDEX.EQ.100) GO TO 99
C READ IN THE DATA
      DO 2 IQ=1,N
      CALL READ(RB,LEN,0,LX,8)
      MM=0
      DO 2 JQ=NS,NF
      MM=MM+1
    2 X(IQ,MM)=RB(JQ)
      GO TO 30
   99 CALL PULSE(TS,R,ISE)
   30 IF(JPLOT.EQ.100) CALL PLIT(TLN,CSEP,SCL,HT,NTS,
     ;1,XPOS,YPOS)
C PLOT THE INPUT TRACES
C
      DO 1 I=1,NOUT
      DO 10 J=1,NLAG
      LL=J+1
      DO 10 IJ=1,NLAG
      DQ(LL,IJ)=0.0
   10 CONTINUE
      IR1=1
      IT=0
      NQQ=NOFS
      DO 3 J=1,NTS
      II=I+1
      III=I+2
      XX(J)=X(I,J)
      DELT(1,J)=X(II,J)-X(I,J)
      DELT(2,J)=X(III,J)-X(I,J)
    3 CONTINUE
      NQ=0
      DO 7 IB=NS1,NF1
      NQ=NQ+1
    7 X1(NQ)=XX(IB)
C CALCULATE R0 AND G0 AND PLACE IN THE AUTOCORRELATION
C AND CROSS CORRELATION MATRICES
C
      DO 4 J=1,NB
      MN=0
      DO 4 JJ=NS1,NF1
      MN=MN+1
```

```
    4 DEL1(J,MN)=DELT(J,JJ)
      CALL VMULFP(DEL1,DEL1,NB,NTT,NB,NB,NB,C1,NB,IER)
      CALL MACRON(A,C1,NB,NOFS2,NQQ,IR1,1,NTT)
      CALL VMULFP(DEL1,X1,NB,NTT,1,NB,1,G1,NB,IER)
      CALL MULTI(B,G1,IT,NB,1,NTT,BS2)
      NMN=1
C CALCULATE THE OTHER AUTOCORRELATION AND CROSS CORRELATION
C TERMS AND PLACE THEM IN THEIR RESPECTIVE MATRICES
      DO 5 J=1,NLAG
      NQQ=NQQ-1
      IR1=IR1+NB
      NF2=NF1-NMN
      NS2=NS1-NMN
      DO 6 JQ=1,NB
      MN=0
      DO 6 JJ=NS2,NF2
      MN=MN+1
    6 DEL2(JQ,MN)=DELT(JQ,JJ)
      CALL VMULFP(DEL1,DEL2,NB,NTT,NB,NB,NB,C2,NB,IER)
      CALL TRANS(C2,NB,C22)
      CALL MACRON(A,C2,NB,NOFS2,NQQ,IR1,1,NTT)
      CALL MACRON(A,C22,NB,NOFS2,NQQ,1,IR1,NTT)
      CALL VMULFP(DEL2,X1,NB,NTT,1,NB,1,G2,NB,IER)
      CALL MULTI(B,G2,IT,NB,1,NTT,BS2)
      NMN=NMN+1
    5 CONTINUE
C CALCULATE THE FILTERS
      CALL LEQT1F(A,1,NOFS2,NOFS2,B,5,WKAREA,IER)
      WRITE(6,103)
      WRITE(6,102) (B(IB,1),IB=1,NOFS2)
      WRITE(6,100) NB,NS,NF,NOFS,NTT
C CALCULATE THE OUTPUT
      DO 11 J=1,NB
      ML=-1
      DO 26 JJ=1,NOFS
      ML=ML+1
      MS=0
      NTS1=NTS-ML
      DO 26 IQ=1,NTS1
      MS=MS+1
      MT=MS+ML
   26 DQ(JJ,MT)=DELT(J,IQ)
      DO 36 JQ=1,NOFS
      JB=((2*JQ)+(J-1))-1
   36 FF(JQ,1)=B(JB,1)
      CALL VMULFM(DQ,FF,NOFS,NTS,1,NOFS,NOFS,CT,NTS,IER)
      DO 47 JQ=1,NTS
   47 XXX(J,JQ)=CT(JQ,1)
   11 CONTINUE
      DO 50 IH=NSQ,NFQ
```

```
   50  OT(I,IH)=XX(IH)+XXX(1,IH)+XXX(2,IH)
    1  CONTINUE
       IF(INDEX.EQ.100) GO TO 41
       DO 92 JT=1,NOUT
       DO 93 JQ=1,NTS
   93  OTT(JQ)=OT(JT,JQ)
   92  CALL WRITE(OTT,LEB,0,LY,1)
   41  IF(JPLOT.EQ.100) CALL PLIT(TLN,CSEP,SCL,HT,NTS,
      ;2,XPOS,YPOS)
C  PLOT THE OUTPUT
       WRITE(6,211) RECORD
       WRITE(6,212) SCL
       IF(JPLOT.NE.100) GO TO 42
       CALL PLOT(0.0,0.0,999)
   42  STOP
       END




       SUBROUTINE PULSE(TS,R,ISE)
       COMMON/STORAG/X(11,250)
       REAL TS(64),R(15)
       PI=3.1415926
       DO 6 I=1,16
       JR=I-1
       TS(I)=-0.5*SIN(PI/16*JR)
    6  CONTINUE
       DO 7 I=17,32
       JP=I-17
       TS(I)=SIN(PI/16*JP)
    7  CONTINUE
       DO 8 I=33,48
       JQ=I-33
       TS(I)=-0.75*SIN(PI/16*JQ)
    8  CONTINUE
       DO 9 I=49,64
       JC=I-49
       TS(I)=0.25*SIN(PI/16*JC)
    9  CONTINUE
       R(1)=0.0
       R(2)=0.0
       R(3)=0.25
       R(4)=0.5
       R(5)=0.25
       R(6)=0.0
       R(7)=-0.25
       R(8)=-0.5
       R(9)=-0.75
       R(10)=-1.0
```

```
      R(11)=-0.75
      R(12)=-0.5
      R(13)=-0.25
      R(14)=0.0
      R(15)=0.0
      DO 1 I=1,3
      DO 1 J=1,250
   1  X(I,J)=0.0
      IL=0
      DO 3 IQ=1,3
      DO 4 I=1,3
      DO 5 J=1,64
      IJ=(I-1)*64+34+IL+J
   5  X(IQ,IJ)=TS(J)
   4  CONTINUE
      IL=IL+ISE
   3  CONTINUE
      DO 10 I=1,3
      DO 11 J=1,250
      IF(J.GT.66.AND.J.LT.82)  X(I,J)=X(I,J)+R(J-66)
      IF(J.GT.130.AND.J.LT.146)  X(I,J)=X(I,J)+R(J-130)
  11  CONTINUE
  10  CONTINUE
      RETURN
      END




      SUBROUTINE PLIT(TLN,CSEP,SCL,HT,NTS,
     ;INDIX,XPOS,YPOS)
      COMMON/STORAG/X(11,250)
      COMMON/STORE/OT(9,250),N,NOUT,RECORD(5),RY(250)
      T=TLN/250.0
      XLEN=FLOAT(NTS)*T
      ABSINT=1.0/TLN
      TSTART=6.0+(100.0/250.0)
      GO TO (20,30),INDIX
  20  DO 27 J=1,N
      DO 22 JA=1,NTS
  22  X(J,JA)=X(J,JA)*HT/SCL
  27  CONTINUE
      CALL PLOT(XPOS,YPOS,-3)
      CALL PLOT(0.0,-1.0,-3)
      CALL SYMBOL(0.0,1.5,0.2,RECORD,0.0,20)
      CALL SYMBOL(0.0,1.0,0.15,'DISTANCE BETWEEN TRACES
     ;IS 0.146 KM.',0.0,35)
      CALL AXIS(0.0,0.0,'TIME IN SECONDS',+15,XLEN,0.0,
     ;TSTART,ABSINT)
      GO TO 45
```

```
30  DO 10 J=1,NOUT
    DO 5 JA=1,NTS
 5  OT(J,JA)=(OT(J,JA)*HT/SCL)*5.0
10  CONTINUE
45  GO TO (40,50),INDIX
40  CALL PLOT(0.0,-2.0,-3)
    DO 41 J=1,N
    DO 42 JA=1,NTS
42  CALL PLOT(RY(JA),X(J,JA),2)
    CALL PLOT(0.0,-CSEP,-3)
41  CONTINUE
    GO TO 46
50  CALL PLOT(0.0,-2.0,-3)
    CALL AXIS(0.0,0.0,'TIME IN SECONDS',+15,XLEN,0.0,
   ;TSTART,ABSINT)
    CALL PLOT(0.0,-2.0,-3)
    DO 43 J=1,NOUT
    DO 44 JA=1,NTS
44  CALL PLOT(RY(JA),OT(J,JA),2)
    CALL PLOT(0.0,-CSEP,-3)
43  CONTINUE
46  RETURN
    END




    SUBROUTINE MULTI(V,RR,IS,NRA,NCA,NTT,BSN)
    DIMENSION V(256),RR(NRA,NCA)
    DO 1 L=1,NCA
    DO 2 J=1,NRA
    IS=IS+1
 2  V(IS)=(RR(J,1)/FLOAT(NTT))*BSN
 1  CONTINUE
    RETURN
    END




    SUBROUTINE MACRON(A,R1,NRA,NOFS2,NST,NBL1,NBL2,NTT)
    DIMENSION A(NOFS2,NOFS2),R1(NRA,NRA)
    IZ=NBL1-NRA
    IS=NBL2-1
    DO 1 I=1,NST
    IZ=IZ+NRA
    DO 2 J=1,NRA
    IS=IS+1
    IF=IZ-1
    DO 2 L=1,NRA
```

```
      IP=IP+1
    2 A(IS,IP)=R1(J,L)/FLOAT(NTT)
    1 CONTINUE
      RETURN
      END




      SUBROUTINE TRANS(C2,NB,C22)
      DIMENSION C2(2,2),C22(2,2)
      DO 1 I=1,NB
      DO 1 J=1,NB
    1 C22(J,I)=C2(I,J)
      RETURN
      END
```